Real-Time Dilepton Selection for the HADES Spectrometer

Inaugural-Dissertation
zur Erlangung des Doktorgrades der Naturwissenschaften
der Justus-Liebig-Universität Gießen
Fachbereich 07 (Mathematik und Informatik, Physik, Geographie)

vorgelegt von
Michael Traxler
aus Marburg/Lahn

II. Physikalisches Institut
der Justus-Liebig-Universität Gießen
November
2001

Dekan:	Prof. Dr. A. Beutelspacher
I. Berichterstatter:	Prof. Dr. W. Kühn
II. Berichterstatter:	Prof. Dr. C.-D. Kohl

Tag der mündlichen Prüfung: 21.12.2001

Table of Contents

4 The Matching Unit

5 Results and Perspectives

Abstract

The HADES spectrometer (**H**igh **A**cceptance **D**i**E**lectron **S**pectrometer) at GSI (Gesellschaft für Schwerionenforschung) is currently going into operation. It is designed to investigate various aspects of hadron and heavy ion induced reactions, in particular the electromagnetic structure and in medium modifications of hadrons.

In these experiments the electromagnetic decay of vector mesons into electron/ positron pairs is examined. These decays are very rare (probability of $\approx 10^{-5}$) and are accompanied by a large hadronic background of up to 200 charged particles per event in heavy ion reactions. Therefore, the experiments have to run at high events rates and require a fast, very selective and flexible online trigger system to reduce the amount of data taken. This is realized by identifying electron/positron pairs in a selectable invariant mass region.

The Second Level Trigger System developed by the Gießen HADES Trigger Group is presented. The first step of the trigger is to find electron signatures in the various subdetectors by **I**mage **P**rocessing **U**nits (IPU).

In the framework of this thesis the **M**atching **U**nit (MU) was developed, which in a second step collects the electron signatures found in each subdetector by the IPUs and combines this information to electron/positron pairs and determines their invariant mass. If the mass is within a selectable window the MU gives a positive final trigger decision which initiates the storage of this event. A negative decision discards the data. Using this scheme the raw event rate is reduced by a factor of 100.

The concept, the algorithm and the realization of the Matching Unit are described. The MU is a VME module based on **D**igital **S**ignal **P**rocessors (DSPs). To guarantee a high event rate, it is required that the MU provides a trigger decision every 10 µs on average. Since there are various experimental questions, the MU has to be flexible and fast enough to perform different trigger algorithms. To fulfill this requirement the hit information of the IPUs is simultaneously transferred to the MU and then distributed to DSPs which work in parallel. The parallel architecture is appropriate since the events are independent of each other. Furthermore, the combinatorial nature of the algorithm results in variable computation times which can be handled best by devices working in parallel.

The MU was used during several experiments with heavy ion beams and the results of its efficiency and performance are presented.

Abstract

Zusammenfassung

Das HADES-Spektrometer (**H**igh **A**cceptance **D**i**E**lectron **S**pectrometer) an der GSI (Gesellschaft für Schwerionenforschung), welches zur Zeit in Betrieb genommen wird, wurde konzipiert um verschiedene Aspekte der Hadronen- und Schwerionenphysik zu untersuchen. Von besonderem Interesse ist hierbei die Untersuchung der elektromagnetischen Struktur sowie die Suche nach Medium-Modifikationen von Hadronen.

In diesen Experimenten wird der elektromagnetische Zerfall von Vektormesonen in Elektron/Positron-Paare untersucht. Diese Zerfälle sind sehr selten (mit einer Wahrscheinlichkeit von $\approx 10^{-5}$) und werden von einem starken hadronischen Untergrund von ca. 200 geladenen Teilchen pro Ereignis (in Schwerionenreaktionen) begleitet. Daher wird in diesen Experimenten mit sehr hohen Ereignisraten gearbeitet und man benötigt ein schnelles, sehr selektives und flexibles Trigger-System, um die Menge an Daten direkt in Echtzeit zu reduzieren. Dies wird durch Selektion von Elektron/Positron-Paaren in einem wählbaren invarianten Massenbereich erreicht.

Das Second Level (LVL2) Trigger-System des HADES Detektors wird vorgestellt, welches von der Gießener HADES-Gruppe entwickelt wurde. Im ersten Schritt sucht der LVL2-Trigger nach Elektronensignaturen in den verschiedenen Subdetektoren. Dies leisten subdetektorspezifische Mustererkennungs-Einheiten (IPUs).

Im Rahmen dieser Arbeit wurde die Matching Unit (MU) entwickelt, welche in einem zweiten Schritt diese Elektronen/Positronensignaturen der IPUs der verschiedenen Subdetektoren sammelt, diese Informationen zu Elektronpaaren zusammenfügt und ihre invariante Masse bestimmt. Falls die Masse innerhalb eines wählbaren Bereichs liegt, wird die MU eine positive Trigger-Entscheidung treffen, welche die Speicherung des Ereignisses veranlasst. Eine negative Entscheidung verwirft die Ereignisdaten. Dieses Konzept ermöglicht eine Reduktion der ursprünglichen Ereignisrate um etwa den Faktor 100.

Das Konzept, der Algorithmus und die Verwirklichung der Matching Unit werden beschrieben. Die MU ist ein VME-Modul, welches auf **D**igitalen **S**ignal **P**rozessoren (DSPs) basiert. Um die hohe Ereignisrate zu gewährleisten, muß im Mittel alle 10 µs eine Trigger-Entscheidung fallen.

Da sich die experimentellen Fragestellungen ändern, muß die MU flexibel und schnell genug sein, um unterschiedliche Trigger-Algorithmen abarbeiten zu können. Dies wird dadurch erreicht, daß die Daten der IPUs gleichzeitig zu MU übertragen werden und dort auf parallel arbeitenden DSPs verteilt werden. Die parallele Architektur ist vorteilhaft, da jedes Ereignis vom nächsten unabhängig ist. Weiterhin führt der kombinatorische Algorithmus zu variierenden Rechenzeiten, der am Besten in parallel arbeitenden Einheiten abgearbeitet wird.

Die Matching Unit wurde während mehrerer Strahlzeiten erfolgreich eingesetzt; die gewonnen Ergebnisse werden in dieser Arbeit vorgestellt.

Die Arbeit ist folgendermaßen strukturiert:

Kapitel 1 gibt eine Einführung in die physikalischen Fragestellungen und die daraus folgende Motivation zum Bau des HADES Detektors. Es wird auf die elektromagnetische Struktur von Hadronen und deren Beschreibung mit Hilfe von Formfaktoren eingegangen. Weiterhin wird auf das Vektormesondominanzmodell eingegangen, welches den Pionen-Formfaktor sehr gut beschreibt, aber z.B. den Übergangsformfaktor des ω-Mesons nicht konsistent beschreiben kann.

Massenmodifikationen von Hadronen in hadronischer Materie werden diskutiert, die durch eine teilweise Wiederherstellung der Chiralen Symmetrie hervorgerufen werden können. Hier wird auf verschiedene theoretische Modelle eingegangen, die unterschiedliche Vorhersagen treffen. Zur Untersuchung dieser Effekte eignet sich der Zerfall von leichten Vektormesonen in ein Elektron/Positron-Paar sehr gut, da Leptonen nicht der starken Wechselwirkung unterliegen und somit Informationen aus dem inneren von hadronischer Materie fast ungestört nach außen tragen können.

Weiterhin werden frühere Experimente und ihre Ergebnisse erwähnt, die die physikalischen Fragestellungen schon untersucht hatten und das HADES Spektrometer wird motiviert, welches durch seine Konstruktion eine präzise Messung der vorhergesagten Effekte ermöglicht.

Im Kapitel 2 wird das HADES Spektrometer im Detail vorgestellt. Das Spektrometer besteht aus verschiedenen Subdetektoren, deren physikalische Funktionsweisen, sowie ihre Verwirklichung für HADES dargelegt werden. Hierbei wird auch basierend auf Simulationsergebnissen auf die erreichbare Massenauflösung sowie Ratenfestigkeit eingegangen. HADES ist ein Magnetspektrometer mit effizienter Elektronenidentifikation. Es hat neben der Möglichkeit der hochauflösenden Spurrekonstruktion von Teilchen, die durch ein toroidales Magnetfeld abgelenkt wurden, auch Subdetektoren, die selektiv Elektronen und Positronen erkennen können und somit den hadronischen Untergrund diskriminieren können.

Da die Untersuchung von sehr seltenen elektromagnetischen Zerfällen von Vektormesonen eine hohe Ereignisrate impliziert, ist im Konzept des HADES Spektrometers das schnelle und effiziente Triggersystem von zentraler Bedeutung, wobei der Schwerpunkt auf dem Second-Level-Trigger liegt. Das Triggersystem wird in Kapitel 3 erläutert. Es wird auf die Algorithmen eingegangen, die notwendig sind um Elektronensignaturen in den verschiedenen Subdetektoren zu finden. Die Verwirklichung dieser Algorithmen in Hardware, den sogenannten Image Processing Units (IPUs), wird beschrieben. Diese müssen die gesamten Detektordaten im Mittel innerhalb von 10 μs auf Elektronensignaturen untersuchen.

Im Rahmen dieser Arbeit wurde die Matching Unit konzipiert, hergestellt, programmiert und am Experiment in Betrieb genommen. Dies ist Inhalt von Kapitel 4.

Die Algorithmen mit allen Teilschritten, wie z.B. die Zuordnung von Treffern in den Subdetektoren zu Leptonenkandidaten, die Impulsbestimmung sowie die Bestimmung der invarianten Massen von Dileptonen wird dokumentiert. Danach wird das Konzept der entwickelten Hardware erläutert und die benutzten Komponenten beschrieben. Weiterhin werden die Schnittstellen zu den anderen Teilen des Second-Level-Triggersystems festgehalten.

Da der Algorithmus der Matching Unit in Software abläuft, werden die zur Implementierung erstellten Module beschrieben und die Möglichkeiten der

Einflußnahme auf den Algorithmus von außen beschrieben. Hiermit können dann für jedes Experiment spezifische Parameter gewählt werden.

In Kapitel 5 werden die Resultate der letzten Strahlzeiten gezeigt und Perspektiven für die Weiterentwicklung der Matching Unit aufgezeigt.

Die Matching Unit wurde erfolgreich eingesetzt. Die Funktionalität des Triggeralgorithmus unter Strahlbedingungen wurde durch Analyse der erzeugten Daten der MU auf Richtigkeit untersucht. Weiterhin werden die erreichten Triggereffizienzen des gesamten Second-Level-Triggers diskutiert.

Chapter 1

Motivation and Introduction

The standard model of particle physics describes the current physics understanding of matter on a microscopic scale. For this it uses two fundamental forces: The electroweak force and the strong force. Together with gravity, these forces can in principle describe the dynamics of matter in our world.

Quantum Chromo Dynamics (QCD) is the theory of the strong force. The elementary particles of QCD are the quarks and gluons. Due to confinement (single quarks have never been observed), these form color neutral objects, called hadrons. These are the baryons (consisting of three quarks), which include the nucleons, the building blocks of the matter we consist of, and the mesons (consisting of a quark and an antiquark).

For processes at high energies, where large 4-momentum transfers are involved, the equations of QCD are perturbatively solvable. For low 4-momentum transfers a numerical solution is achieved by Lattice QCD calculations, which is strongly limited by the computing technology available today. Therefore, one needs to use effective theories for describing processes at low 4-momentum transfer. These theories are based on principle symmetries of the QCD or use model assumptions from phenomenological indications resulting in solvable equations.

Since QCD is the theory of the strong force, its purpose is to explain the properties of hadronic matter and its dynamics we find in nature. The characteristics of the hadrons can be found listed for example in the *Particle Physics Booklet* [PDG00], where the world data is summarized. The most essential properties include the charge, the mass, the life time, the decay channels and the spin, etc. Many of these fundamental features are well known and understood, but there are still many open questions.

These properties are measured in vacuum and one expects changes when these particles are surrounded by hadronic matter. By analogy, this is similar to the *effective* mass of an electron moving in a crystal lattice; the surrounding potentials of the lattice result in a change of the mass used in the differential equations of their motion.

A great effort is being made for the experimental observation and theoretical interpretation of these fundamental features of matter, to get a better understanding of the laws of nature.

A special class of hadrons are the so called light vector mesons. These mesons have a rare electromagnetic decay channel into an electron/positron pair. This is remarkable, since these leptons do not interact strongly with hadronic matter and therefore penetrate hadronic matter undisturbed. For example, these light vector mesons can be produced in

heavy ion experiments. If they decay while they are still in hadronic matter, their dilepton decay products are an ideal probe to *look* inside nuclei. By changing the experimental conditions (beam energy, reaction target) one can measure the properties of the vector mesons (invariant mass, decay width, etc.) at different hadronic densities and temperatures.

These processes can be quantified by the spectroscopy of the produced electron/positron pairs.

Some properties of hadrons and the theoretical description of these are outlined in the following sections. The available experimental data related to the discussed properties motivate the HADES spectrometer. The rest of this thesis will deal with the HADES detector and the essential trigger system, where the emphasis is set on the Matching Unit, the part of the trigger, which generates the final decision to select electron/positron pairs out of a large hadronic background.

The Matching Unit has been developed in the framework of this thesis, this includes the concept, the algorithm, the realization in hardware, the programming and the commissioning of the Matching Unit at the experimental site.

1.1 The Structure of Hadrons

Hadrons are bound systems consisting of quarks (with the gluons as the field quanta of the strong interaction between the quarks), and one is interested in their internal structure. This can be described by quantities such as magnetic moment, polarizability and form factors and by parton distribution functions obtained from deep-inelastic scattering (for nucleons).

1.1.1 Form Factors

With the scattering of electrons on hadrons the internal electric structure becomes visible, if the momentum transfer is large enough. Additionally, since the electrons have spin 1/2 the magnetic structure also influences the scattering. The differential cross section for elastic scattering is given by the Rosenbluth formula [Ros50]:

$$\frac{d\sigma}{d\Omega} = \left(\frac{d\sigma}{d\Omega}\right)_{Mott}\left[\frac{G_E^2(Q^2) + G_M^2(Q^2)}{1+\tau} + 2\tau G_M^2(Q^2)\left(\tan\frac{\Theta}{2}\right)^2\right] \qquad (1.1)$$

where $\left(\frac{d\sigma}{d\Omega}\right)_{Mott}$ is the Mott differential cross section (which describes the elastic electron scattering taking the electron spin into account), $Q^2 = -q^2$ is the 4-momentum transfer $q^2 = (E/c)^2 - p^2$, $G_E(Q^2)$ is the electric, $G_M(Q^2)$ is the magnetic form factor and $\tau = \frac{Q^2}{4M^2c^2}$.

The non relativistic interpretation of the form factor $G_E(Q^2)$ is the fourier transformation of the spatial distribution of charge and $G_M(Q^2)$ for magnetic moment. These form factors are determined in the following way: First the elastic scattering cross section for a fixed q^2 as a function of the scattering angle is measured. This is repeated for different values of q^2. The resulting data is analyzed in terms of the Rosenbluth formula yielding $G_E(Q^2)$ and $G_M(Q^2)$. The q^2 dependence of the measured form factors then leads to the spatial distribution of charge and magnetic moment.

For elastic scattering q^2 is negative involving only 3-momentum transfer, no energy transfer. This region is called the space-like region. For annihilation processes (like $e^+e^- \rightarrow \pi^+\pi^-$) q^2 is positive involving only energy transfer, no 3-momentum transfer. This region is called the time-like region. The corresponding Feynman graphs can be found in fig. 1.1.

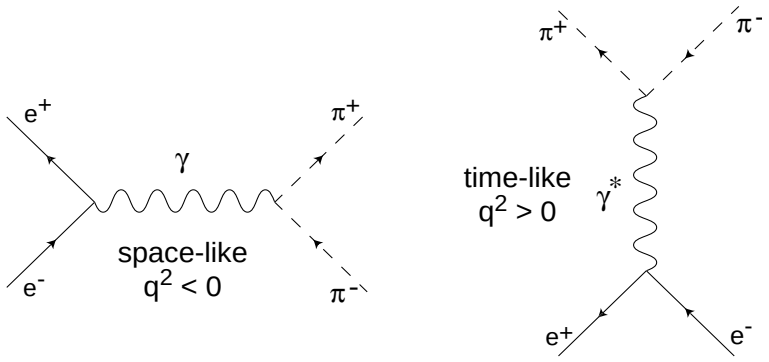

Fig. 1.1: *Feynman graphs for the space-like pion scattering (only 3-momentum transfer) and the time-like electron positron annihilation (only energy transfer).*

With scattering and annihilation processes it is possible to scan the electromagnetic form factor for the whole physical accessible region of the 4-momentum transfer q^2. For annihilation processes, the region $0 \leq q^2 < (2m_{particle})^2$ is not accessible, as the energy transfer is not enough to generate the 2 particles in the outgoing channel. This region of q^2 values is called the unphysical region.

1.2 Vector Meson Dominance Model

The measurement of the total cross section of the e^+e^--annihilation to $\pi^+\pi^-$ [Bar85] reveals a remarkable structure, which is shown in fig. 1.2.

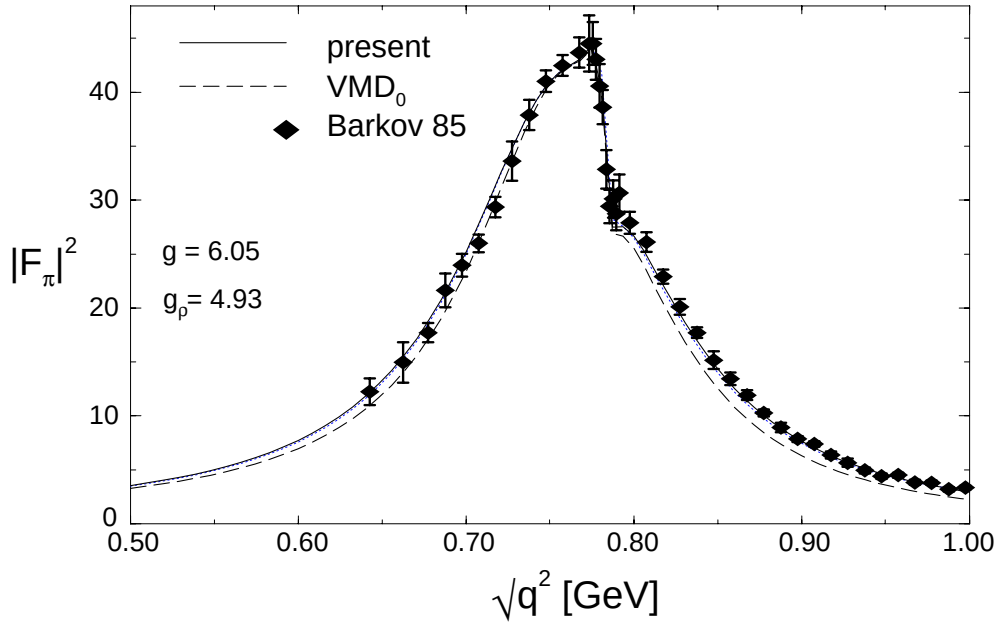

Fig. 1.2: *Pion form factor of the e^+e^--annihilation to $\pi^+\pi^-$ in the time-like region. The peak at the ρ and ω vector meson masses can be explained by the **V**ector **M**eson **D**ominance Model (VMD). A comparison of the data to calculations which include ρ/ω mixing is shown [Kli96].*

The peak and the sudden fall off in form factor squared appears exactly in the mass region of the light vector mesons ρ and ω. Some important properties of the light vector mesons in vacuum are shown in table 1.1. [PDG00]

Vector Meson	Mass [MeV/c²]	Width [MeV/c²]	Life Time [fm/c]	Main decay	Branching ratio to e^+e^-
ρ	769	150	1.3	ππ (100%)	$4.5\cdot10^{-5}$
ω	783	8.4	23	$\pi^+\pi^-\pi^0$ (89%)	$7.1\cdot10^{-5}$
ϕ	1019	4,5	44	K^+K^- (49%)	$2.9\cdot10^{-4}$

Table 1.1: Properties of the light vector mesons in vacuum.

This peak can be explained in the **V**ector **M**eson **D**ominance Model (VMD) [Sak69][Fey72]. In this model the coupling of hadrons to virtual photons is determined by intermediate vector mesons.

Since the quantum numbers of the vector mesons and the virtual photon are the same ($J^p = 1^-$), the off shell photon can convert to a vector meson. The decrease at the ω mass

can be explained as an interference between the ρ and ω meson and is called the ρ/ω mixing. The Feynman graphs in fig. 1.3 show the conversion of the photon to vector mesons.

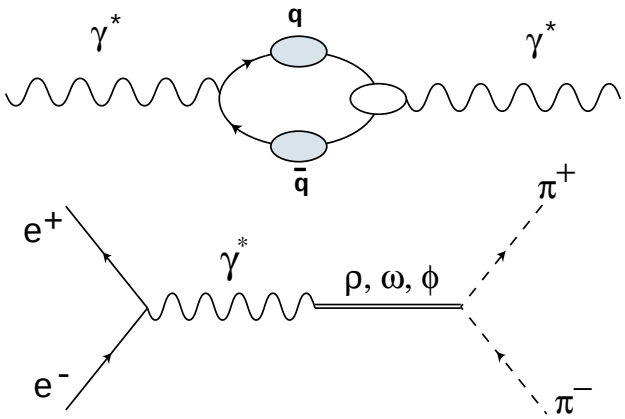

Fig. 1.3: *The upper Feynman graph shows the conversion of the virtual photon to a vector meson. The virtual photon couples to the charge of the quark-antiquark pair and can convert to a vector meson, since the photon and the vector meson have the same quantum numbers. The lower Feynman graph shows the annihilation of e^+e^- and the strong decay of the vector meson to pions. This process is described by the Vector Meson Dominance Model (VDM).*

As explained earlier these annihilation processes are in the time-like region, therefore the form factor measurement always include an experimentally inaccessible region in q^2.

In fig. 1.4 the qualitative dependence of the form factor of the e^+e^- annihilation process is shown.

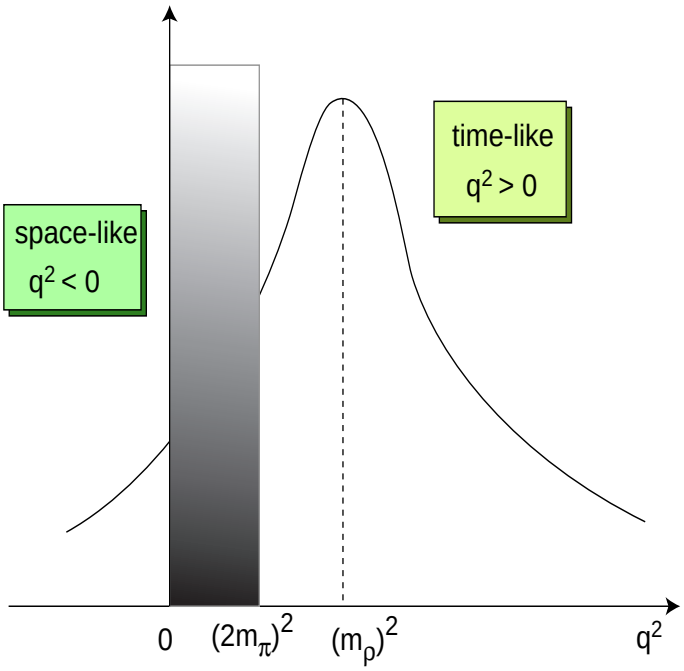

Fig. 1.4: *Dependence of the pion form factor on the 4-momentum transfer. The region from 0 up to 4 times the pion mass squared in the time-like region is experimentally not accessible. [Lan85]*

1.2.1 Transition Form Factors

Neutral pseudoscalar mesons (π^0, η) can not decay directly into e^+e^-, due to C-parity conservation. They can decay in conversion processes like the Dalitz decay $A \rightarrow B\gamma^* \rightarrow B + e^+e^-$. These processes are described with transition form factors. With VMD calculations the transition form factor of the η decay can be described very well.

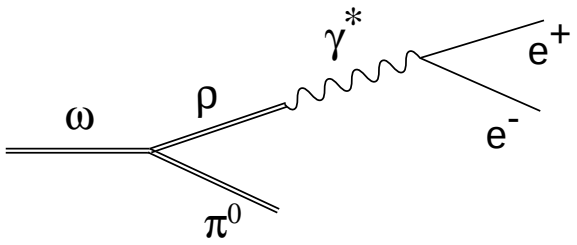

Fig. 1.5: *Feynman graph of the ω Dalitz decay described by the VMD.*

In contrast, for the ω meson the transition form factor data differ significantly from the VDM calculations. (the corresponding Feynman graph is shown in fig. 1.5). The data available [Dzh81][Dru93] for this reaction and various calculations (Vector Meson Dominance and variations of it) [Kli96] are shown in fig. 1.6.

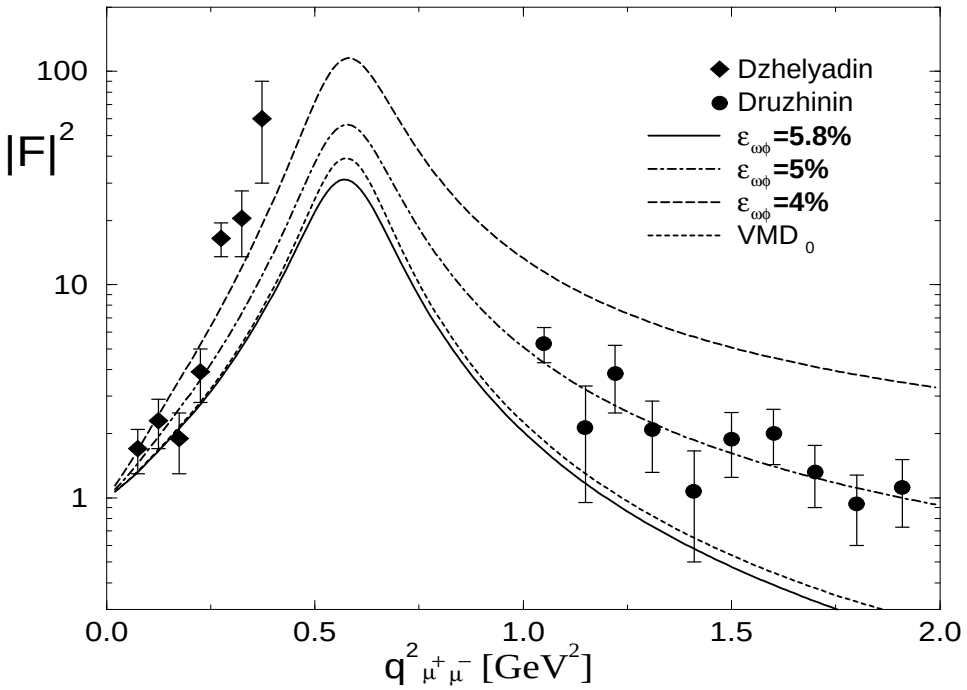

Fig. 1.6: *Time-like transition form factor $|F|^2$ obtained from measurements of the Dalitz decay $\omega \rightarrow \pi^0\mu^+\mu^-$ (diamonds) and annihilation $e^+e^- \rightarrow \pi^0\omega$ (filled circles) as a function of the invariant mass squared of the lepton pair. The data is from [Dzh81] and [Dru93]. VMD calculations are shown as lines [Kli96]. The standard VMD calculation and ωφ mixing calculations are shown ($\varepsilon_{\omega\phi}$ is a parameter which describes the strength of the ωφ mixing).*

Due to the small number of data points and their large error bars, it is not clear if the observed discrepancy is due to experimental problems or a result of a failure of the VMD model.

The detailed knowledge of these form factors is not only important for understanding the fundamental structure of the hadrons, it has also an important implication in interpreting the dilepton spectra from heavy ion collision experiments, for example the CERES data [Dre97] (details in chapter 1.4 on page 23).

Another point of interest are the time-like form factors of baryons. For example, neutron form factors in the time-like region have only been investigated by the FENICE experiment [Ant98]. They were measured through the annihilation experiment $e^+e^- \to n\bar{n}$. The experimental result is shown in fig. 1.7.

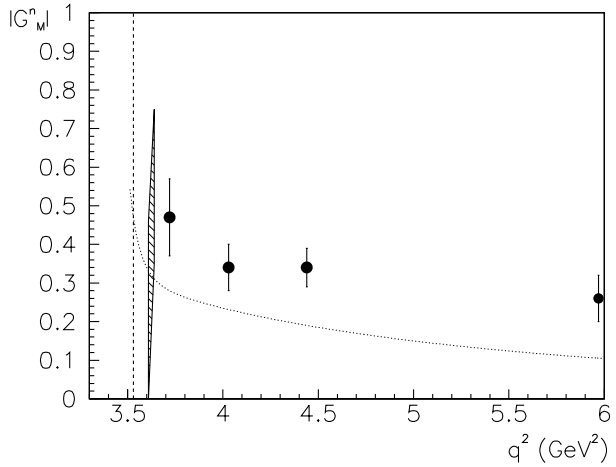

Fig. 1.7: *The time-like magnetic form factor of the neutron in dependence of q^2. The threshold for this reaction is drawn as a vertical line. The dotted line is a parametrization of the proton form factor [Ant98].*

The measured form factors are based on 74 events and have therefore very large uncertainties. The dotted line is a parametrization of the proton form factor. This leads to an ratio of $\left|G_M^n\right| / \left|G_M^p\right| > 1$. But from QCD calculations [Hye93] this ratio is expected to be smaller than 1. The origin of this discrepancy is unknown.

QCD calculations predict [Lep79] that for large momentum transfer q^2 $\left|G_M\right|$ should be proportional to the square of the running coupling constant of the strong interaction $\alpha_s(q^2)$. As a consequence time-like form factors at high q^2 are expected to approach space-like form-factors.

A collection of measurements of the proton time-like form factor at large momentum transfers are shown in fig. 1.8 [Cal01].

The measured magnetic form factors in the time-like region are twice as large as the corresponding ones in the space-like region. This discrepancy to QCD predictions has to be confirmed and understood.

Additional experimental information about time-like form factors of hadrons can be obtained by Dalitz decays of baryon resonances, i.e. $\Delta^+ \to pe^+e^-$.

Nearly no data exists to test models of the processes shown in the Feynman diagram in fig. 1.9. For the realization of such measurements one needs a pion beam, which the SIS at GSI is able to deliver since 1998.

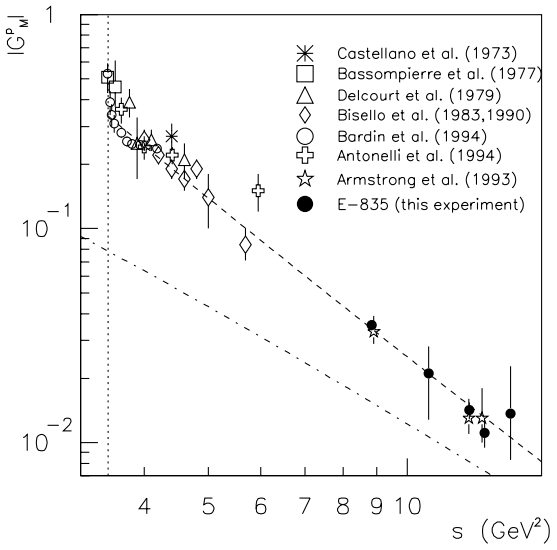

Fig. 1.8: *The proton magnetic form factor in dependence of q^2. The dashed curve shows a fit to the measured data in the time-like region. The dot-dashed curve is the magnetic form factor in the space-like region [Cal01].*

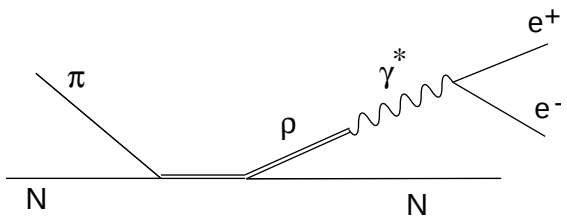

Fig. 1.9: *Feynman graph of an inelastic pion-nucleon process. The time-like form factor of baryons can be measured with such reactions and compared with model predictions.*

1.3 Medium Modifications of Hadrons

1.3.1 Chiral Symmetry

Symmetries always imply conservation laws, for example invariance of the Lagrangian under translations in space and time results in momentum and energy conservation. The QCD Lagrangian for massless quarks shows a symmetry under a vector and axial transformation. This symmetry is called *Chiral Symmetry.* The symmetry of vector transformations leads to the conservation of the Isospin, which is well known for hadrons [Koc95]. For the axial transformation the symmetry implies the same mass for the chiral partners, e.g. ρ and a_1. This is obviously not the case (m_ρ = 770 MeV/c^2 and m_{a_1} = 1260 MeV/c^2).

This large discrepancy can not be explained by the *explicit* symmetry breaking of the Lagrangian due to the finite current quark masses. As the masses of the light quarks are about 5 - 10 MeV/c^2 and the relevant energy scales of QCD of about 200 MeV is much larger, one can speak of an approximate symmetry.

The solution to this is that the vector-axial symmetry is *spontaneously* broken, which means that the symmetry of the Lagrangian is not realized in the ground state. This can be illustrated in a mechanical analog shown in fig. 1.10 [Koc95].

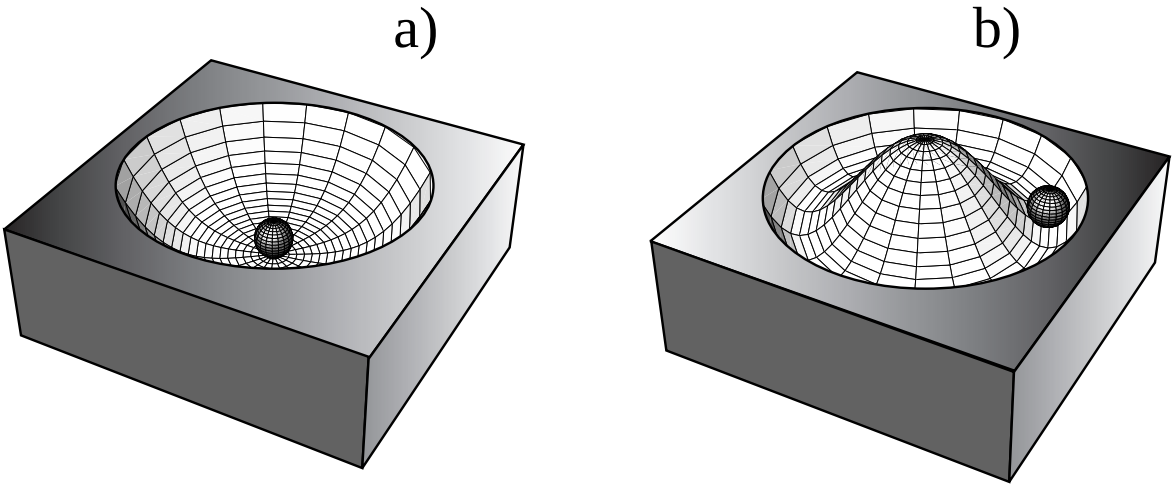

Fig. 1.10: *Classical mechanics potential model illustrating chiral symmetry breaking. The potential in a) is symmetric. In b) the potential is still symmetric, but the symmetry of the ground state is spontaneously broken as the ball rolls to a certain point in the potential and selects a direction, which breaks the symmetry. However, a rotation (moving the ball in the valley) does not cost energy [Koc95].*

The implications of this symmetry breaking are a massless Goldstone boson π and a massive σ. The π is obviously not massless, however its mass is much smaller compared to all other hadrons. In the classical mechanics analogy, the π corresponds to a mode where the ball moves in the valley and the σ corresponds to radial motion. The mass difference of the chiral partners ρ and a_1 is also explained with this model.

The non zero mass of the π is caused by the *explicit* Chiral Symmetry breaking which corresponds in the classical mechanics analogy to a tilt of the potential. Here, the rotational mode will cost energy for the π. The explicit symmetry breaking is a consequence of the small but finite current quark masses.

The spontaneous symmetry breaking is related to a non vanishing scalar quark condensate $\langle q\bar{q}\rangle \cong -(225\ \mathrm{MeV})^3 \cong -1.5\mathrm{fm}^{-3}$ [Tho01].

One expects that at high temperatures and/or densities the finite expectation value of the scalar quark-condensate is vanishing and that, as a consequence chiral symmetry will be restored. In this phase, the chiral partners σ/π and ρ/a_1 would be degenerate and the π would become massive.

One expects on basis of lattice QCD calculations (with extrapolations to finite baryon chemical potential) at very high temperatures and/or densities a phase transition from the hadronic phase to the *Quark Gluon Plasma*, where quarks and gluons are *deconfined*. This transition is shown in fig. 1.11 [BMu98].

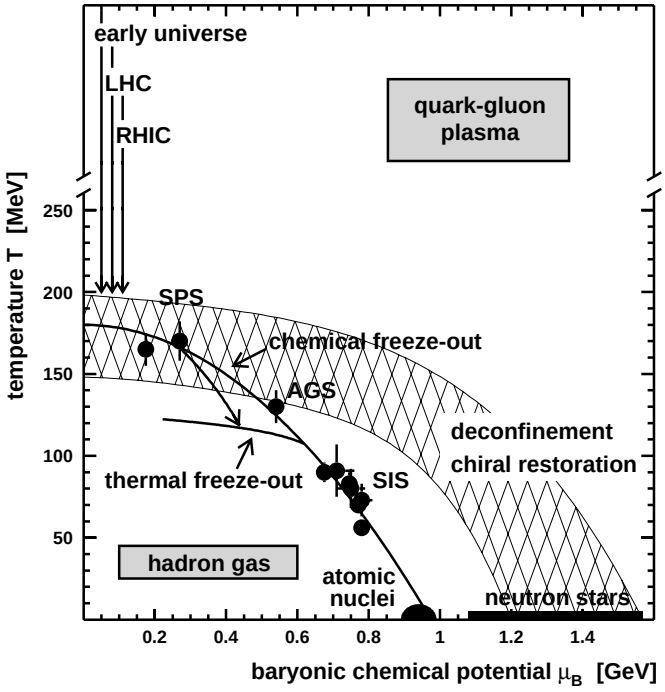

Fig. 1.11: *QCD phase diagram in the baryon chemical potential and temperature plane [BMu98]. The dots correspond to regimes accessible by the accelerators SIS (GSI Darmstadt), AGS (BNL) and SPS (CERN).*

When the quarks deconfine, the quark-condensate decreases at the same time.

Effects from the partial restoration of symmetry should be already visible at temperatures / densities well below the phase transition. At finite temperatures it follows directly from chiral symmetry that the chiral condensate scales as [Koc95]

$$\langle q\bar{q}\rangle_T \;=\; \langle q\bar{q}\rangle_0 \left(1 - \frac{T^2}{8f_\pi^2}\right), \tag{1.2}$$

where f_π is the pion decay constant (f_π = 93 MeV).

In contrast, at finite density one expects a linear scaling with the density as

$$\langle q\bar{q}\rangle_\rho = \langle q\bar{q}\rangle_0 \left(1 - 0.35\frac{\rho}{\rho_0}\right). \tag{1.3}$$

This amounts to a change of 35 % at normal nuclear matter density. This formula is only valid for small ρ.

Brown and Rho [Bro91] suggested that the masses of hadrons can directly be linked to the chiral condensate. This implies that at finite densities a reduction of the hadron masses is expected. For example, within this model the ρ-meson mass is supposed to drop by about 15 - 20 %.

Calculations on basis of the Nambu-Jona/Lasinio [Kli90] model describe the dependency of the expectation value of the quark condensate from temperature and nuclear density. This is shown in fig. 1.12.

Also indicated are the regions in temperature and density which are accessible by accelerators. SIS at GSI and SPS at CERN are marked.

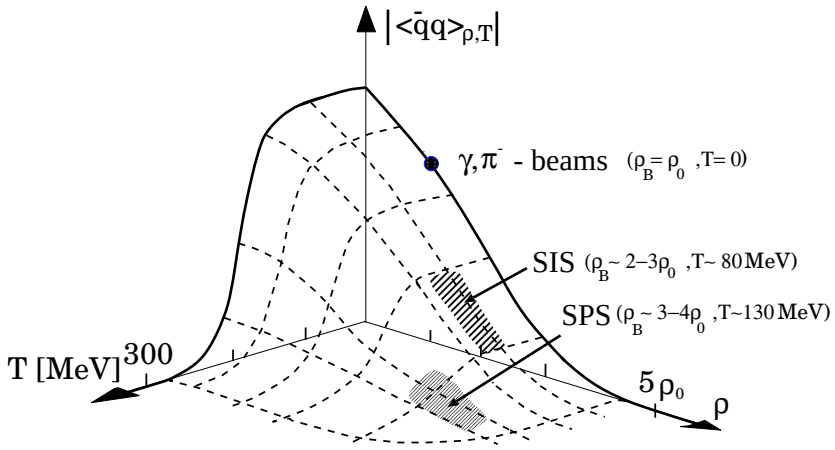

Fig. 1.12: *Effects of the temperature and density on the quark condensate. At high temperatures and densities the chiral symmetry is restored. [Kli90]*

The effect of chiral symmetry restoration and the decreasing expectation value of the quark condensate on the masses of vector mesons is described by many models, where some of these are discussed in the following.

1.3.2 Mass Modifications of Vector Mesons

Vector mesons have a decay channel to dileptons. As these leptons do not strongly interact with the surrounding hadronic matter in, e.g., a heavy ion experiment, they are an ideal probe to measure the invariant mass of the decayed vector mesons in medium.

For this reason, vector mesons are of particular interest and will be discussed in the following.

A useful quantity for a discussion of the in-medium properties of any particle is its spectral function. It is defined as the imaginary part of the propagator and can be interpreted as the mass distribution of the particle.

The presence of nuclear matter breaks the Lorentz invariance, so the spectral function depends on the Energy ω and the three-momentum $\vec{q}$ of the meson.

$$A(\omega, \vec{q}) = \frac{1}{\pi} \frac{\mathrm{Im}\Sigma(\omega, \vec{q})}{(\omega^2 - \vec{q}^2 - m^2 + \mathrm{Re}\Sigma(\omega, \vec{q}))^2 + \mathrm{Im}\Sigma(\omega, \vec{q})^2}, \tag{1.4}$$

where Σ is the self energy.

In the case of vector mesons, one has to keep in mind that at finite 3-momentum transversely and longitudinally polarized mesons are modified differently from the surrounding nuclear medium, which leads to the existence of two independent spectral functions.

At sufficiently low nuclear densities the self energy Σ of the meson (Σ can be described as an effective potential that acts on the meson) can be expressed within the *low-density* approximation [Dov71].

$$\Sigma_{medium}(q) = \frac{1}{8m_N} \rho_N T_{vac} \tag{1.5}$$

where T_{vac} is the vacuum forward scattering amplitude.

Thus, in a first approximation, the medium properties are governed by the vacuum scattering amplitude. However, this quantity is not directly accessible from the experiment and one needs to set up a model for T_{vac}.

In the following it is reviewed how the forward scattering amplitude is modelled in various approaches and the differences in predictions to the in-medium mass modification of vector mesons these theories result in.

Klingl and Weise [Kli97] start with an effective chiral Lagrangian and take the hadronic two body processes of the nucleon, pion and vector meson into account to calculate T_{vac}. The result for the spectral functions of the ρ and ω meson is shown in fig. 1.13.

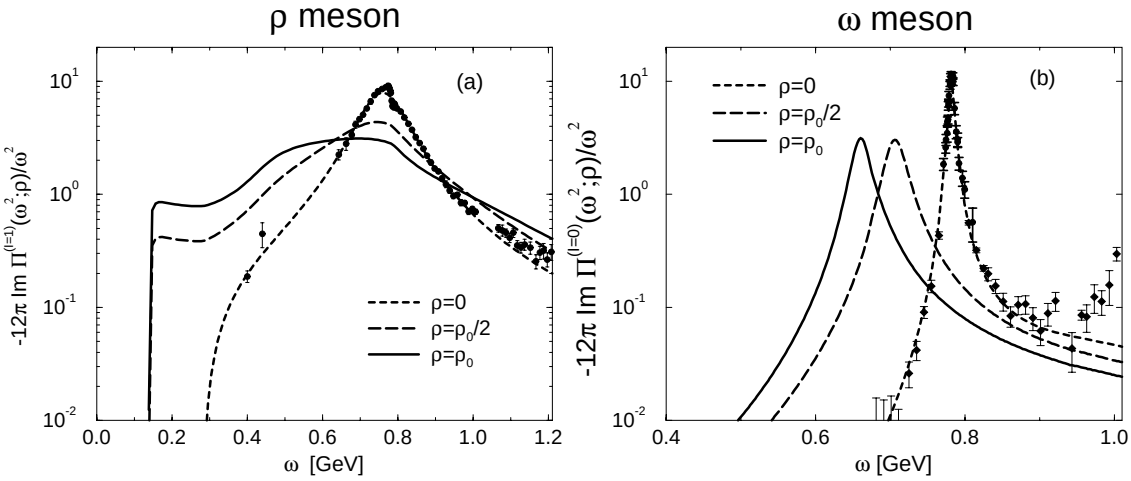

Fig. 1.13: *Spectral functions of the ρ and ω meson for various densities of nuclear matter. The ρ shows a broadening, whereas the ω shows a shift to smaller masses [Kli97].*

A shift of the ω meson mass to lower values is predicted, as well as a broadening of the spectral function.

Post et al. [Pos00] instead consider resonances (for example the $D_{13}(1520)$, which plays an important role in ρN scattering) in their model. This approach leads to the spectral functions for the ρ meson shown in fig. 1.14.

Here, in addition to the broadening, the ρ shows a second or even more peaks in the spectral functions. The ρ in medium modeled this way shows a much more complex behavior than seen in the result of Klingl et al.

Rapp et al. [Rap98] consider the reduction of the pion mass in medium. This leads to a larger phase space for the reactions and thus to a broadening of the ρ meson.

However, recent investigations indicate an increasing pion mass in hadronic matter of 167 ± 3.5 MeV/c^2 [Gil97][Fri98].

This very short review demonstrates that many different theories have been developed to describe in medium effects, while all of them result in an mass shift and in an change of decay width. These effects can be experimentally examined by heavy ion and hadron induced experiments.

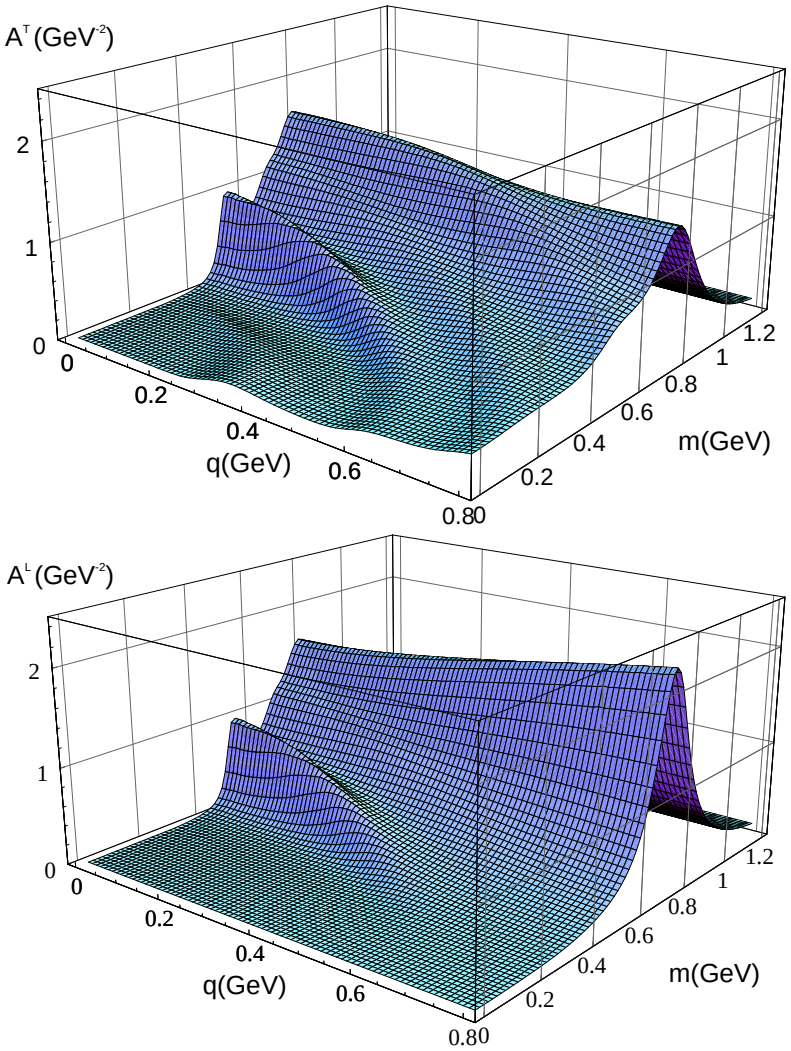

Fig. 1.14: *Spectral functions (transversal part in the upper part and the longitudinal part in the lower part) of the ρ meson in nuclear matter. The model includes resonant processes (like the $\Delta_{13}(1520)$ resonance) and the spectral function shows two peaks [Pos00].*

1.4 Experiments

As described in the previous chapter the electromagnetic decay of vector mesons give us the opportunity to probe the properties of these mesons in matter, as the leptons do not interact via the strong force.

Signals for the described in medium effects can therefore be examined by studying the decay of the ρ, ω and ϕ mesons in detail (an overview of the properties are shown in table 1.1 on page 12).

By reconstruction of the momentum of the electron/positron pair (or muon pair), the invariant mass of the vector meson at the instant of its decay can be calculated. A change of the properties of the vector meson is expected if it decays in the hadronic matter, which is definitely true for the ρ meson with a life time of 1.3 fm/c in vacuum.

Measuring the dilepton spectrum in a heavy ion experiment is challenging, since there are many other sources of leptons. Hence, one has to determine all contributions to the lepton cocktail.

Dielectron spectra have been measured by the CERES detector at CERN (SPS) (at high energies) and **D**i**L**epton **S**pectrometer (DLS) at BEVALAC [DLS95]. Additionally, dimuon spectra up to the J/Ψ region have been measured by the HELIOS-3 [Hel95] and the NA38/NA50 [Abr96] collaborations at CERN SPS.

The CERES data show an excess of dielectrons in the invariant mass region of 0.2 up to 1.5 GeV/c^2 by a factor of 3 to 5 as seen in fig. 1.15.

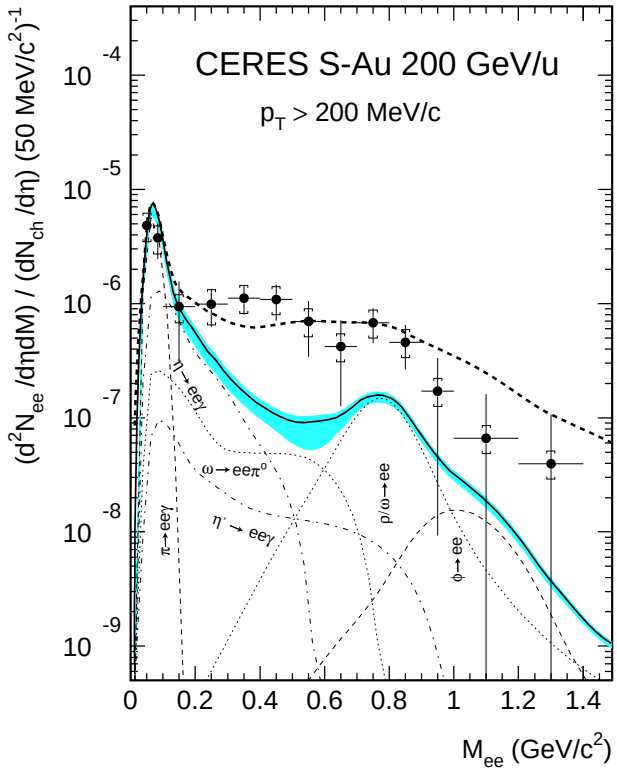

Fig. 1.15: *Dilepton spectrum measured by the CERES experiment at CERN-SPS for the reaction S+Au at 200 AGeV. The "cocktail" of known contributions expected from nucleon-nucleon collisions is shown. A significant excess of dileptons by a factor 3 to 5 is seen in the data, especially just below the region of the ρ and ω vector mesons [Dre97].*

The enhancement is found in the data in the region where the Dalitz ω decay has the largest contribution to the e^+e^--pairs.

As shown in fig. 1.6 on page 14 the relevant transition form factor of the ω has large uncertainties. There is an ongoing theoretical effort to explain this discrepancy of the

data to the known dilepton sources. In-medium effects have been successfully used to reproduce the data.

The only measurements of dilepton spectra at projectile energies of up to 2.1 AGeV have been done by the DLS spectrometer. The data [DLS95] and a simulation of the known contributing sources is shown in fig. 1.16 for Ca+Ca at 1 AGeV [Bra98].

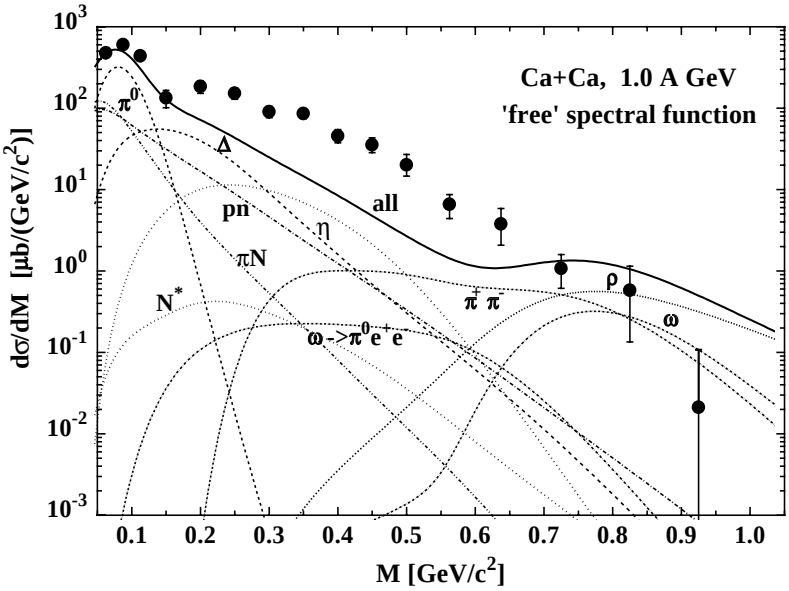

Fig. 1.16: *Dilepton spectrum of the reaction Ca+Ca at 1 AGeV with the DLS acceptance taken into account [DLS95]. Simulation for the different contributing sources done by [Bra98].*

The data show a significant excess of dileptons for invariant masses from 0.2 to 0.6 GeV/c^2 compared to the sum of the known contributions. This discrepancy is not consistently reproduced by theories.

An additional discrepancy arises from the fact that the η production rates measured by the DLS experiment are higher than the results of the TAPS [Hol97] experiment.

The DLS experiment has several deficiencies: The fixed two arm setup leads to a very limited geometrical acceptance and the mass resolution of only 12% is not sufficient to separate the signals from the ρ and ω mesons.

Recently, Ozawa et al. published [Oza01] that they observed medium modifications of vector mesons at normal nuclear matter density for p + A reactions at 12 GeV. The measured invariant mass spectrum of e^+e^- pairs is shown in fig. 1.17.

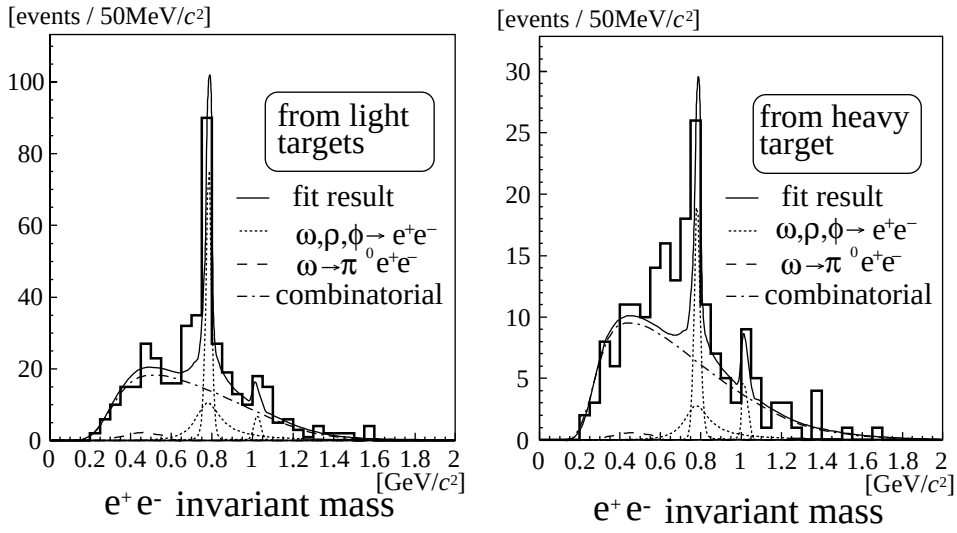

Fig. 1.17: *Invariant mass spectrum of the e^+e^--pair measured by the KEK-PS E325 experiment [Oza01]. The spectrum was taken or a carbon (left spectrum) and a copper target (right spectrum). The solid line indicate the results for the known hadronic sources with the combinatorial background. The dotted lined show contributions from the ρ, ω and ϕ decays.*

The significant enhancement below the ω peak for the copper target compared to the carbon target can be explained by in-medium modifications of the ρ and ω meson at normal nuclear matter density.

1.5 Dielectron Spectroscopy with HADES

The **H**igh **A**cceptance **DiE**lectron **S**pectrometer HADES [Had94] at GSI is a electron/positron spectrometer built by the european HADES collaboration, consisting of groups from 19 institutions in 9 countries (currently 120 members, for a full list refer to "HADES Collaboration" on page 99).

The physics program of HADES is the systematic study of e^+e^- pair production in hadron and heavy ion induced collisions. The energy regime available at the SIS (*Schwerionensynchrotron)* of 1-2 AGeV allows to access densities up to 3 times the nuclear density and temperatures of up to 80 MeV, which gives the possibility to investigate precursor effects of chiral symmetry restoration.

To quantitatively understand and interpret the measured electron/positron spectra it is planed to investigate elementary reactions (πp, pp), hadron induced nuclear reactions (pA, pA) and heavy ion collisions (AA).

Compared to DLS, HADES has a significantly improved mass resolution of about 1% as well as a 10 times larger geometric acceptance for e^+e^- pairs. These features provide the resolution and statistics to separate the ρ and ω peaks in the invariant mass spectrum.

In chapter 2 the subdetectors of the HADES spectrometer are discussed in detail. The small branching ratio of light vector mesons into electron/positrons demands a high event rate of the experiments to increase statistics. Therefore, the HADES detector requires a selective trigger system, to reduce the amount of data to be stored. This trigger system is presented in chapter 3, with the focus on the second level trigger, designed and built in Gießen.

The Matching Unit, which was designed and built in the framework of this thesis, is described in chapter 4. It allows to combine the electron signatures of the subdetectors to electron candidates, find electron/positron pairs and select the ones in an invariant mass regime to determine the second level trigger decision.

In chapter 5 the results obtained with the second level trigger during the last beam times are discussed.

Chapter 2

The Hades Detector System

In this chapter the HADES spectrometer (**H**igh **A**cceptance **D**i**E**lectron **S**pectrometer) is introduced. It is set up at the *Schwerionensynchrotron* (SIS) at the *Gesellschaft für Schwerionenforschung* (GSI). It is operational (data of all subdetectors has been taken) and in its final configuration (only additional extensions are planed for the future). The physics questions asked in the first chapter also indicate the requirements the detector has to fulfill.

2.1 Requirements

As described earlier (chapter 1) the HADES project has several objectives, including
a) to determine form factors of vector mesons (and baryons) in the time-like region
b) and to examine of hot and dense nuclear matter.

Therefore, one has to find the e^+e^--pairs from the decaying vector mesons which are produced by the heavy ion or pion induced reactions.

Due to the electromagnetic branching ratio in the order of 10^{-5}, the detector has to be very selective for dileptons and must be able to run with high event rates. For example, in a Au+Au-collision at 1 AGeV 10^{-6} dileptons from ρ-decays are produced per central collision. To acquire sufficient statistics for a high precision experiment (same reaction as above) the detector has to cope with a primary beam intensity of 10^8 particles/s and 10^6 collisions/s (1% interaction target).

Additionally, in each central collision the multiplicity reaches up to 200 charged hadrons. Therefore, the detector has to be very selective in identifying electrons and positrons (in the following “electrons and positrons” will be abbreviated with “electrons”) and discriminate against protons and pions.

Moreover, there are other sources of electron pairs from conversion of photons from π^0 decays as well as π^0 Dalitz decays. Independent of that there is an uncorrelated combinatorial background over the whole mass region.

The mass resolution is one of the most important issues of the HADES detector. To discriminate a narrow ω signal from the broad ρ, one has to assure a mass resolution of 1% in the region of interest (fig. 2.1).

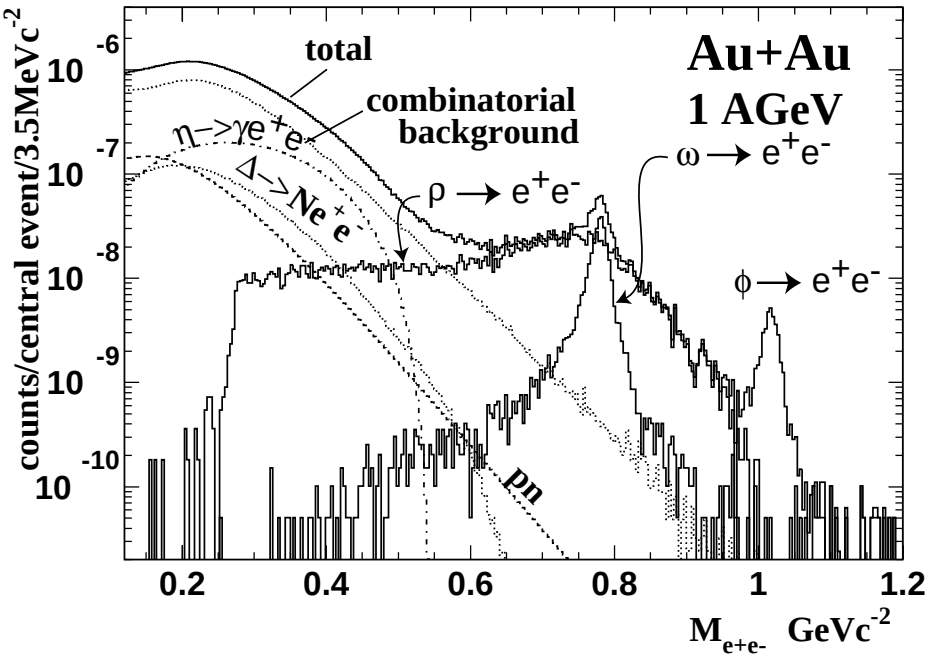

Fig. 2.1: *Simulated dilepton spectrum for the reaction Au+Au at 1 AGeV with the detector acceptance taken into account [Sch95]. The individual distributions are shown: The 1% mass resolution is enough so that one can easily distinguish between the ω and φ.*

This demands subdetectors of low as possible density to minimize multiple scattering and production of secondary particles and requires high resolution in track reconstruction.

The HADES detector is designed to acquire high statistics for the very rare electromagnetic decays of light vector mesons, thus a high geometrical acceptance is needed. Furthermore, the high acceptance will minimize the introduction of systematic errors for acceptance corrections. HADES has therefore the full azimuthal acceptance (except the mounting structures) and in polar angles from 18° to 85°. This implies that 45% of the solid angle and about 45% - 50% of all decays in dileptons will be in this region. The momenta of these electrons will be in the range of 0.1 - 2 GeV/c.

In fig. 2.1 [Sch95] one can see a simulated dilepton spectrum for the HADES detector (Au+Au at 1 AGeV) with the acceptance taken into account. The mass resolution is good enough to discriminate between the signals of the ρ and the ω.

2.2 The HADES Spectrometer at a Glance

Taking all these requirements into account, the following detector system has been built (fig. 2.2 on page 30) [Had94] [Sal95] [Gar98A].

The central part is a superconducting toroid consisting of 6 coils. This six-fold geometry is also found in all other detectors. The magnet produces a toroidal magnetic field of 0.26 to 0.9 T (at 3525 A). At 0.5 T this magnetic field results to a transversal momentum kick $\Delta p_t / p$ of about 15% for leptons originating from ω decays.

The toroidal magnet together with the two modules (6 planes each) of mini drift chambers (MDC) in front and two planes of MDC behind the magnet build a magnetic spectrometer for measuring momenta of charged particles.

The following three subdetectors are the electron identifying detectors.

In front of the magnet a RICH detector can be found. From the point of view of electron identification this detector is the most essential, because it is hadron blind. For the second level trigger this detector delivers the most important information for the data reduction, because it produces a clean signal for electrons.

Behind the magnet at large polar angles (45° - 85°) there is a Time of Flight (TOF) wall, where a selection on the time of flight of the particle is used to suppress hadrons. For small polar angles (18° - 45°) a Shower detector finds electromagnetic showers of electrons, which also suppresses hadrons.

2.3 The Subdetectors

2.3.1 The Ring Imaging Cherenkov Detector

For each central collision 200 charged particles are produced, thus one needs a very effective identification of electrons.

The momenta of all particles produced in heavy ion collisions at SIS energies (1 - 2 AGeV) are in the region of 0-2.5 GeV/c. Therefore, the velocity (γ) of electrons and positrons (m_0 = 511 keV/c^2) is much higher than those of hadrons (m_0 > 140 MeV/c^2). Hence, a Cherenkov detector is applicable.

Whenever a particle in a medium has a velocity *v*, which is higher than the phase velocity of light c_n in medium with the index of refraction *n*, the particle emits light under a fixed angle Θ_c to its trajectory [Cher37].

$$v > c_n = \frac{c}{n} \tag{2.1}$$

This means that emission of Cherenkov radiation starts with a threshold velocity of $\beta > 1/n$, where $\beta = \frac{v}{c}$.

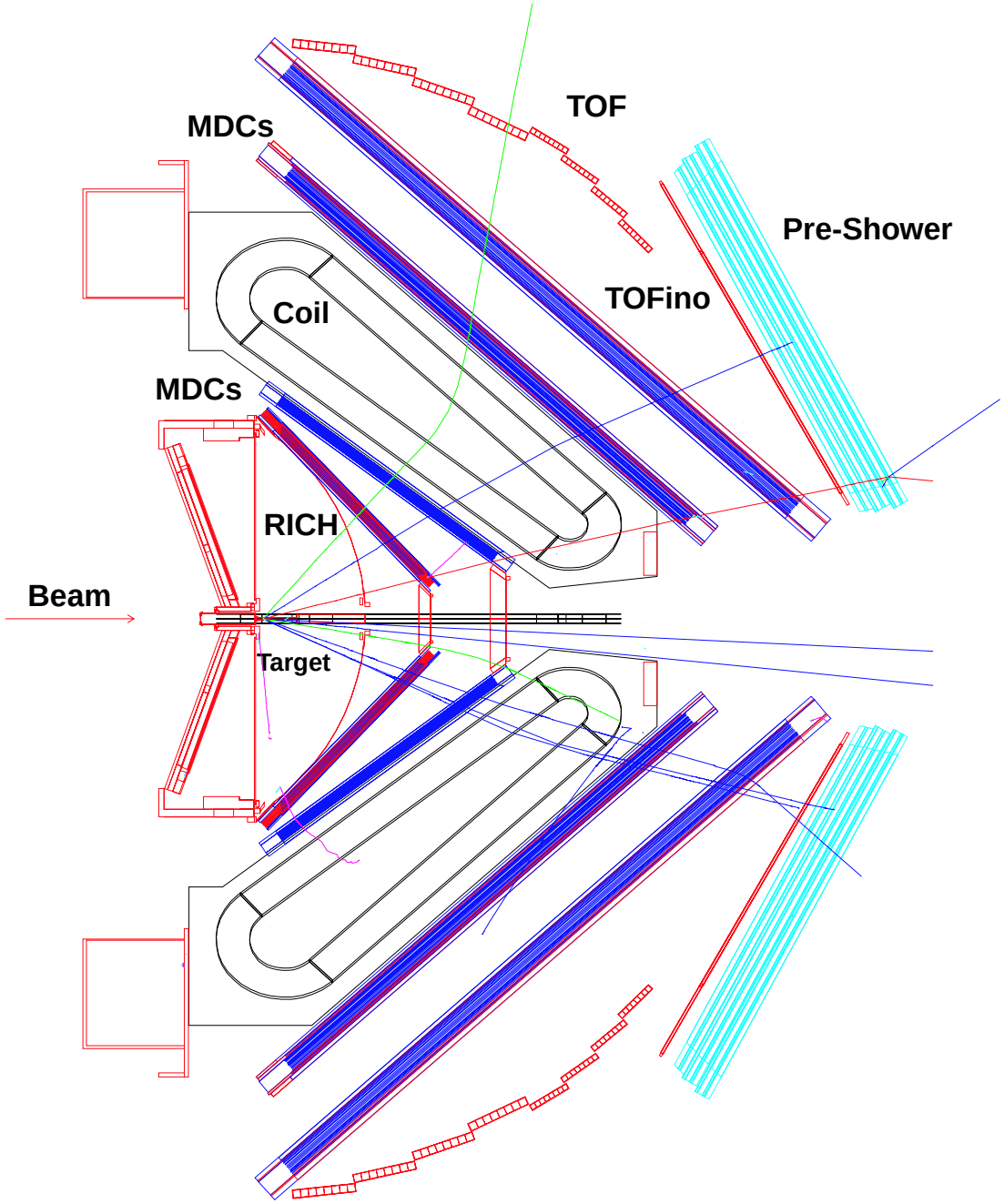

Fig. 2.2: *A Cross-section of the HADES detector. From the six segments two are shown. A particle crosses the detector. From the target through the RICH, two planes of MDC modules, the toroidal magnet, again 2 planes of MDC, the TOF wall and for small polar angles the shower detector. The particle tracks are shown from a simulation of C+C at 1.5 AGeV [HaC01].*

The half-angle of the cone of the emitted light is

$$\Theta_c = \operatorname{acos}\frac{1}{n\beta} \approx \sqrt{2\left(1-\frac{1}{n\beta}\right)} \text{ for small } \Theta_c. \tag{2.2}$$

With the selection of the appropriate dielectric as the radiator medium (selecting the index of refraction) one can determine the threshold for Cherenkov light to

$$\gamma_{thr} = \frac{E}{m} = \frac{1}{\sqrt{1-\beta^2}} = \frac{1}{\sqrt{1-\frac{1}{n^2}}}. \tag{2.3}$$

The most simple way to discriminate particles with the Cherenkov effect is to use this threshold velocity. The radiator medium is chosen such that in the interesting momentum region one particle is above and one below the Cherenkov threshold.

Differential Cherenkov detectors use photon detectors at a fixed angle and are able to measure directly the velocity of the particle, but with the disadvantage of the very small velocity window they can cover.

One step further is the usage of the complete angular information of the emitted light. These detectors are called **R**ing **I**maging **Ch**erenkov (RICH) detectors [Yps94][Seg94]. The idea of these detectors is that one uses a two dimensional photon detector (for example drift chambers or multi wire chambers) and is able to detect several rings, even with different diameters, at the same time. This diameter is then a method to discriminate between particles due to their different γ factor (particle ID). Furthermore, with the position of the detected rings one can reconstruct the emission angle of the particle.

A cross section of the HADES RICH is shown in fig. 2.3.

Charged particles produced in the target will enter the gas radiator and emit Cherenkov light in a cone, if their $\gamma > \gamma_{thr}$. This light is then reflected at the spherical mirror and travels through a CaF_2 window, which separates the radiator gas from the detector gas. CaF_2 crystals were chosen, because of their high transmittance of UV light. Then the light hits the photon detector and is imaged as rings due to the imaging properties of the mirror.

The diameter of the CaF_2 window is 1.45 m and the radius of the spherical mirror is 0.87 m.

The HADES RICH is designed to be “hadron-blind”, that means the radiator must have a very high γ_{thr}. The radiator gas is C_4F_{10} (n = 1.0015, radiation length X_0 = 34.52 g/cm^2, this gives a radiation length of about 3200 cm for the HADES gas radiator). The gas has a γ_{thr} = 18 and a very high transmission in the UV region. Therefore, only electrons and positrons emit Cherenkov light. Above p > 100 MeV/c the asymptotic angle of emittance is Θ_c = 3.18°, this results in rings of constant diameter of about 5 cm on the photon detector. From the point of view of the second level trigger it is faster and easier to recognize rings with fixed radius.

The photon detector is a multi-wire proportional chamber (MWPC) with a segmented CsI photocathode. The electrons which are emitted by the photocathode due to the Cherenkov photons are amplified by a factor of 10^5 by the MWPC. These electrons will again induce electric charge on the photocathode, which is then measured. The cathode consists of 4712 pads per sector with a constant width of 6.6 mm and a height

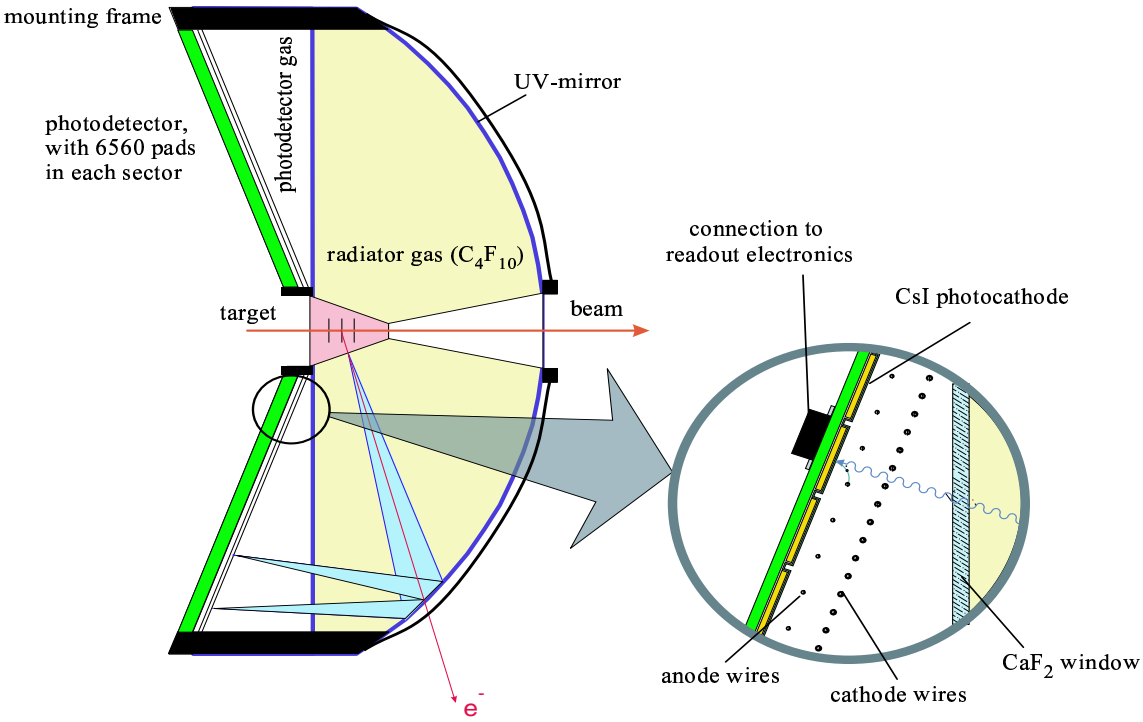

Fig. 2.3: *Cross-section of the HADES RICH. The cones show the Cherenkov light emitted in the gas radiator, reflected by the mirror and detected on the photon detector as rings. The two gas volumes are divided by a segmented CaF_2 window [Böh99].*

of 4.5 - 7.0 mm, which varies to compensate the deformation of Cherenkov rings for larger polar angles caused by distortions due to the spherical mirror.

2.3.2 Mini Drift Chambers

The mini drift chambers (MDC) are mounted in front and behind the magnet. They are used for very precise tracking and determination of momenta of the electrons. There are two modules of MDC in front and two modules behind the magnet, where each plane has 6 planes (6 fold symmetry of the detector).

The modules consist of 6 planes of drift-cells [Gar98]. One cell is built out of 2 layers of foil, which are cathodes, two field wires with one sense wire (anode) in between. To assure multi-hit capability even with about 25 charged particles per segment and a very high event rate, the drift cells have to be very small. The size of the drift cells varies from 5 mm x 5 mm up to 10 mm - 14 mm, thus the name “mini” drift chamber. This increase in size of the drift cells is due to the fact, that the outer drift chambers are much bigger and to achieve the same granularity in all modules, the outer ones do not need the fine grid of the inner modules. This size of the cells results in a drift time smaller than 1 µs.

The dead time is smaller than 10 μs, which allows operation at the required high rates. These drift cells are then stacked, but rotated by 0, ±20, ±40 (see fig. 2.4).

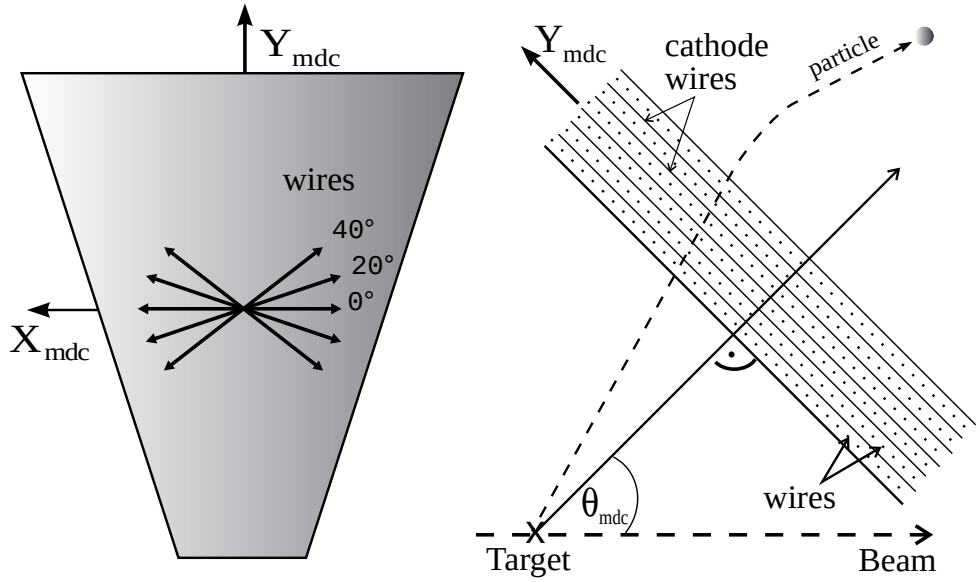

Fig. 2.4: *Schematic drawing of the HADES MDC. The 6 layers of sense wires are oriented as shown on the left side. On the right side the orientation of the MDC in the detector and a trajectory of a particle is shown.*

The signals of the total of 26828 sense wires are then fed into ASICs (Application Specific Integrated Circuit), which were especially developed for HADES, where the drift times are digitized and zero suppressed.

The spatial resolution for the drift chambers is 35-50 μm in polar directions and 85-125 μm in azimuthal direction, which is enough to reach the required momentum resolution of 1%.

2.3.3 The Shower Detector

Charged particles (other than electrons) with momenta from 10 MeV/c^2 up to GeV/c^2 lose energy in matter primarily by ionization. The mean rate of energy loss is given by the Bethe-Bloch equation [Bet30]

$$-\frac{dE}{dx} = Kz^2\frac{Z}{A}\frac{1}{\beta^2}\left[\frac{1}{2}\ln\frac{2m_e c^2\beta^2\gamma^2 T_{max}}{I^2} - \beta^2 - \frac{\delta}{2}\right] \qquad (2.4)$$

where K/A is 0.307 MeVg^{-1}cm^2 for A = 1 g/mol, A is the atomic mass of medium, Z is the atomic number of medium, ze is the charge of the incident particle, $\beta = v/c$, I is the mean excitation energy, δ is a density effect correction to ionization energy loss and T_{max} is the maximal kinetic energy. This formula is not correct for electrons because of spin, kinematics and identity of the incident electron with the electrons

which it ionizes [ICR84]. But nevertheless, for low energy electrons dE/dx for ionization depend logarithmically on the energy of the particle.

For high energy electrons and positrons the predominant energy loss in matter is due to bremsstrahlung, because dE/dx for bremsstrahlung rises nearly linearly with the energy of the particle. This effect dominates for electrons above a few tens of MeV and is negligible for heavier particles like protons and pions.

When a high-energy electron travels through matter, it initiates an electromagnetic cascade (shower) as the bremsstrahlung photons produce e^+e^--pairs (pair production) with lower energy.

This is exactly the effect which the HADES shower detector uses to discriminate between electrons and hadrons: electrons will produce an electromagnetic shower, whereas pions and protons will not.

The shower detector for HADES [Bal98] is used for small polar angles (18°-45°) (dimensions of one module (sector) are 1.5 m x 1.3 m). Each segment consists of three multi-wire chambers. In between the planes there is a lead converter with a thickness of about 1 cm (two times the radiation length) as seen in fig. 2.5.

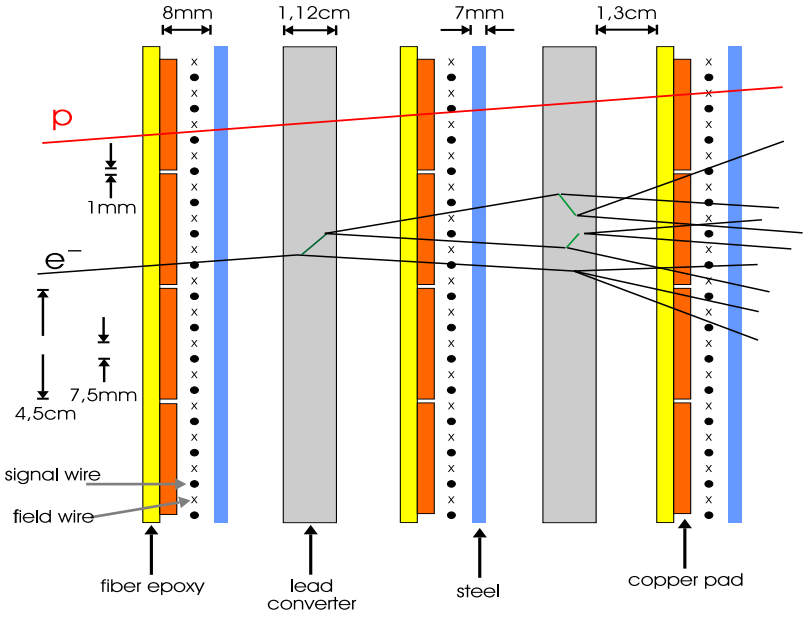

Fig. 2.5: *A cross section of the shower detector. There are three MWDC, which are separated by lead converters. Shown is a electron, which produces an electromagnetic shower as well as an proton which does not.*

Each MWC consists of a layer of field and sense wires in a distance of 7.5 mm to each other and two cathode planes, where one is segmented. The segmented plane is divided into 942 pads and provide the position information. There are 32 pads in the polar direction and in the azimuthal direction the number varies from 32 (at large polar angles) down to 20 pads (at small polar angles).

A charged particle traveling through a gas produces electron-ion pairs along its path (primary ionization). These are separated by the electric field and the electrons are col-

lected by a thin anode wire. The increasing field strength (1/*r*) accelerates the electrons enough to allow for secondary ionization and this leads to an avalanche effect. This produces a signal which is proportional to the primary ionization (proportional region).

Quenching gases (organic molecules with low transparency for light) are added, because they absorb most of the photons which are produced during the avalanche development, and thus keeping the avalanche region localized.

The MWC are operated in the self quenching streamer mode (SQS mode) [Ale80] [Ata82]. In this mode the produced electric charge is nearly independent of the primary ionization. That means that the total signal sensed at a pad is proportional to the number of charged particles which passed the MWC.

Therefore, an electromagnetic shower from an electron traversing the lead converters will be detected as an increase in the detected charge from one layer of MWC to the other. Protons and pions can change their primary ionization from one layer to the next (see Bethe-Bloch), but as the detector runs in the SQS mode, this will not be seen as an increase of charge in the signal.

Multiple scattering leads to a lateral distribution which is described by the Moliére radius R_m, given by [Nel66] [Bat70]

$$R_m = X_0 \frac{E_s}{E_c} \tag{2.5}$$

where E_c is the critical energy (the energy at which the ionization loss per radiation length is equal to the electron energy) and $E_s \approx 21\text{MeV}$.

For the shower detector this means the charge integral over a 3 x 3 pad region must be taken in order to determine the number of particles belonging to one single electromagnetic shower traversed through the chamber.

2.3.4 Time of Flight Wall

The TOF detector is used for particle identification (angles > 45°) as well as the first level triggering, which is based on the multiplicity trigger of charged particles.

It consists of 1056 plastic scintillators which are oriented perpendicular to the beam axis (see fig. 2.6).

Charged particles traversing these scintillators produce light (blue to green) [Bir64], which is detected by photomultiplier tubes on each end of the scintillator. These signals are then discriminated by a CFD (Constant Fraction Discriminator, it produces a signal at a time which is in a certain region independent of the signal height) for the time to digital converters (TDC). The signal heights are also converted by analog to digital converters (ADC)[Bas98]. With this data and the start signal (the time when the beam particle hits the target) the time of flight and the hit position can be determined.

The discrimination between electrons and pions/protons is done by the difference of their velocity ($v_e \cong c$) and thus their time of flight until they reach the detector. With the time resolution of 150 ps it is possible to identify electrons with a fake rate of n_{fake} = 1-2 for each sector in the polar region > 45°. For smaller angles the hadrons have higher velocities and therefore the probability to misidentify a hadron as an electron rises sharply.

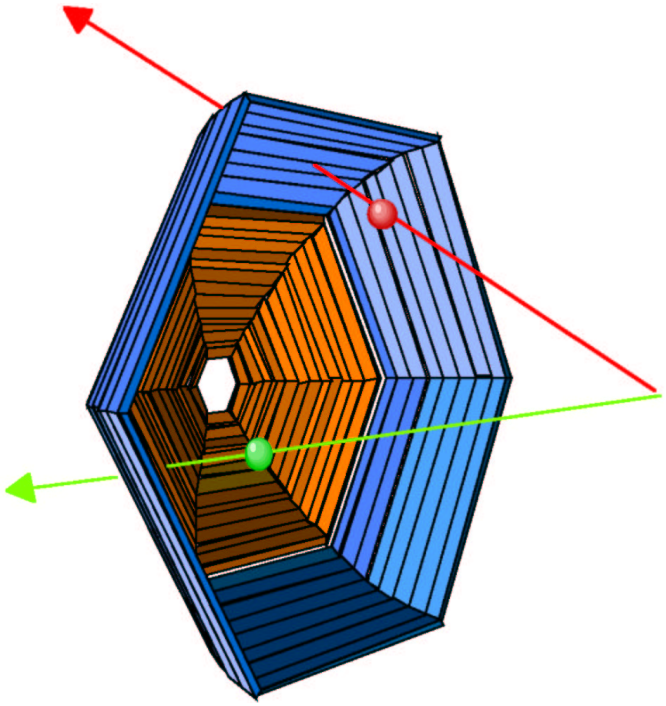

Fig. 2.6: *Schematic view of the TOF wall.*

The inner TOF (18°<θ<45°) is not yet constructed. It is substituted by the so called "Tofino" detector, which consists of 4 scintillator plates per segment, which are read out by one photomultiplier tube each. The disadvantage of this low granularity solution is, that the particle identification only works for experiments with light nuclei (e.g. C+C). With heavy systems (e.g. Au+Au) the multiplicity will lead to multiple hits.

2.3.5 Start Detector

The HADES start detector is a polycrystaline chemical vapor deposition diamond with metal electrodes to apply a potential. Passing charged particles produce electron/hole pairs and therefore a electrical current will flow, which can be amplified, digitized and processed by a digital electronic circuit.

The setup for HADES is shown in fig. 2.7. The start detector signals incoming beam particles 75 cm in front of the target, and the veto detector signals particles 75 cm behind the target. Particles which are detected on the start and on the veto detector did not react with the target and should not be triggered. The position resolution is provided by the segmentation of the start and veto diamond into 8 stripes. The start detector delivers the precise time reference for the TOF detector. As this time information is crucial for the experiment, dedicated electronics were developed, which has a resolution better than 60 ps [Lic99]. Additionally, the start detector is used for an online monitoring of the beam quality and the spill structure. This is done by connecting a fast counter (*scaler*) to each of the 8 channels of the detector, which must be capable to count the 10^8 particles per second.

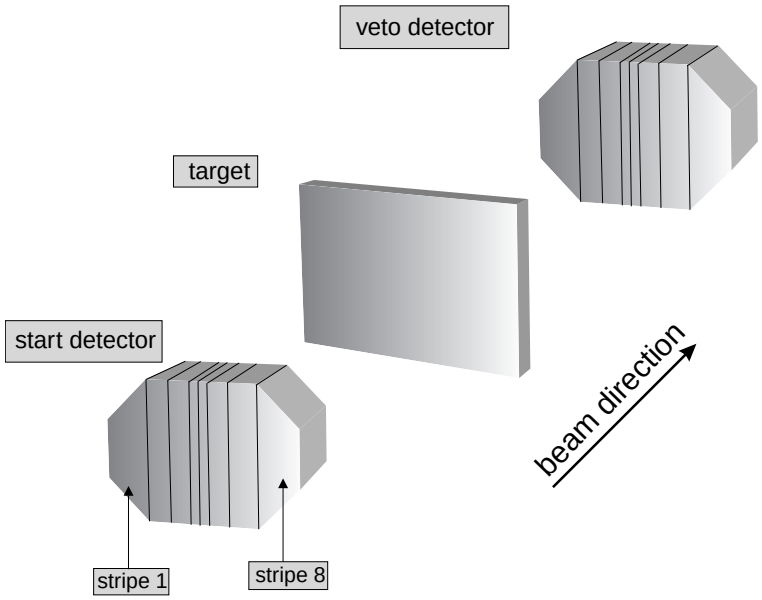

Fig. 2.7: *The setup of the start and the veto detector. The distance to the target is 75 cm for both.*

2.4 The Working Instrument

In fig. 2.8 a picture of the HADES Spectrometer is shown. It is taken from the backside of the detector, the beam is approaching the camera.

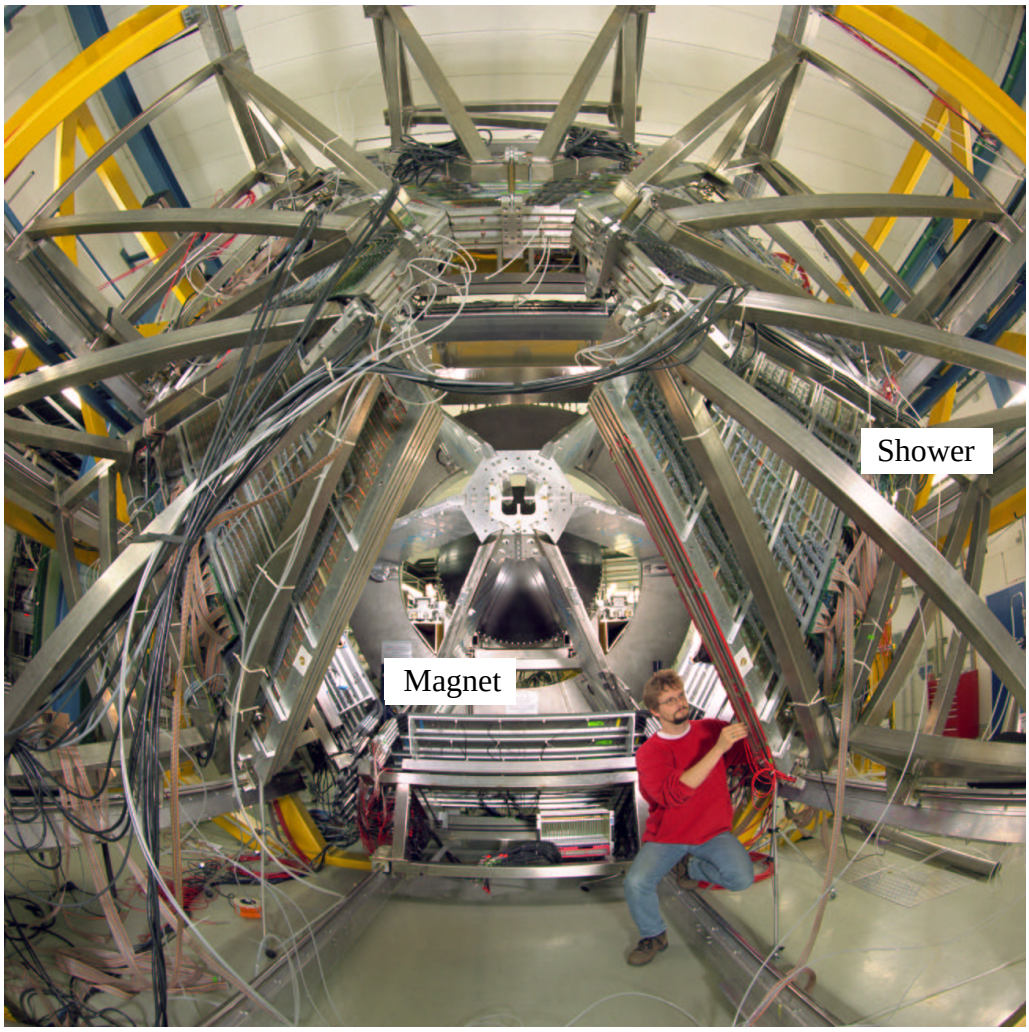

Fig. 2.8: *View of the HADES detector from the back, the beam is approaching the camera. The superconducting magnet and the Shower detector in the six fold symmetry can be seen.*

One can see the superconducting toroid with the six coils in the center and the six segments of the Shower detector.

In fig. 2.9 a side view of the detector is shown. The RICH and MDC, which are mounted close to each other, are moved out of the magnet. All subdetectors are mounted on slides, to allow the access all the detectors for maintenance.

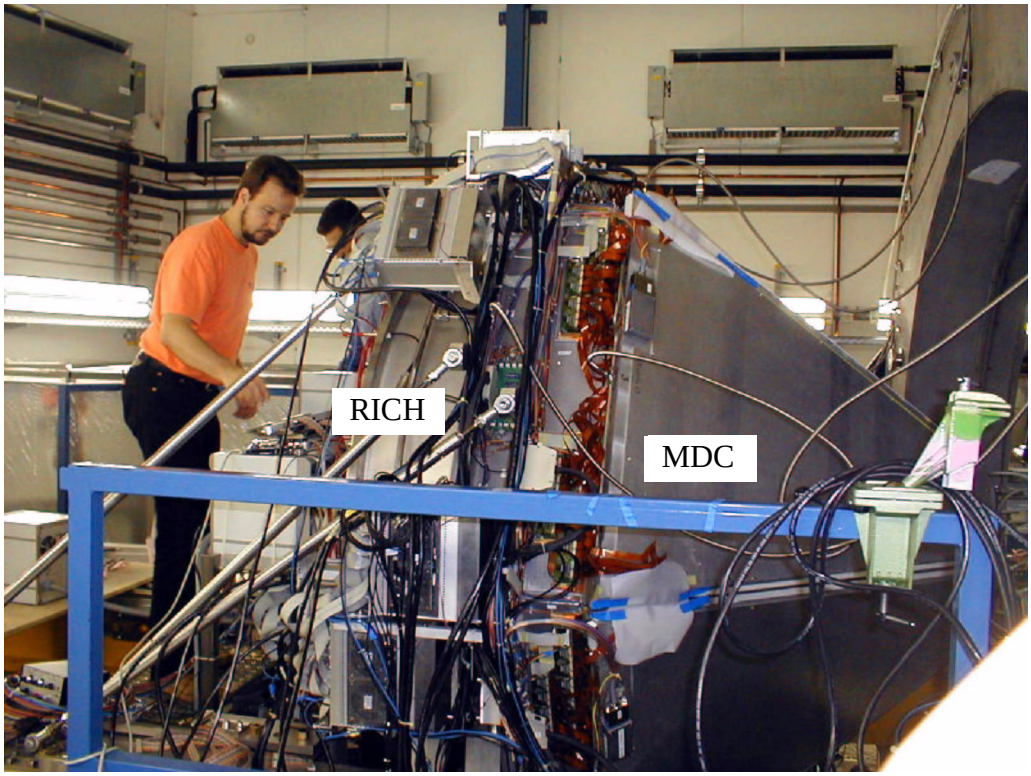

Fig. 2.9: *Side view of the detector. The RICH and the two modules for each sector in front of the magnet of MDC are moved out of the magnet for maintenance. The beam is coming from the left.*

Chapter 3

The Three Levels of the HADES Trigger

The purpose of the HADES detector is to measure dileptons from the decay of light vector mesons (ρ,ω,ϕ), therefore one has to consider the branching ratios for these decays. As these are in the order of 10^{-5} to 10^{-6} it is necessary to use high beam intensities in order to achieve good statistics of the experiment. The SIS accelerator at GSI is able to use beam intensities of up to 10^8 particles/s. With a thin target (1% interaction length) the resulting total nuclear reaction rate is 10^6 s^{-1}. The target must be very thin, to reduce the creation of conversion electrons which produce combinatorial background. In addition, this lowers multiple scattering in the target, which leads to a decreasing momentum resolution.

With a multiplicity trigger in the TOF wall (selecting central events), a reduction by a factor of 10 can be obtained. This results in an event rate of 10^5 s^{-1}. With this rate all the subdetectors are read out, all analog signal are digitized and stored in buffers. This means that the approximately 100.000 channels of the HADES detector produce a raw data rate of 3 GByte/s. For the HADES experiment these amounts of data can not be stored and analyzed. Therefore, it is essential to realize a very efficient online trigger system which reduces the event rate by several orders of magnitude. The trigger is divided into several steps, due to the increasing complexity of the algorithms to achieve a reduction. The HADES trigger reduces the event rate by a factor of 10000, where the essential and most demanding part is the reduction of the second level trigger by a factor of 100.

The complete trigger is divided into three steps, where in the following the focus is set on the second level trigger (LVL2) [Leh97] [Tra00].

The third level trigger (LVL3) described in chapter 3.3 on page 55 is a future extension and has not yet been implemented.

In fig. 3.1 an overview of trigger system is shown.

The large number of asynchronous working modules at different places at the detector also requires a flexible and stable trigger distribution system (see chapter 3.2.4 “Trigger Distribution System” on page 50).

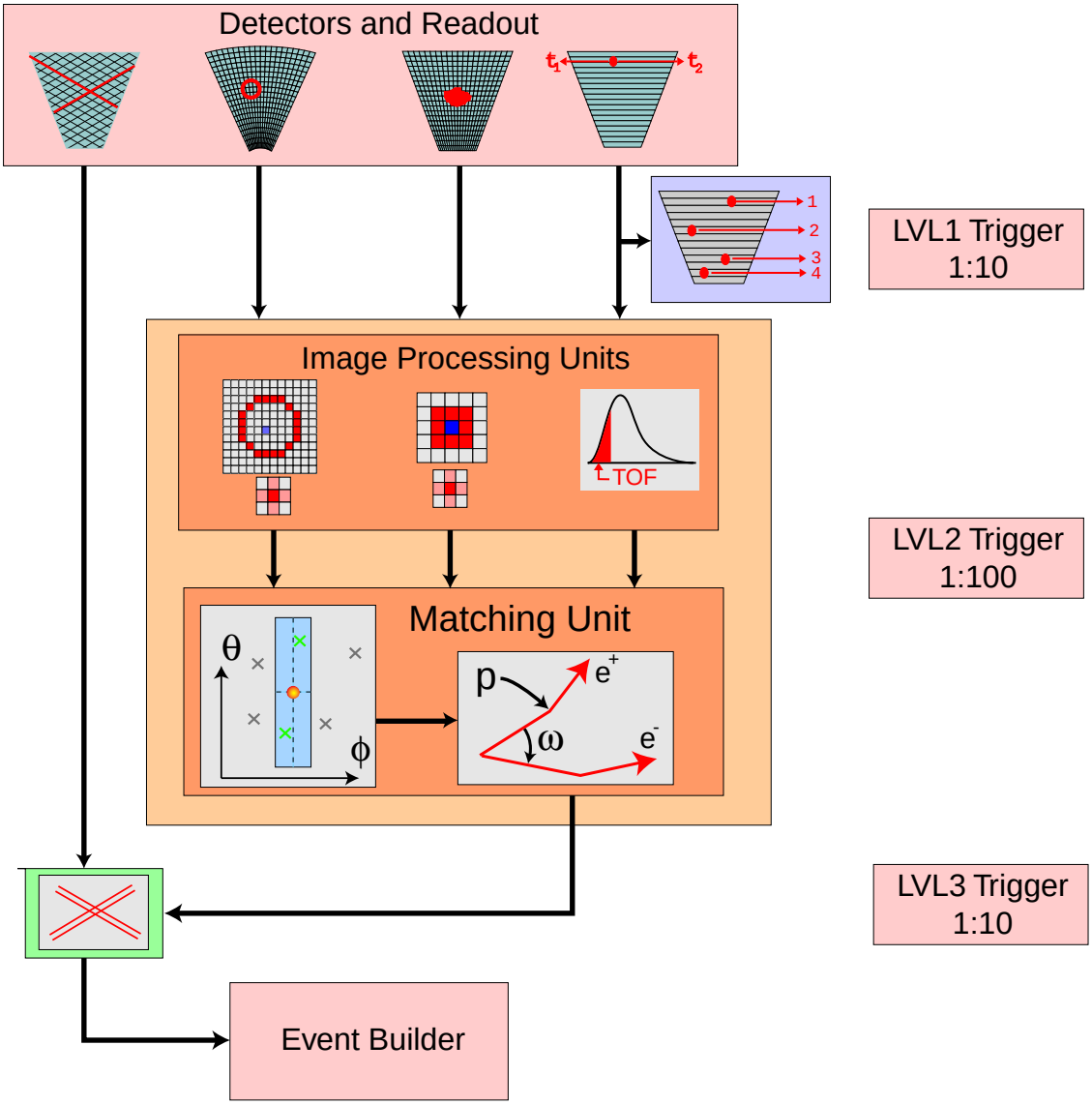

Fig. 3.1: *Overview of the HADES Trigger. It is divided into three steps. The LVL1 (the first level trigger) is a multiplicity trigger in the TOF wall on central events (1:10 reduction of event rate). The LVL2 trigger recognizes electrons in the subdetectors (RICH, TOF and Shower) by pattern recognition, that is ring finding for the RICH IPU, searching for electromagnetic showers in the Shower IPU and selecting a range of the time of flight in the TOF IPU. Then this information is combined to electron-positron pairs by hit matching and from these, dileptons in a selectable invariant mass window are chosen (1:100 reduction of event rate). The LVL3 trigger (not implemented yet) also uses the MDC information to verify the LVL2 decision by MDC hit patterns (1:10 reduction). The information gathered by the trigger is then added to the event stream and stored by the Event Builder.*

3.1 LVL1 Trigger (Multiplicity Trigger)

For decreasing impact parameter *b* the number of nucleons participating in a reaction is increasing, this also results in an increasing number of particles emitted at large angles.

Charged particles produce scintillation light in the TOF wall. The individual signals are added (analog) by the MTU (Multiplicity Trigger Unit) and discriminated to deliver the LVL1 trigger.

If the multiplicity threshold is selected such that the impact parameter $b < 4$ fm, the event rate will be reduced by a factor of 10 for the Au+Au system (see fig. 3.2). This

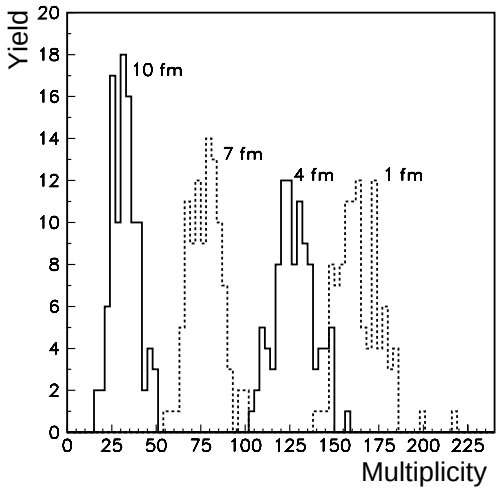

Fig. 3.2: *Histogram of the charged particle multiplicities in simulated AU+AU collisions at 1 AGeV for the given impact parameters b [GAR93].*

reduces the total event rate to 10^5 s^{-1}, which is manageable by the following trigger levels. An overview of the resulting data rates of the subdetectors is shown in table 3.1.

Detector	Max. Event Size (kByte)	Average Event Size (kByte)	Average Data Rate (MByte/s)
RICH	60	<10	1000
MDC	100	10	1000
TOF	8	1,6	160
Shower	36	7	700

Table 3.1: The average event sizes and data rates for 10^5 readouts per second for Au+Au at 2 AGeV. The max. event size is the size of an event when all channels fire simultaneously.

3.2 LVL2 Trigger (Dilepton Trigger)

The second level trigger consists of two stages:

In the first stage the various subdetectors are read out and dedicated hardware looks for electron signatures in the data. This will be explained in the following for each subdetector.

In the second stage the hit information of electron candidates in the subdetectors is transferred to one central module, the Matching Unit, which has been designed and built as part of this thesis. It combines the hit information from the IPUs and performs a "hit matching" to look for electron/positron trajectories (which also can be called rough tracking). These electrons and positrons are then combined to dileptons. The combination of the momentum of the electrons and the opening angle of the lepton pair allows dileptons within an invariant mass window to be selected. The Matching Unit and its algorithm is discussed in detail in chapter 4.1 "The Algorithm" on page 59.

Since the system is running asynchronously, the data in the readout systems has to be stored in pipes (pipes are data buffers, implemented as FIFOs (**F**irst **I**n **F**irst **O**ut) or Dual Ported SRAMs), until a trigger decision for that event arrives from the Matching Unit. Depending on the trigger decision, the data is either discarded or sent to the next pipe or to the central Event Builder (fig. 3.3). As long as there is no LVL3 trigger, the LVL2 pipe

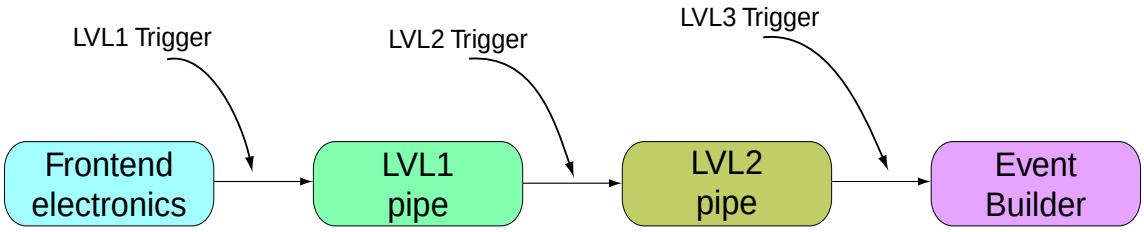

Fig. 3.3: *The data transport is controlled by the three levels of trigger decisions.*

is not used.

In the following the detector specific electron identifying hardware modules are called Image Processing Units (IPUs). To be more exact, they use pattern recognition algorithms because of the limited complexity of algorithms that one can implement in hardware. For the TOF the term IPU is used for consistency, since no pattern recognition is done here.

In addition, since the data processing of the IPUs is so closely connected to the raw data of the subdetector, the Shower IPU and TOF IPU serve as both read-out system and IPU.

3.2.1 RICH IPU

As discussed in chapter 2.3.1 "The Ring Imaging Cherenkov Detector" on page 29 each lepton with $\gamma > 18$ will emit Cherenkov light in the detector's gas radiator. The photons are reflected at the mirror to form ring patterns on the photon detector. The IPU then

searches for possible ring centers on every pad of the squared 96x96 detector plane, containing the more irregularly shaped real pad plane.

In the invariant mass region of interest, the electrons have sufficiently high momentum so that the rings have a constant diameter of 5 cm, which corresponds to a diameter of 8 pads on the pad plane. One difficulty with the search for rings is the low photon statistics and the background. For HADES experiments, a ring consists of less than 15 photons [Zei99]. The background consists of several sources, such as scintillating light in the radiator gas and electronic noise.

Therefore, several algorithms have been tested [Leh00], where the following was chosen.

For every possible ring center (96x96 = 9216) a 13x13 pad region is analyzed. The hits on a ring with a radius of 4 pads are added to the value “ring region”. There are two veto regions inside and outside the ring region, where also the pads are added. These hits account to the veto region. In the implementation in hardware not all hits were actually added, first some areas of pads on the ring are combined to a group and a logical or of these pads is performed. Then, the groups are added. This method saves

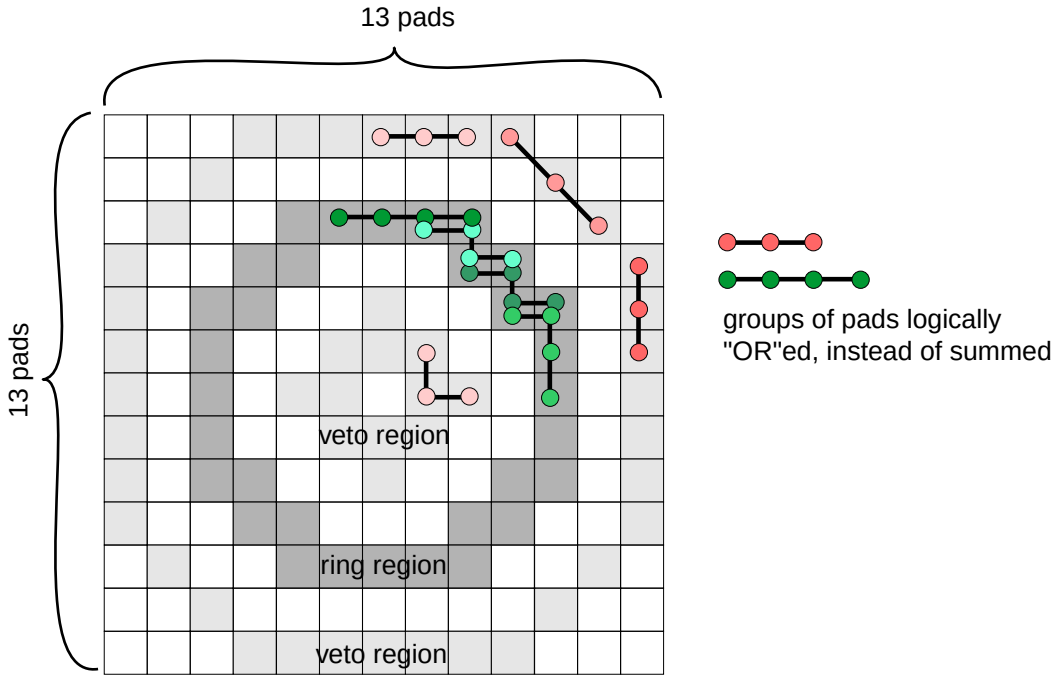

Fig. 3.4: *Ring recognition algorithm in the RICH IPU. The 13x13 pad region, the ring region and two veto regions are shown. Ring hits are summed not individually, first groups of hits are “OR”ed to save resources.*

resources in the hardware, since OR-gates are abundant in FPGAs, whereas adding numbers needs registers, which are “more expensive” (see fig. 3.4).

Now one can chose different thresholds for the sum of the ring region as well as for the veto region and can identify the center of a Cherenkov ring of a electron. Addition-

ally, a local maximum search is performed on neighboring pads, to prevent the IPU from finding rings with adjacent centers from the pads associated with a real ring.

The RICH IPU is implemented on two 6U-VME boards for each of the 6 detector segments. One pattern reconstruction card (PRC) reconstructs the hit pattern of the complete 96x96 virtual pad plane (not every pad corresponds to a existing pad in the detector). The ring recognition unit (RRU) searches for potential ring center pads on all 96 columns of the hit pattern (see block diagram of RICH IPU in fig. 3.5).

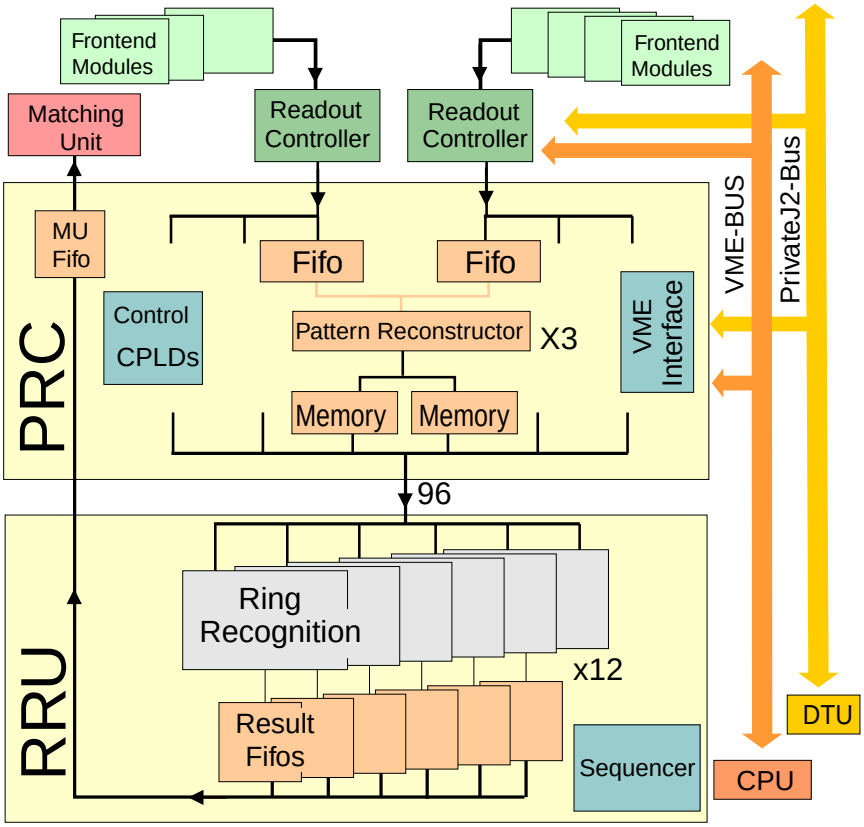

Fig. 3.5: *RICH IPU block diagram. The Pattern Reconstruction Card (PRC) and the Ring Recognition Unit (RRU) are shown with the interfaces to the readout controllers and the MU.*

Position information from all pads on the detector plane with a pulse height value above a specific threshold is transferred at 16 MHz from 2 RICH readout controllers (RC) in parallel to the PRC. The position words from both RCs are pre sorted in three buffer FIFOs where each contains 32 columns of the pad plane. This data is then transferred into two 16 bit wide dual ported SRAMs where the hit pattern is reconstructed. The second port of these SRAMs is then used to transfer complete reconstructed rows to the RRU. The RRU performs the algorithm described above. It is implemented in 12 Xilinx XC4028EX-4 FPGAs each containing 8 dedicated ring recognition units for one column of the pad plane. The pipelined realization of the algorithm in the FPGAs allows the ring finding to be finished in about 10 µs.

The results are then collected on the PRC and then read out by the Matching Unit by a 20 Mbytes/s RS485 bus.

3.2.2 TOF IPU

The TOP IPU selects electrons by discriminating particles by their velocity. Hence, one has to measure the time of flight from the target to one strip of the scintillating TOF wall, to determine their velocity. In fig. 3.6 simulations (for central Au+Au collisions)

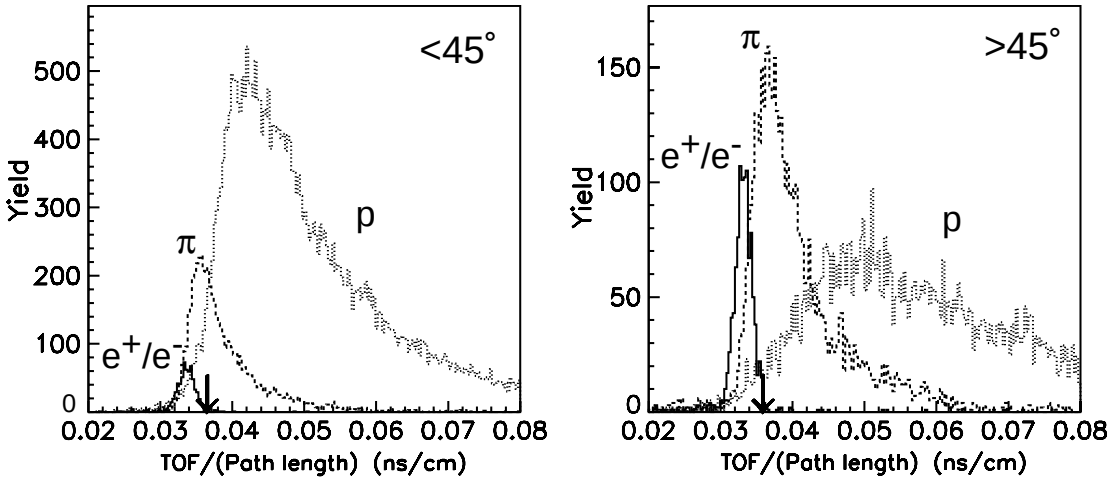

Fig. 3.6: *Simulation of the velocity of electrons, pions and protons for different polar angles (central Au+Au collisions). The discrimination of electrons is much more effective for polar angles > 45° (plot on the right), than for angles < 45° [Gar93].*

[Gar93] of the velocity distribution of different particles in the HADES detector is shown for different polar angle regions. Here one can see, that a discrimination of the electrons from heavier particles is possible in a polar angle region > 45°, which leads to a significant reduction in electron candidates.

The TOF IPU receives 2 TDC (Time to Digital Converter) and 2 ADC (Analog Digital Converter) values per scintillation strip. The TDC values correspond to the time difference between the start signal and the stop signal. This is not exactly the time the particle needed to travel from the start detector to the plastic scintillator. To get the velocity one has to make several calibrations and corrections:

a) Convert the TDC channel number to time (linear function)
b) Walk correction with the ADC values
c) Add the time signals on both sides of the detector strip
d) Correct the time of flight by the start detector time
e) Calculate the velocity by considering the path length

Although, the amount of data the TOF IPU has to process is smaller than for either the RICH or the Shower IPU (see table 3.1 on page 43), the algorithm is more complex.

Therefore, the TOF readout and TOF IPU is implemented by using Digital Signal Processors (DSPs), which are able to perform floating point calculations. The block diagram of the TOF readout and IPU is shown in fig. 3.7 [Lin01].

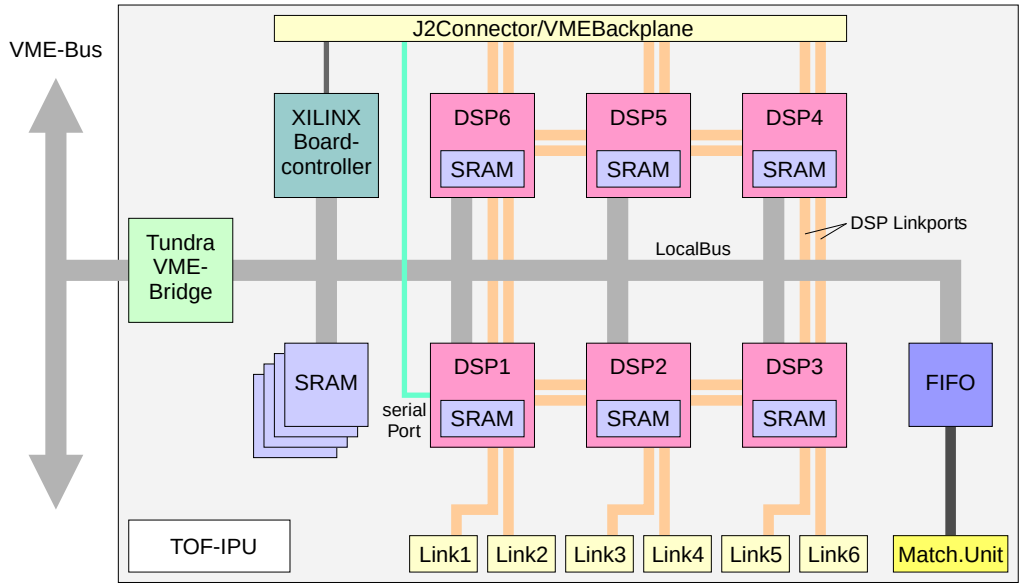

Fig. 3.7: *Block diagram of the TOF readout and IPU.*

The task is performed in an array of six ADSP2106x (SHARC) DSPs (for details see chapter 4.2.3 “Digital Signal Processors” on page 67) in a pipelined architecture (80 MFLOPS each). These data from the TDCs and ADCs are transferred via a VME bridge (SCV64 from Tundra) on the VME bus by a chained block transfer. These data are then transferred to one DSP via the SHARC link ports which performs one part of the algorithm. After that it will transfer the event to the next DSP, and so on. Each TOF IPU can process 2 sectors of the HADES detector.

The positive triggered events are transferred via LVDS (Low Voltage Differential Signals) to a concentrator board in a different crate. It is essentially the same board, but with different I/O configuration and different software running on the DSPs. It will collect the read out data from the TOF IPUs and build subevents, which then are read out by a VME CPU which sends the event via ATM to the HADES Event Builder.

3.2.3 Shower IPU

The Shower IPU has to find electron signatures in the three layers of the Shower detector. As discussed in “The Shower Detector” on page 33 the electromagnetic shower in the lead converters increases the number of charged particles. As the multi-wire chambers run in the Self Quenching Streamer Mode only the number of charged particles determines the amplitude of the signal. Therefore, the Shower IPU has to search for a

increase in charge in the deeper layers, which is done by adding the charge in 3x3 pad regions (see fig. 3.8).

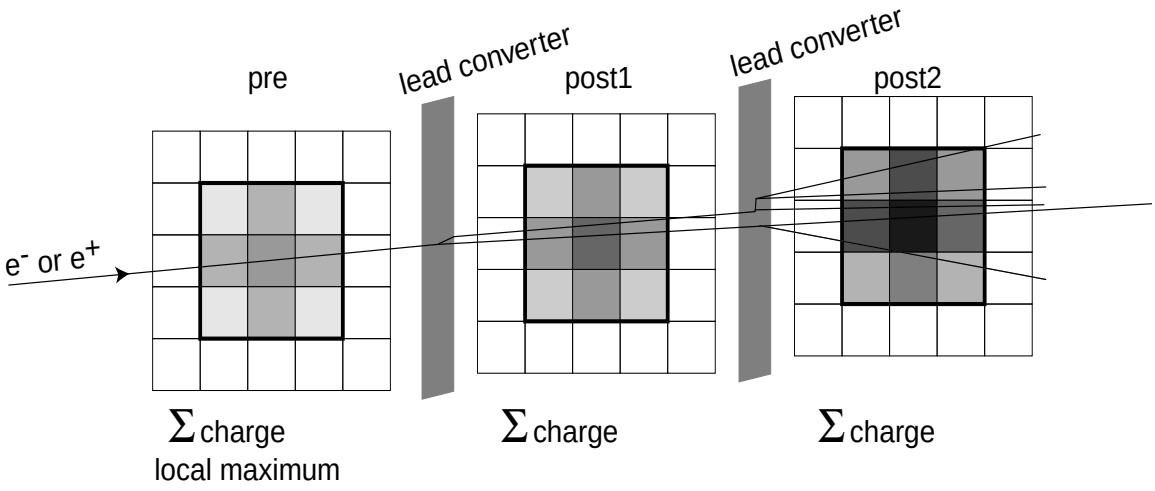

Fig. 3.8: *Schematic view of the Shower IPU algorithm. In all three layers the charge for 3x3 pad regions are added. An increase in charge is an electron signature.*

Subsequently, a local maximum search is performed. It uses the full 8 bit pulse height information of the front-end electronics of all 16956 pads. Additionally, the Shower IPU also performs the readout of the detector.

The block diagram of the Shower IPU is shown in fig. 3.9 [Pet00].

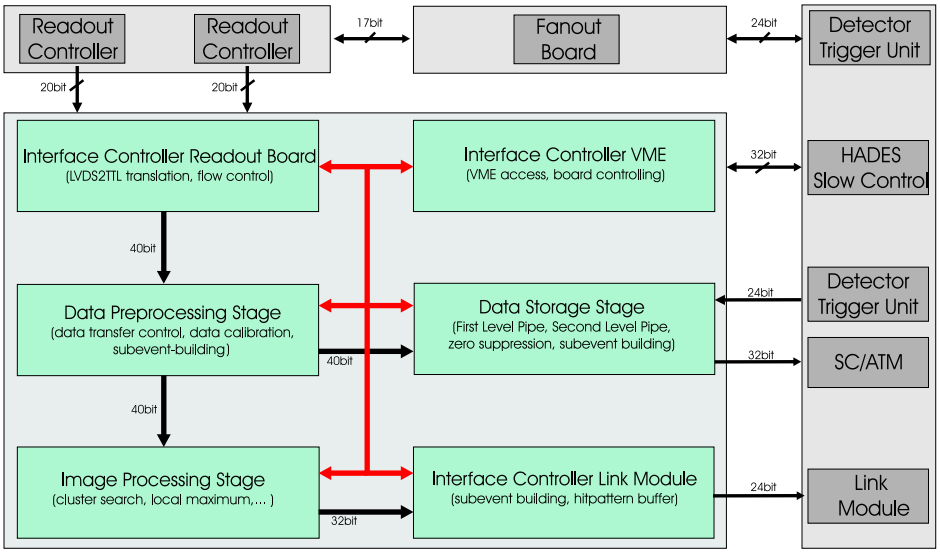

Fig. 3.9: *Functional block diagram of the Shower IPU with all its interfaces [Pet00].*

The realization of the IPU is similar to that of the RICH IPU. The data is processed in parallel by FPGAs (Altera EPF10K100ARC), where the algorithm is implemented in

a pipelined fashion, row by row. Due to the additional task of readout, pedestal correction, zero suppression and storage of the data in pipes for later readout (if the LVL2 decision was positive) the Shower IPU for the complete HADES detector consists of 12 VME boards (motherboard with add-on).

3.2.4 Trigger Distribution System

Since the IPUs and readout systems are working asynchronously separated by large distances, it is necessary to have an efficient trigger distribution system. It has to send all LVL1 and LVL2 trigger decisions and trigger identifying information to the various subdetectors distributed around the whole HADES detector. This information then has to be converted into subdetector specific signals and sequences. The information identifying the trigger is the trigger tag and the trigger code.

The trigger tag is an 8 bit number, which increments for every event. It allows the asynchronous data streams to be synchronized after a positive LVL2 trigger decision. 8 bits are sufficient, because this number is just needed to find matching events in the LVL1 pipes (which are typically of 20 events deep), not to uniquely identify a event in an experiment.

The trigger code is a 4 bit number which identifies the type of the event and thus the way the readout and trigger should treat the data (see table A.1 on page 101). For example one needs periodic (10 Hz) calibration events for the MDC detector to account for temperature induced changes in the drift time. These events are generated uncorrelated with the LVL1 trigger and it has to be assured by the Matching Unit, that these events are triggered positively and are sent to the Event Builder. Therefore, the MU has to decode the LVL1 trigger codes which are incorporated in the IPU data, and send the LVL2 trigger decision encoded in a trigger code, corresponding to the table A.1 on page 101.

Additionally, the trigger distribution also has to transfer status and error conditions from the subdetectors to a central trigger unit, for example a busy condition, when one sub system is currently not able to accept more triggers of a certain level. The central trigger unit has to inhibit new triggers for all detectors while this condition is true.

This concept is realized by the use of one Central Trigger Unit (CTU) which centrally distributes the LVL1 trigger from the Start Detector and the LVL2 decision from the Matching Unit. These triggers are then distributed to many local trigger modules, the Detector Trigger Units (DTU), which provide an interface to the specific needs of the readout electronics of the subdetector. The communication between the CTU and the

DTUs is via a differential bus (RS485), one for each level (see block diagram in fig. 3.10) [Lin01].

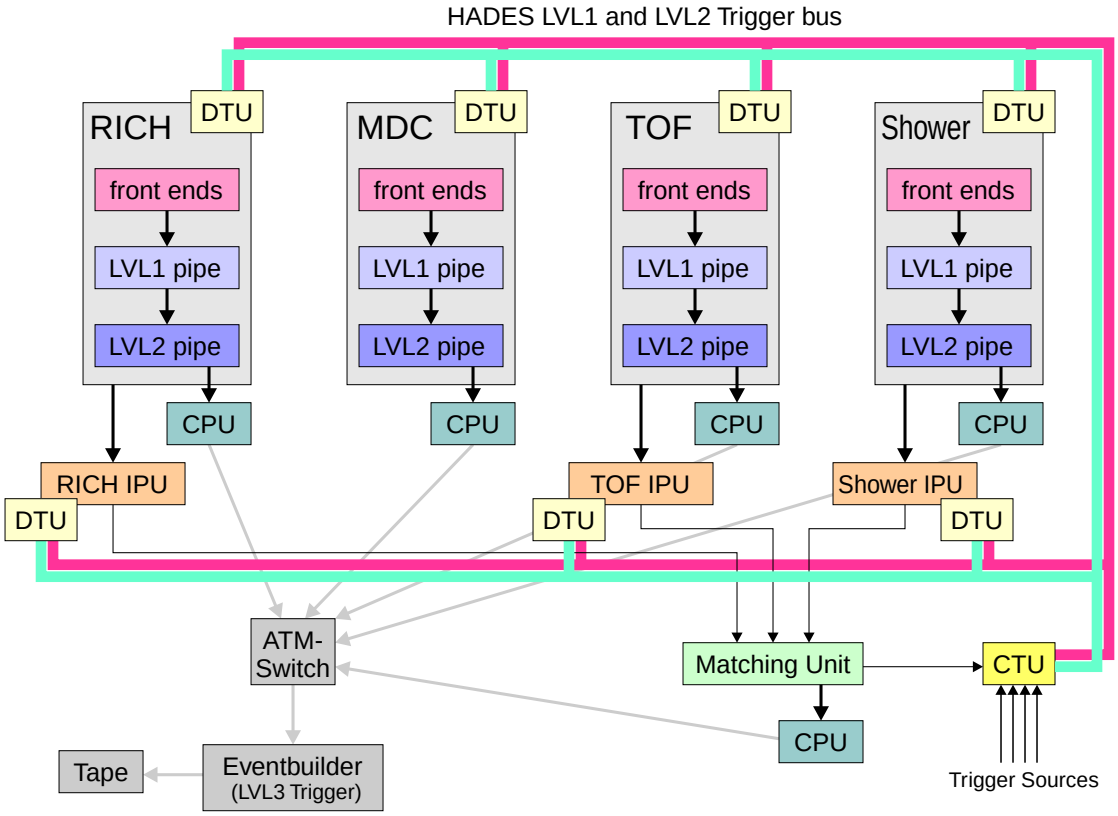

Fig. 3.10: *Block diagram of the trigger distribution system with data acquisition.*

The VME modules of the CTU and DTU use the same components, but the programming of the FPGA which contains all the logic, is different. The special needs of the subdetectors are met by subdetector specific add-on boards.

For the communication of the CTU with the Matching Unit the VME backplane (P2, custom defined pins) are used.

At this point it is possible to make a case study of one complete second level trigger to illustrate the interaction of all involved parts (as illustrated in fig. 3.11).

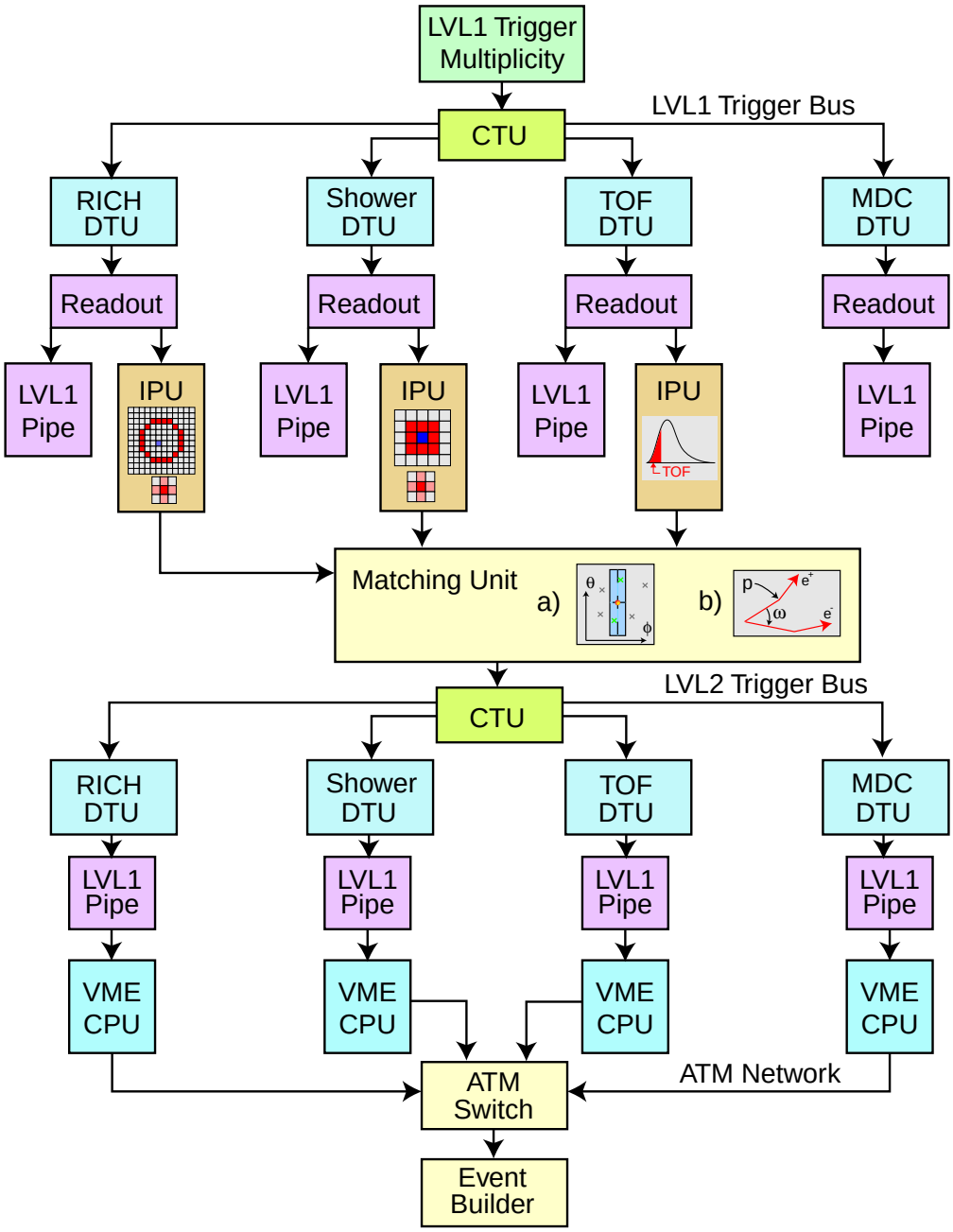

Fig. 3.11: *Flow diagram of a LVL2 trigger.*

First a start signal is delivered by the multiplicity logic to the CTU, the CTU distributes this first level trigger to all DTUs (3 RICH, 2 MDC, 1 Shower, 4 TOF) on the common LVL1 trigger bus, these start the readout of the front end boards. This data is then transferred to the level 1 pipe and to the IPUs (RICH IPU, TOF IPU, Shower IPU). The IPUs search for electron signatures and transfer the found hit information to the Matching Unit. The MU tries to match these hits and sets a window on the invariant mass of the found dileptons. The MU then sends the decision to the CTU, which then distributes this

decision on the LVL2 trigger bus to all DTUs. Then, depending on the decision, they discard the data in the level 1 pipe or this data is sent to a buffer for readout by a local CPU and sent via ATM to the central Event Builder, including the data from the MU, which lead to the decision.

3.2.5 Trigger Performance

As discussed earlier the second level trigger system has to run at an event rate of 10^5 Hz, that means that on average every 10 µs the second level trigger must be able to process a new event. This does however not mean that all the complex algorithms and data transports have to be completed in that time.

This can be accomplished by splitting the whole process into small steps, each of which can be processed in the required time of 10 µs. Every small step then transfers the data to the next (pipelining). If the steps do not require a fixed time, but can vary, the data has to be buffered in memory in between these steps.

This way one can assure, that new data can be accepted every 10 µs. This scheme introduces a larger time delay from the LVL1 trigger until the LVL2 trigger, the latency. This latency is fixed for the Shower IPU, as it is processing all the raw data every time in parallel. The RICH IPU has a fixed latency for the ring recognition but a variable latency for transferring the data from the readout controller to the IPU. For the DSP based TOF IPU and the Matching Unit this latency is determined by the event size, since they working sequentially.

As the buffer memories on the readout systems are fixed to a maximum of about 20 events, the maximum latency allowed for the whole LVL2 trigger is 200 µs.

3.2.6 Efficiency Reduction and Fakes

Due to limits of the detectors and the algorithms to find dileptons, one has to expect events which are triggered negatively by the LVL2 trigger, even if they should be triggered positively (good for bad, reduction of efficiency), as well as events which are triggered positively, even if they should not be (bad for good, fake rate).

The problems which arise are for example:

The photon statistics in the RICH is so low, that rings are sometimes not recognized. The background on the other hand sometimes looks like a ring, which is not real.

The discrimination of electrons and pions in the TOF wall is only partly possible (see fig. 3.6), which gets worse for small polar angles.

In the Shower detector double hits (for example photon and proton) lead to electron signatures. For low momentum particles (< 400 MeV/c) the efficiency drops down to 30%.

Simulations of the detector performance show the following efficiencies and fake rates [Had94] [Sch95].

Detector	Polar Region	Efficiency	Fake Rate
RICH	18°-85°	90%	0.5
TOF	45°-85°	85%	6
Shower	18°-45°	85%	6

Table 3.2: Efficiencies and fake rates for the subdetectors for m_{inv} = 0.5-1.0 GeV/c^2.

The fake rate will be reduced by the Matching Unit, as it searches for corresponding signatures in the other detectors. Due to the combinatorial nature of the Matching Unit algorithm this fake rate has to be small.

3.3 LVL3 Trigger (Tracking in MDC)

This step is a future extension for the HADES trigger system. It is a consistency check of the LVL2 trigger. Is uses the particle tracks in the MDC detector to cross-check the found electrons in the dilepton trigger. This again reduces the event rate, because it will suppress events where the LVL2 trigger found matches between uncorrelated hits in the RICH and TOF or Shower. For example, low momentum electrons will make a ring in the RICH but they can not cross the magnet. This can however be matched by the LVL2 trigger with a pion in the TOF detector (see fig. 3.12).

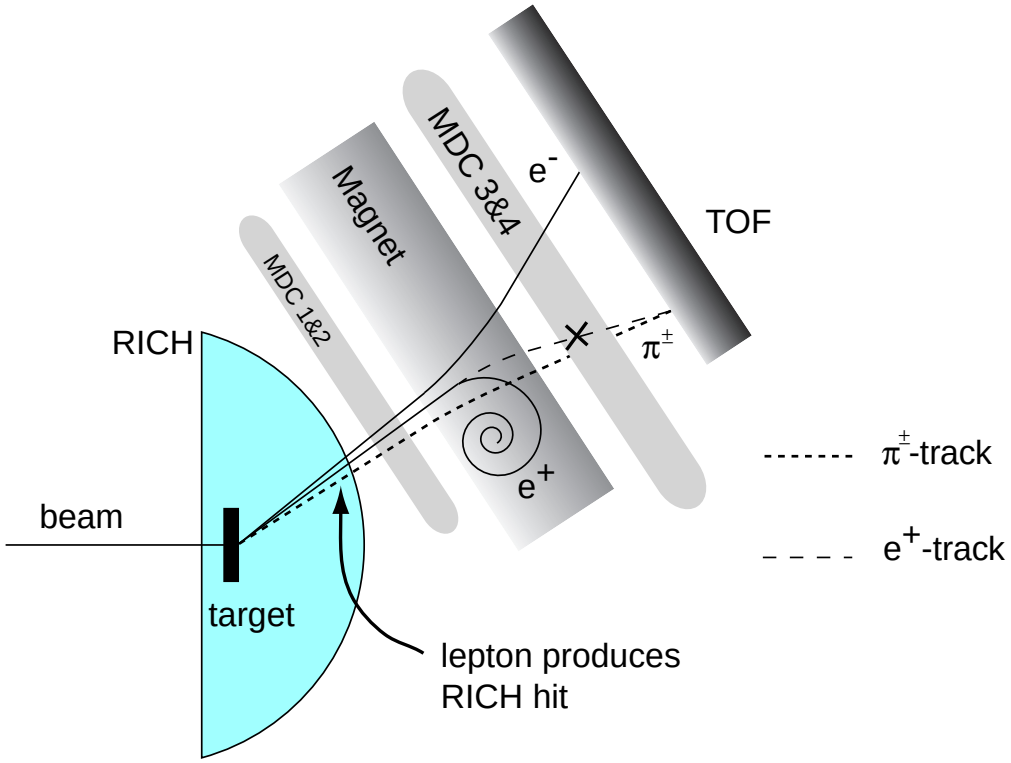

Fig. 3.12: *An example for an misidentified dilepton pair by the second level trigger. One of the leptons did not have enough momentum to cross the magnet (e.g. from π^0-Dalitz decay). The pion hits by chance the TOF at the position where the positron is expected. This can be suppressed by demanding a track in the MDC at the cross, which is missing.*

This can be avoided by checking, if there is a track in the MDC along the trajectory between the RICH and the TOF or the Shower. As a result the data rate can be suppressed by a further factor of 10.

The LVL3 trigger is planed to be implemented in software and run on fast computers, rather than on custom built hardware.

Chapter 4

The Matching Unit

The Matching Unit is responsible for the final decision of the second level trigger. Its task is to find correlating electron signatures in the data of the Image Processing Units belonging to the subdetectors (RICH IPU, TOF IPU and Shower IPU), to find electron "tracks" and with their deflection in the magnetic field the momentum, combining electrons and positrons to dileptons and calculating the invariant mass of found dileptons. By setting a window on this mass, the MU decides if the data of the corresponding event is kept or discarded. The position of the Matching Unit in the context of the LVL2 trigger system data flow is shown in fig. 4.1.

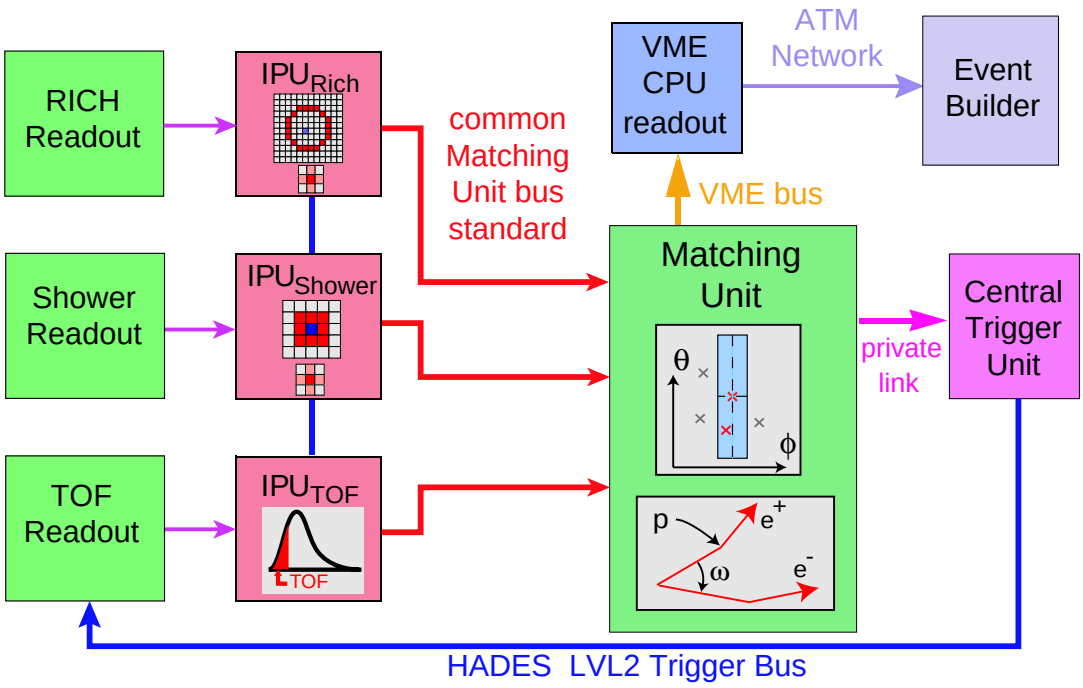

Fig. 4.1: *The Matching Unit shown in the context of the data flow of the complete second level trigger system. All the IPU data is processed and the LVL2 trigger decision is sent to the CTU, which gives the feedback to the readout controllers. Finally, the MU delivers all the gathered information to the Event Builder.*

In the following the Matching Unit algorithm, the hardware concept, its implementation and its interfaces to the other modules of the second level trigger are described.

The Matching Unit was developed in the framework of this thesis. This development includes all steps which are involved in such a project:

a) The determination and evaluation of the physics task the MU has to fulfill and the algorithm the MU has to process,
b) setting a time schedule to fit the requirements of the trigger and detector development,
c) the survey of technologies available on the market which are able to fulfill the requirements within the given budget of the project,
d) introducing new **P**rinted **C**ircuit **B**oard (PCB) production methods in the laboratory,
e) creating the schematics and layout of the PCB, mounting and soldering of the components on the PCB,
f) programming the hardware in VHDL (**V**ery High Speed Integrated Circuit **H**ardware **D**escription **L**anguage), programming the DSPs (DMA data transfers with interrupts, multitasking environment, algorithm),
g) and commissioning the complete trigger system at the detector at GSI.

Here, I would like to stress the point that a major part of the work was the implementation of the stable, fast and simultaneous transfer of the data to and from the MU. As the Matching Unit is a central part of the trigger system which all other components are connected to, the commissioning of the trigger system was a lengthy but successful big effort of the whole trigger team. The cooperation and teamwork made the working trigger system possible.

4.1 The Algorithm

4.1.1 Electron/Positron Identification

As described in chapter 2.2 on page 29 the HADES detector uses a toroidal magnet to determine the momentum of charged particles. To first order this magnetic field deflects the particle only in the polar direction, whereas the azimuthal angle will be constant (shown in fig. 4.2).

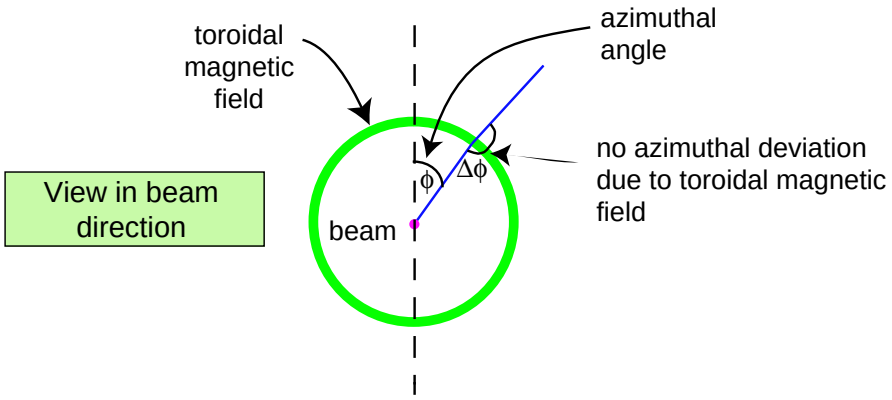

Fig. 4.2: *The basic principle of the Matching Units algorithm. In this picture the view in beam direction is shown. The deviation of a charged particle in the azimuthal direction is zero to first order due to the toroidal shape of the magnetic field.*

This property is used by the Matching Unit to find possible electrons and positrons.

After a high momentum electron crosses the RICH (as shown in fig. 4.3), it is deflected in polar direction by the magnet and hits the TOF or Shower detector. To find possible electron candidates, the MU sets a small window in azimuthal angle (which in first order does not change) and a large window in polar angle (where the deflection is momentum dependent).

Hence, the MU tries to match every hit in the RICH IPU with all the hits in the TOF and Shower IPU. If there are several hits in a given polar and azimuthal angle window, then the MU will find several electron/positron candidates for this one RICH hit. The matching in the θ–ϕ plane with the applied window is shown in fig. 4.4.

For matching and momentum determination the MU needs the azimuthal angle ϕ and the polar angle θ of the hits found by the IPUs. The IPUs, which are constructed with FPGAs, can only deliver position information in coordinates of their pad plane, which is a representation of the x (rough azimuthal correlation) and y (rough polar correlation) coordinates. To determine the mapping between x/y to the corresponding θ and ϕ ray tracing has to be performed. This is done with a Monte-Carlo simulation in the case of the RICH. Many randomly distributed particles with known θ and ϕ are tracked through a three dimensional model of the detector and the hit positions (for the RICH these are the ring centers of the cone of the Cherenkov light) on the xy-pad plane

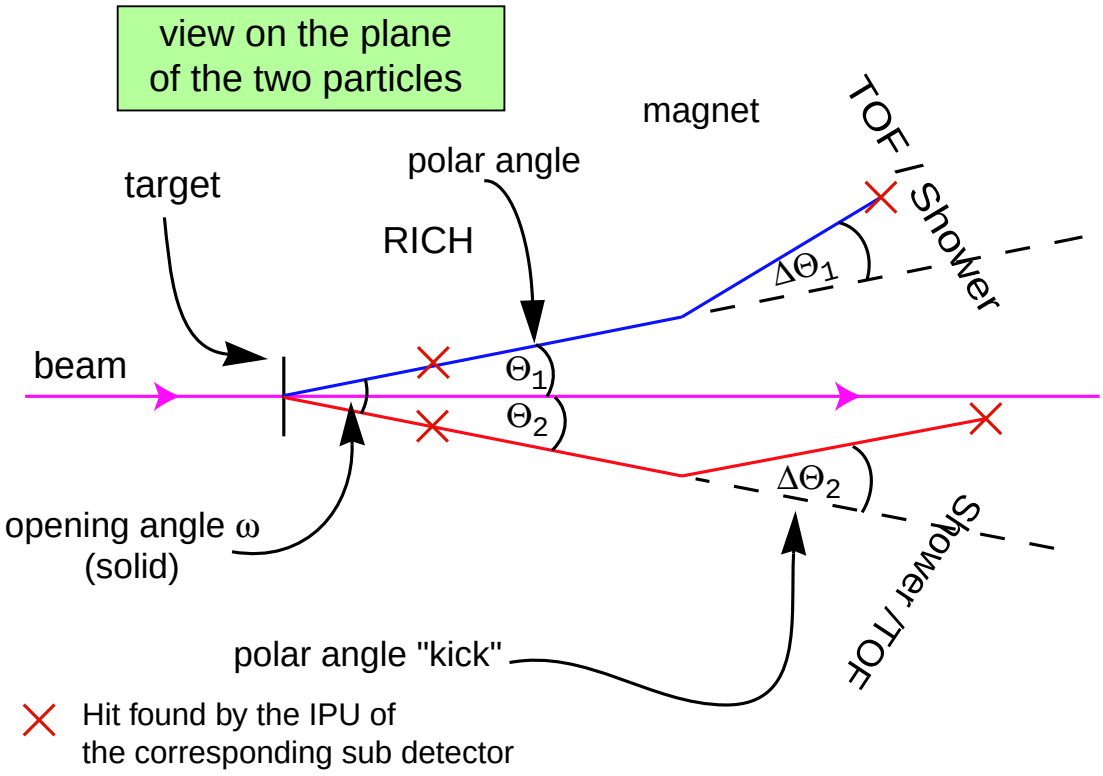

Fig. 4.3: *The basic principle of the Matching Units algorithm. The electron and positron each suffer a deflection in the polar angle direction related to the momentum of the particle.*

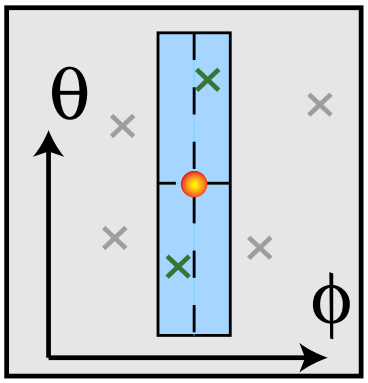

Fig. 4.4: *Window set by the MU in the θ and ϕ plane. The hit coordinates of the RICH is in the center of this window (disc). Several hits of the TOF and Shower IPU are distributed across the plane (crosses). The ones which fall into the window are then accepted, defining an electron candidate. In the picture two electron candidates are found, which are then further analyzed.*

are recorded. For the RICH detector this results in a mapping which is shown as an example for the polar angle in fig. 4.5.

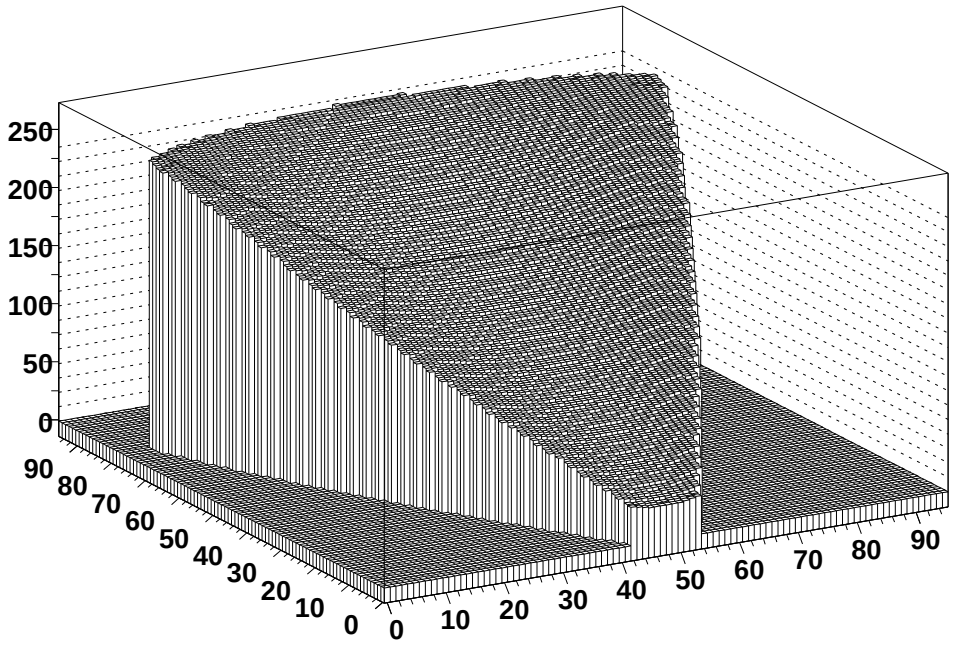

Fig. 4.5: *Result of a Monte-Carlo simulation to determine the mapping of the virtual pad plane of the RICH detector to* θ *angles needed by the Matching Unit. The x and y coordinates are the ones of the virtual pad plane, the z coordinate corresponds to the polar angle* θ *(where* θ *= 250 means 90°).*

4.1.2 Momentum Determination

The momentum of an electron is determined by its deflection in the magnetic field. For the offline software analysis one has the full tracking information of the MDC1 and MDC2 before the magnet and MDC3 and MDC4 behind the magnet. The Matching Unit receives only information of hits in the RICH, TOF and Shower detector. With the assumption that the particle originates from the target, one also can determine trajectories and thus the deviation in the magnetic field.

To determine the momentum of the particle the approach of a “kick plane” is used. The idea is to assume that the deflection of a track in the HADES magnetic field just takes place at one point in space, where the particle suffers a momentum kick. It can be proven that this momentum kick for all tracks occurs on a surface, which is flat for a homogeneous magnetic field (see fig. 4.6).

Since the HADES magnetic field is not homogeneous a simulation has to determine the real kick plane [San00]. The resulting hyper-surface, where all deviations due to the inhomogeneous magnetic field are incorporated, is then parameterized by a function. Especially at the corners of a sector there are larger deviations to the ideal toroidal magnetic field.

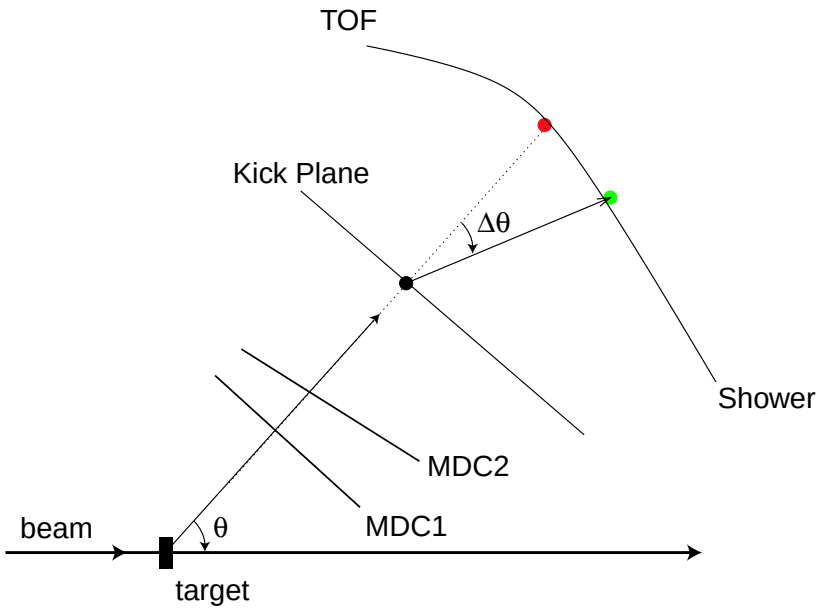

Fig. 4.6: *A particle passing through the HADES detector: Instead of tracking the particle step by step through the magnetic field, it is assumed that the whole deflection takes place at one point in space. These points lie on a hyper-surface, the so called "kick plane".*

By transforming the kick angle to the appropriate parameters known by the Matching Unit, namely the original θ of the particle detected in the RICH and Δθ, the difference of θ_{RICH} and the θ_{Shower} or θ_{TOF}, it is possible to transform these parameters to the momentum of the particle.

Moreover, one has to consider the different behavior of electrons and positrons in the magnetic field. The deflection Δθ is only to first order the same for electron and positron of the same momentum, because the trajectory for an electron is bent towards the beam, whereas for a positron it is bent away from the beam (the direction is certainly dependent on the direction the current is flowing through the magnet). This results in a longer path for positrons in the magnetic field and therefore a larger deflection Δθ.

The necessary calculations are all done offline and for the Matching Unit a table is provided, where the angle θ, the deflection Δθ, the azimuthal angle ϕ and the kind of particle (electron/positron) is mapped to the momentum of this particle. The range in momentum of this table from 50 MeV/c up to 1 GeV/c. The granularity of this table is the same as the granularity of the subdetectors.

4.1.3 Dileptons and Invariant Mass

The Matching Units task is to calculate the invariant mass of dileptons by finding and matching electron/positron pairs. Electrons and positrons are distinguished by the differ-

ent sign of their polar deflection in the magnetic field. After finding the dileptons, the MU determines the spatial opening angle, as shown in fig. 4.3 on page 60:

$$\cos\omega = \frac{\vec{a}\cdot\vec{b}}{|a|\cdot|b|}, \tag{4.1}$$

where $\vec{a}$ and $\vec{b}$ are the vectors determined by the target (0,0,0) and the xyz-coordinate of the hits in the RICH detector. Therefore, the θ/ϕ is converted to cartesian coordinates.

With the information of the opening angle ω and the momenta $\vec{p}_{1,2}$ of the electron and the positron, the invariant mass m_0^2 can be determined as follows:

$$\hat{p}^2 = E^2 - p^2 = m_0^2, \tag{4.2}$$

where $\hat{p}$ is the 4-momentum.

$$m_0^2 = (\hat{p}_1 + \hat{p}_2)^2 = \hat{p}_1^2 + \hat{p}_2^2 + 2\hat{p}_1\hat{p}_2 \tag{4.3}$$

Since the mass of the electron is small compared to the total energy of the individual leptons (typically 0.1-1 GeV/c^2), it follows

$$m_0^2 = 2(E_1E_2 - \vec{p}_1\vec{p}_2) = 2p_1p_2(1-\cos\omega). \tag{4.4}$$

With the correct units, this results to

$$m_0^2 = \frac{2p_1p_2\left(\sin\frac{\omega}{2}\right)}{c^2}. \tag{4.5}$$

With this calculation the Matching Unit is able to determine the invariant mass of any matched e^+e^- pair. Now, by applying a window only electron/positron pairs within an invariant mass range of vector mesons are accepted and will result in a positive LVL2 trigger.

4.1.4 Combinatorial Problem

One must consider the multiplicities in the different subdetectors, due to the combinatorial nature of the Matching Unit algorithm. Simulations have determined [Sch95] the figures given in table 4.1.

IPU	average number of hits	max. number of hits considered
RICH	1.2	4-5
TOF	6	12
Shower	6	12

Table 4.1: Number of hits the IPUs detect per event on average and at maximum for Au+Au at 2 AGeV [Sch95].

Here, the average number of hits in the RICH IPU is relevant, as only hits are matched when there is a hit in the RICH. Thus, this number determines the average computing time of the MU. As long as this number is low, the computation time is reasonably small.

4.2 The Realization in Hardware

As part of the LVL2 trigger, the Matching Unit algorithm has to be processed in real time. The algorithm involves complex calculations with large data rates in the input and output stream, thus the Matching Unit has to be built in hardware.

In the following the concept, the implementation, the interfaces to other modules and the necessary software for the Matching Unit are described.

4.2.1 The Hardware Concept

To perform the Matching Unit Algorithm (as explained above) one has to decide which architecture of the hardware is appropriate. Since each event is independent from the others, the natural idea is to use the algorithm in parallel. That means that every event is distributed to a computation unit, which is able to perform the full algorithm and make a LVL2 trigger decision. This allows the processing time for a single event to be much larger than the required 10 µs on average for a LVL2 decision to be sent to the CTU (for the performance requirements of the trigger system see fig. 3.2.5). The average time of 10 µs between two LVL2 triggers is still guaranteed, but the latency, the time from data input to the Matching Unit to the LVL2 decisions, is increasing. This results in the requirement, that the Matching Unit must be able to accept the data of the IPUs every 10 µs on average.

Another advantage of the parallel concept is, that it is simpler than a pipelined implementation. Pipelined algorithms have in principle the same performance as parallel algo-

rithms, as they also perform many steps of a algorithm in parallel in different units. But they divide the full algorithm into small steps, and transfer only the processed data to the next computation unit. On one hand this method does not need as much computing resources (such as memory), because for every step only the local resources are needed (like lookup tables), but on the other hand, the data transfer from step to step uses resources and every step has to fulfill the time requirements. So, one has to be very careful in dividing a complex algorithm in small steps, which all need the same number of instructions. In total, the parallel algorithm is easier to implement, since a synchronization with the other parallel units only has to be done at the end of a calculation. Due to the combinatorial nature of the algorithm, the Matching Unit can not guarantee a fixed processing time for each step.

The second main decision which has to be taken is the selection of the kind of computational unit. As mentioned in chapter 3.2 “LVL2 Trigger (Dilepton Trigger)” on page 44 the RICH and Shower IPUs are implemented in FPGA (**F**ield **P**rogrammable **G**ate **A**rrays). For the task of the Matching Unit **D**igital **S**ignal **P**rocessors (DSPs) are more appropriate, as they are also able to perform complex calculation. Since they are designed to process continuous data streams and hence can provide the required I/O capabilities needed by the Matching Unit.

These decisions led to the hardware concept of the Matching Unit shown in fig. 4.7.

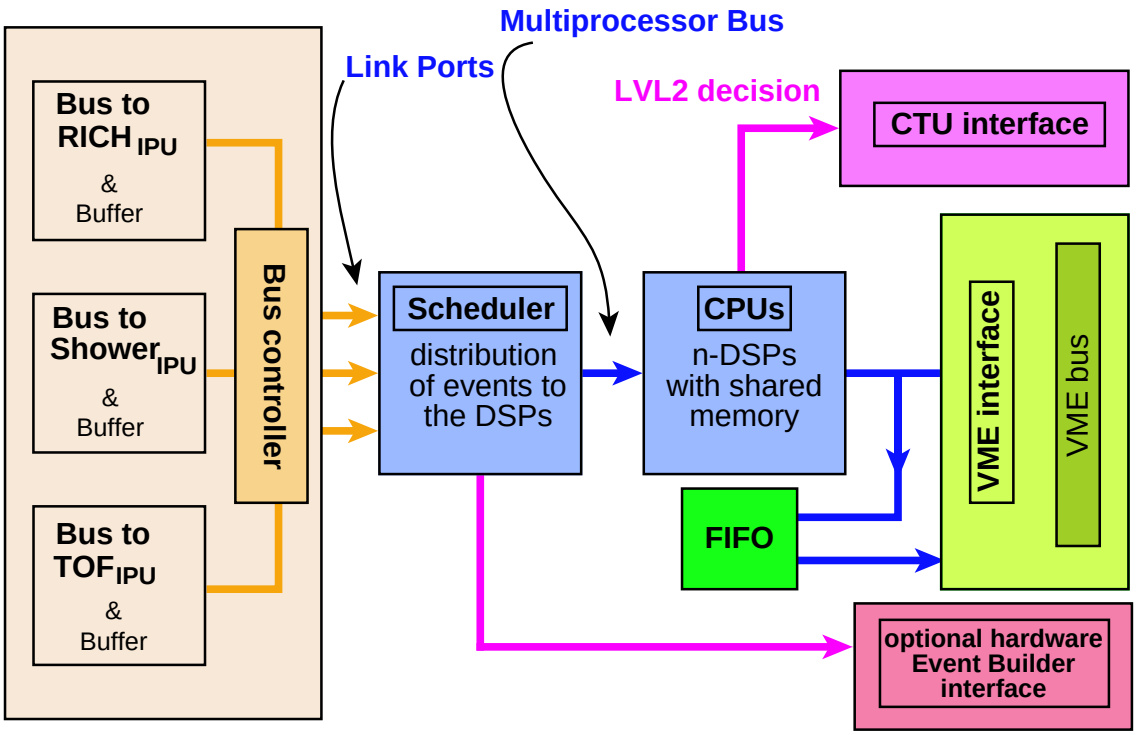

Fig. 4.7: *Block diagram of the hardware implementation of the Matching Unit. It shows the parallel concept of the computation units and the data paths implemented.*

The data from the IPUs is transferred from all IPUs to the MU via a standardized protocol (the HADES common IPU to Matching Unit protocol). A CPLD on the MU

receives this data from the three sources simultaneously, multiplexes it and sends it to a dedicated DSP, which serves as a scheduling DSP. The *scheduler* collects the data from the 3 IPUs, checks for consistency and transmission errors and builds events. These events are sent to one of the DSPs working in parallel. These perform the matching algorithm and after finishing write the raw data as well as the information from the algorithm to a buffer memory (FIFO) which is then read out by the local VME-CPU without interrupting the DSPs in their work. The second level trigger decision is then sent via the VME backplane to the adjacent CTU. Optionally, the data can be sent to a hardware event builder in the same VME crate.

4.2.2 The Matching Unit

To prove that this scheme is applicable a prototype MU has been built, which uses the concept described above, but not optimized to speed. Therefore, the prototype uses only a total of three DPSs which is extendable up to six DSPs.

A block diagram of the prototype with the data paths and their width is show in fig. 4.8.

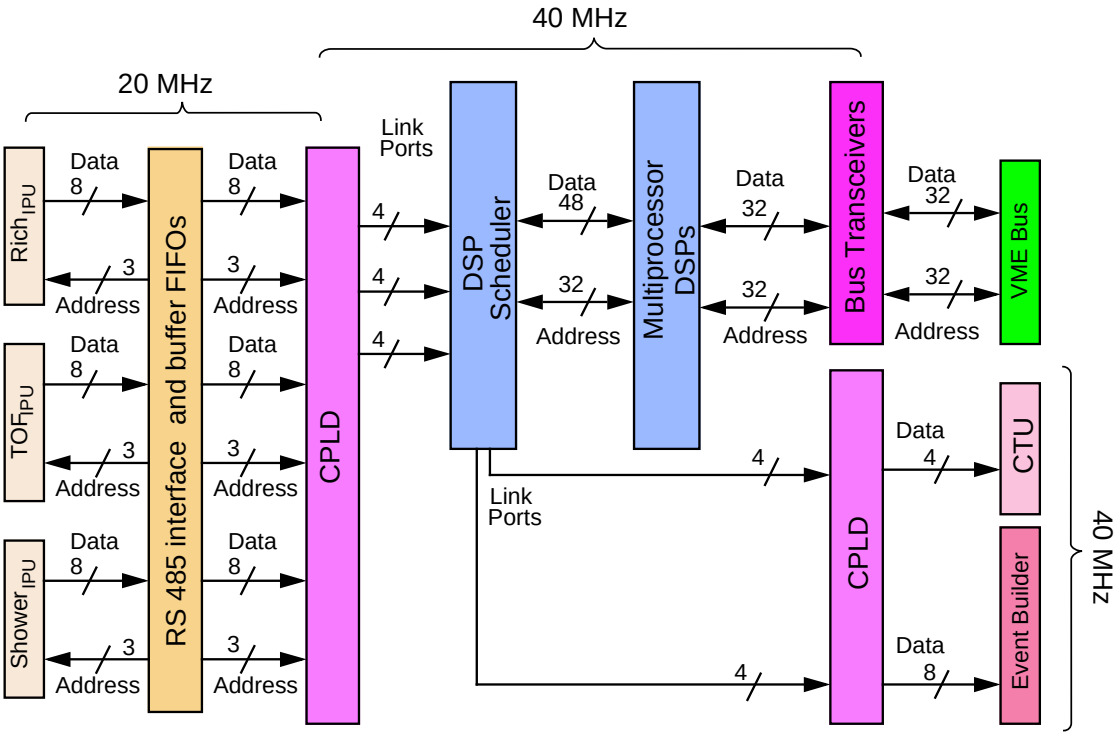

Fig. 4.8: *Block diagram of the prototype of the MU. The different components, the data paths between them, their widths and the frequency they work with are shown.*

This shows that the hit data from three detector sub systems IPUs is transferred to the Matching Unit simultaneously. There are 6 IPUs for the RICH detector, 3 IPUs for the

TOF detector and 12 IPUs for the Shower detector. For the Shower IPU the MU only has to address one “link”-module, which collects the information from the 12 IPUs locally in one crate (this is especially reasonable for the Shower IPU, as all IPUs and read out cards are in just one crate). This data is first stored in a FIFO for each IPU to allow asynchronous operation. The board controller CPLD then multiplexes this data and maps it to the appropriate protocol for the scheduling DSP. The data is then transferred via **D**irect **M**emory **A**ccess (DMA) directly into the memory of the scheduling DSP. This DSP addresses and receives the data from all three IPU systems independently. That means this DSP is responsible for addressing the different IPUs simultaneously, but the IPUs of one type in sequential order (to avoid bus conflicts). After recognizing that a full event is transferred it packs the data of the different IPUs to an event and sends this data to one of the idle DSPs, which is available and has no other task at that moment.

These DSPs then perform the matching algorithm. After making their decision they send their data to the event FIFO, which is a buffer to be read out by the common data acquisition via the VME bus. This read out can be done without interference at the same time as the DSPs use their multiprocessor bus, due to bus transceivers which generate two bus systems on the board (see fig. 4.11 on page 70).

Additionally, the decision has to be sent to the CTU. This information is transmitted via a special VME back plane. Optionally, a connection to a hardware event builder is foreseen.

In the following some of the important components on the MU are discussed in detail.

4.2.3 Digital Signal Processors

The DSPs are the most important devices on the MU. Since they perform the algorithm and receive and send all data, special care has to be taken to choose the appropriate device.

Here, a DSP from Analog Devices has been chosen (ADSP-21060). The most important features of these devices are:

a) The possibility to transfer data to and from the chip via dedicated data links with high speed, without interfering with the core of the DSP. This allows the transport of data and calculating in the **A**rithmetic **L**ogic **U**nit (ALU) simultaneously.
b) The Multiprocessing Feature. Without additional interconnecting logic elements it is possible to connect up to six of them to an array of DSPs with shared memory.
c) An upgrade path. These DSPs are developed further and code compatible DSPs with improved architectures are brought to the market. This gives the ability to build an enhanced Matching Unit in the near future to meet the advanced trigger algorithms needed by upcoming experiments with the HADES detector. This way of increasing processing power to the MU is preferable to the alternative of building one very powerful device in the beginning because of the complexity and costs of such a device. As the product cycle in digital electronics is about two years (i.e. in two years from know, the devices will be twice as powerful than today), it will reduce the complexity (and thus the time needed to build one) and cost of the device significantly to plan the upgrade to a new technology every three years.

In fig. 4.9 the block diagram of the DSP is shown [Ana00].

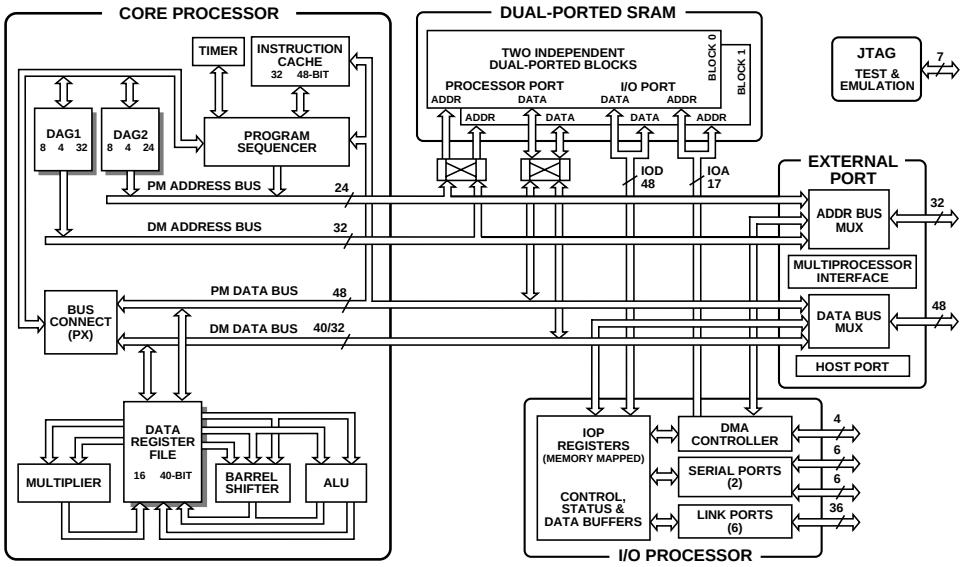

Fig. 4.9: *Block diagram of the SHARC DSP (ADSP-21060) from Analog Devices used by the MU. The advantages of these chips are the two data and address buses (which allow concurrent data transfer and program execution) and the multiprocessing feature with the unified memory architecture.*

The features of this device which are important for the MU are mentioned briefly. The DSP has a 32 bit floating point ALU, which can process 40 million operations of the form $f(x) = ax + b$. It has an internal memory of 512 kBytes, which can also be accessed by random access with 40 MHz. This large memory is necessary for the MU, as it has to store the data from the IPUs and the various look up tables to perform the matching algorithm.

The six link ports allow a data transfer of 40 MBytes/s on each of them without interfering with the ALU, as a dedicated DMA controller is performing the data transport task. These link ports are used by the MU to transport the IPU data to the internal memory of the DSP. Each IPU is connected via the board controlling CPLD (which multiplexes the 8 bit data stream of the IPU to the required 4 bit stream with additional control signals) to one link port.

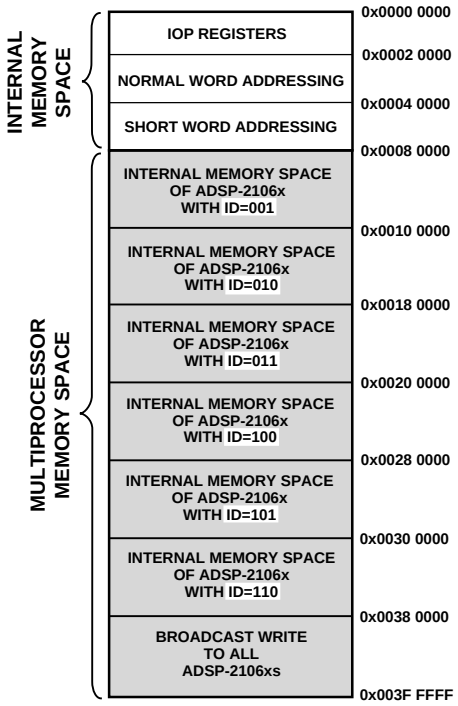

Fig. 4.10: *Unified memory architecture of the ADSP-2106x.*

The possibility of multiprocessing without glue logic allows an array of 6 DSPs with a host controller. The unified memory architecture (fig. 4.10) is essential for the multiprocessing application, as it allows the direct exchange of data between these DSPs (for example implementing semaphores for synchronization I/O operations). The multiprocessing is arbitrated via a *master/slave* scheme. There is always only one DSP which is the *master* and controls the multiprocessing bus, reading and writing to the external memory. It can also write directly into the on-chip memory of every DSP. When a different DSP requires bus access, it has to ask for it via the *bus-request/bus-grant* mechanism. The host controller access is very important for programming the DSPs, writing the lookup tables to the memory, setting various parameters for the current trigger algorithm and accessing internal registers for monitoring purposes during an experiment as well for the test phase. The host controller for the Matching Unit is the local crate CPU and accesses the DSPs via the VME bus.

4.2.4 Board controlling CPLD

The board controller CPLD (**C**omplex **P**rogrammable **L**ogic **D**evice) is responsible for the coordination of all the data transfers to and from the MU.

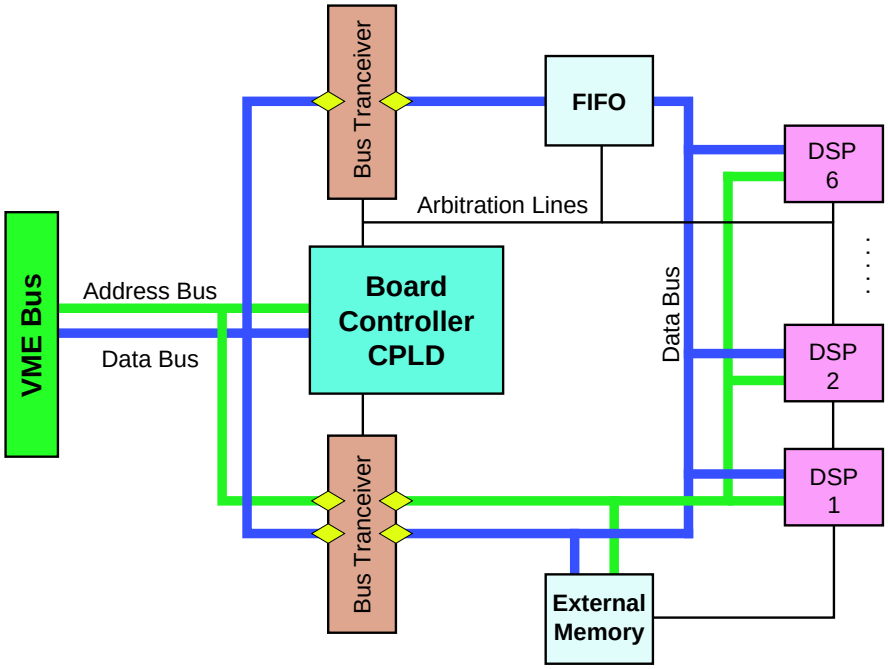

Fig. 4.11: *Functional overview of the data and address buses which can be separated by bus switches to allow simultaneous access of LVL2 trigger data by VME and the usage of the multi-processor bus between the DSPs.*

It activates the corresponding drivers depending on the type of transfer and multiplexes the data from the IPUs.

The following actions and control signals are performed by this CPLD:

a) VME bus interface with the address decoding of all devices accessible by VME. The VME access of the DSPs involves a special handshake mechanism for the host access of the VME CPU. For every access all devices need special signal lines asserted or deasserted to assure that only one is accessed or only one will drive the data bus.
b) Initialization of all devices on the board.
c) Control signals for the input FIFOs on the IPU buses (RESET, Read, Write, Almost Full Flag, Empty Flag, etc.).
d) Multiplexing of the 8 bit data from the IPUs to 4 bit data and generation of control signals for the link port interface of the SHARC DSP. This also includes the appropriate reaction on the state, when there is new data from the IPUs available, but the DSP is not ready to accept it.
e) Sending the LVL2 trigger decision to the CTU via a special VME backplane. The transfer emulates the HADES Trigger bus protocol (see fig. 4.14 on page 74).
f) Controlling all data bus switches on the MU (see fig. 4.11).
g) Display control. On the display the current status and mode of the MU can be seen.

h) Various additional inputs and outputs. For example a standard Lemo connector is added which can generate signals or can be used as an input for further external signals.

The Matching Unit is just another data source from the point of view of the HADES Data Acquisition, thus the local crate CPU has to access the trigger data on the MU. To allow a simultaneous access of the trigger data by the CPU and the usage of the DSP common data and address bus, the MU uses totally switched buses. The DSPs write their data to a large FIFO, which can be read on the other side by the CPU can read from at the same time (achieved by separating the buses). For host controlled access of the DSPs this bus is then switched through. A block diagram of this concept is shown in fig. 4.11.

As explained above, the board controller has to fulfill many tasks with high speed. One possibility to realize this task is to implement each sub task in a separate CPLD. The problem with this solution is the complexity of board layout (uses a lot of space on the printed circuit board), the redundancy which is sometimes required (same function implemented several times in different chips) and manageability of many CPLD designs.

For the MU a different approach is used. It uses a single CPLD, which has a large capacity of logic resources and is able to perform all tasks in one chip. The used device is the PZ3960C from Philips [Phi98], now XRC3960 from Xilinx.

The PZ3960 contains 960 macrocells, entities consisting out of a flip-flop with programmable AND and OR gates. This is sufficient to implement all the required functions. The advantage of a CPLD architecture over an FPGA (**F**ield **P**rogrammable **G**ate **A**rray) is the fixed timing of a signal going through the device. The metallic interconnect allows a fixed timing of about 7 ns from pin to pin for this chip (when no loop backs are used).

This large CPLD has a SRAM to store its configuration which is volatile when the power is switched off. Therefore, the MU needs a second simple CPLD, just for the time after power up until the large CPLD is programmed. This is done by a Lattice 2064 chip. It stores its configuration in an internal non volatile memory and is usable immediately after power up. It provides then a simple VME bus protocol and assures that all configuration pins of the large CPLD are accessible via VME. After the PZ3960 is programed it will show this by a signal which then puts the 2064 into a global three-state mode. In this mode no pins will source or sink current, so in high impedance, but it is still “listening” to the VME bus. The advantage of this scheme is, that the complex design of the board controller can be reprogrammed “in the field” by simple commands from the local VME CPU. That means one does not need to pull out the board from the experiment and put it in the laboratory, where a PC is connected, which can reprogram the chip. This method is needed for the small CPLD with the non volatile memory, but as it is a simple interface, there is no need to do this very often. In practice, this feature turned out to be very useful.

4.2.5 On Board External Memory

In addition to the internal DSP memory, the MU has external memory on the board shared by all 3 DSPs. This memory is 32-bit wide and is used to store large lookup

tables which do not fit into the internal memory of the DSPs. Accessing the external memory requires the DSP to be bus master, as described in chapter 4.2.3 “Digital Signal Processors” on page 67. This will introduce some wait cycles and therefore slow down the table lookup. Hence, the usage of the external memory has to be minimized for full performance. The prototype MU stores the momentum table in the external memory (see chapter 4.1.2 “Momentum Determination” on page 61), since this table is very large and not as often accessed as the x-y to θ–ϕ mapping.

The external RAM devices are SRAMs (**S**tatic **R**andom **A**ccess **M**emory) which allow the fastest access of data at arbitrary positions in the memory without overhead and glue logic (as compared to DRAM).

4.2.6 Physical Interface to the IPUs

There is one common bus standard and physical protocol used to transfer the hit coordinates from the three IPUs to the Matching Unit. The data stream frames are not standardized due to reduction of overhead in the case of the RICH IPU.

In principle, the MU bus is designed to be able to address up to 8 IPUs of each type (RICH, TOF, Shower) as shown in fig. 4.12. The MU initiates a transfer by addressing an IPU via a serial protocol. The addressed IPU on the other hand then switches its drivers to a low impedance mode and starts to send data. The data is sent in 8-bit words but aligned to 32-bit word boundaries. These 32-bit boundaries are a requirement of the SHARC DSPs link ports. The data is then stored in a FIFO, which can buffer a full event of the IPU in case the DSP is busy and can not receive data through its link ports. After receiving a whole sub event from the IPU, the MU addresses the next until all IPUs have sent their data.

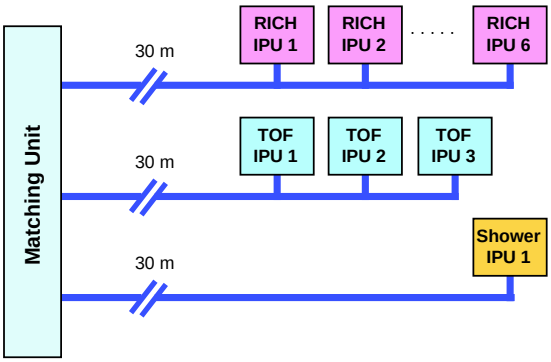

Fig. 4.12: *HADES Matching Unit to IPU bus. It is designed to connect up to 8 IPUs of each type. The current configuration of the experiment is shown.*

The physical link between the IPUs and the MU is according to the RS485 standard. The transfer of data is across twisted pairs of ribbon cable with an impedance of 110 Ω. The ends of the cable have to be terminated to reduce reflections. The transfer is differential, thus any noise will be induced on both wires of the pair and be eliminated at the receiving operational amplifier, as it will only measure the difference in the two signals.

The MU bus works up to 20 MHz over distances tested up to 30 m with 6 receiving/ sending modules connected to the bus. The physical protocol used on the link is shown in fig. 4.13.

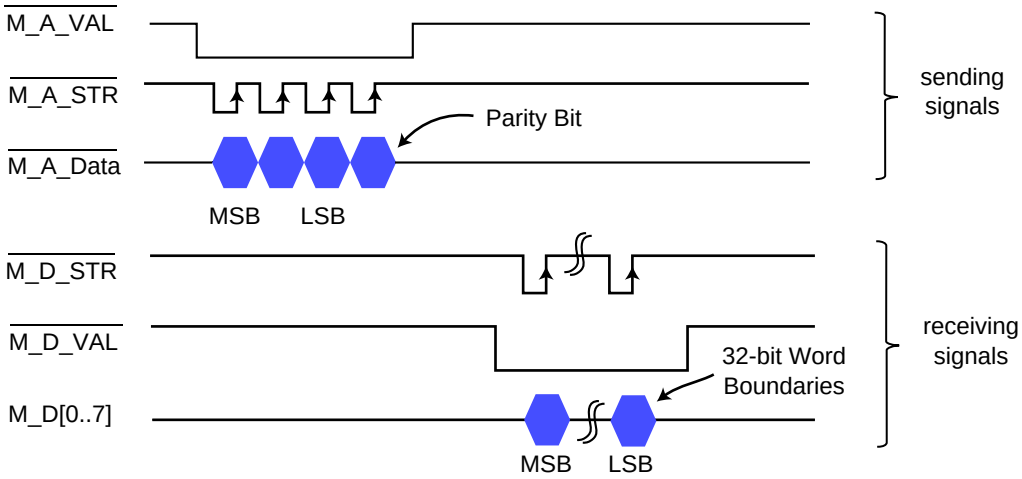

Fig. 4.13: *Protocol of the Matching Unit bus. First a specific IPU is addressed, then this IPU sends its data in 8-bit words, but in 32-bit boundaries.*

The meaning of the signals shown in the figure are as follows:

M_A_VAL:

This signal qualifies the MU address cycle.

M_A_STR:

With the riding edge of this signal, the data bit has to be latched by the IPUs.

M_A_Data:

Data bit of the serial transfer of the address sent to the IPU. It starts with the most significant bit (MSB) and consists of 3 bits. After the least significant bit a parity bit is appended, which is the *XOR* of the 3 bits.

M_D_VAL:

Signal to qualify the data transfer of the IPU to the MU.

M_D_STR:

With the rising edge of this signal, the MU latches the data on the data bus.

M_D[0..7]:

8 data bits to transfer to the MU. The whole data transfer has to be 32-bit aligned.

4.2.7 Interface to the CTU

When the Matching Unit makes its final LVL2 trigger decision, it has to distribute this decision to all detector readout systems. This is done by sending the decision to the CTU which then sends it to all DTUs of every detector sub system.

The MU and CTU are connected via a special backplane on the J2 connector. The protocol of the data transfer is the same as it is used on the HADES trigger bus and is shown in fig. 4.14.

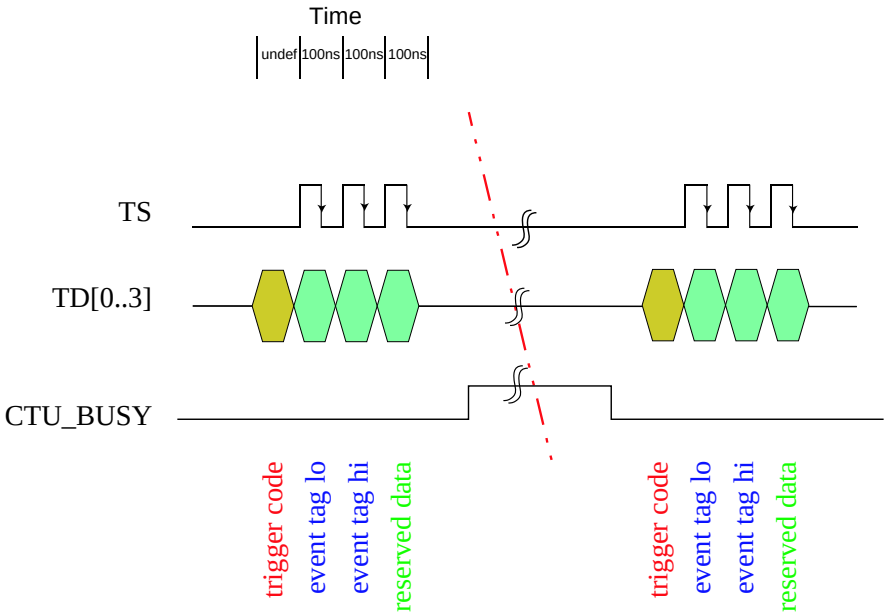

Fig. 4.14: *The transfer of a LVL2 trigger decision to the CTU is shown. The protocol is the same as used on the HADES trigger bus.*

This way of transfer (using only 4 bits to transfer the decision) is slower (especially because the MU has to meet the timing given in the figure) but since the CTU is controlled by a FPGA it is easier for the CTU just to accept the standard format it also uses internally. The MU has to send the trigger tag number of the event and the trigger code for this event, so essentially whether the event should be discarded or read out by the data acquisition. The signals shown in the figure have the following meaning:

T:

Trigger signal. With the falling edge it initiates a transfer of a trigger decision. The trigger code data has to be valid at this time on the TD signals and will be latched by the CTU at this moment. For more information of the trigger code refer to table A.1 on page 101.

TS:

Trigger strobe signal. With its falling edge it qualifies the event tag information. First the lower 4-bit part of the 8-bit word is transmitted, then the upper. The third trigger strobe signal transfers a 4-bit word for future usage.

TD[0..3]:

Trigger data.

CTU_BUSY:

This signal is set by the CTU if it is unable to accept more triggers from the MU. The CTU has the possibility to store up to 15 LVL2 decisions from the MU. When the LVL2 Busy is set by one of the detector sub systems the CTU can not send further LVL2 triggers to the DTUs. If the LVL2 trigger bus is still busy after 15 LVL2 decisions from the MU, also the MU has to stop and wait until the CTU is again able to accept new decisions.

4.2.8 The Matching Unit Printed Circuit Board

The prototype Matching Unit is shown in the following picture (fig. 4.15).

It is a 6 U VME board for usage in standard VME crates. Both sides of the board are equipped with components. On the board the components are surface mounted (**S**urface

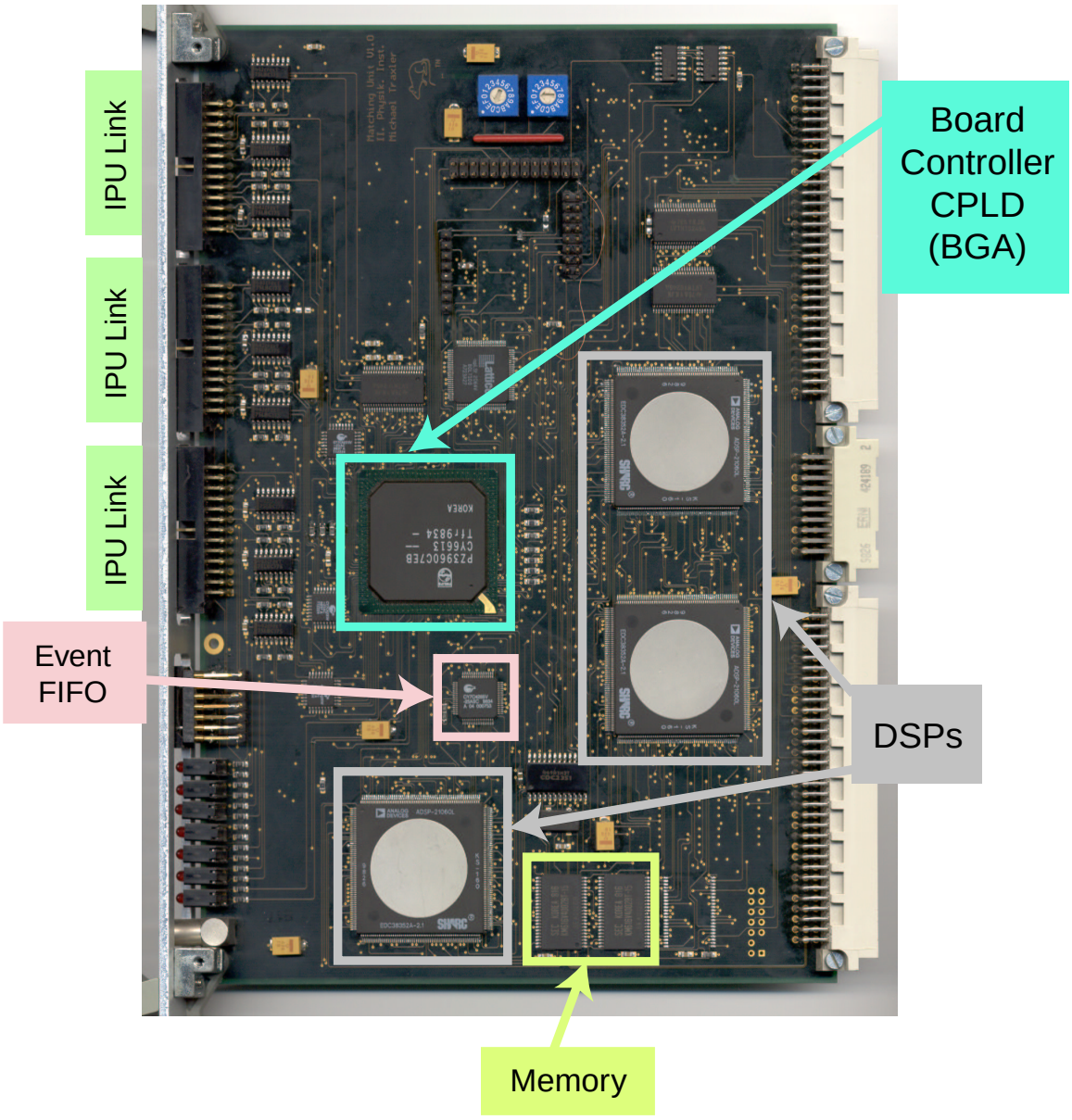

Fig. 4.15: *The prototype of the Matching Unit. The different functional groups on the 6 U-VME board are shown. The right side of the board provides the connectors to the VME bus. On the back side of the board the bus switches are mounted. The board controller CPLD is a Ball Grid Array with 592 balls beneath the chip.*

Mounted **T**echnology, SMT) and the board controller CPLD is a BGA (**B**all **G**rid **A**rray) device, so all 592 connections are beneath the chip. This board has been used in all commissioning beam times as well as for production beam times. It has been shown that all the requirements on the Matching Unit for the second level trigger are met by the prototype, except the processing speed of 100 kHz event rate.

4.3 Software Implementation

4.3.1 IPU to MU Software Protocol

In the previous sections the hardware protocol of the transfer of the hit information of the IPUs to the MU was described. To operate the system one also has to define a higher layer of data protocol. Here the containers for the data have to be defined, because

a) the MU has to know how long every transfer will be, to start a DMA transfer, or to know when it received all the words one IPU has sent.
b) every IPU packs the hit information in a specific way, which is due to the different kind of information and the different abilities the IPUs have.

Detailed information about the exact and most recent data format can be obtained in [MUD01].

RICH IPU Data

The RICH IPUs are all addressed consecutively by the MU. The IPU with the number one corresponds to sector 0 of the detector, and so on. As the RICH IPU has the cleanest hit information available, the expected data volume is the smallest, therefore one needs no DMA transfer (which also implies some overhead) and can use single word transfers.

The structure of the header and data words are shown in fig. 4.16. The header word contains the length of the data sent by this IPU and the trigger tag and code of the event which had these hits. Additionally, the Segment ID is stored there to identify the IPU (to which sector it belongs to).

The data words contain (additionally to the segment ID) the following information:

- The polar (column) coordinates of the hit pattern is found by the formula
  $95 - [8 \cdot (\text{FIFO Nr.-1}) + (\text{position of bit in column pattern which is set})]$.
- The azimuthal (row) coordinate is given by
  Row Number - 23.

These coordinates in the pad plane then have to be converted to real θ and ϕ angles in space, which is done by the transformation described in chapter 4.1.1 “Electron/ Positron Identification” on page 59.

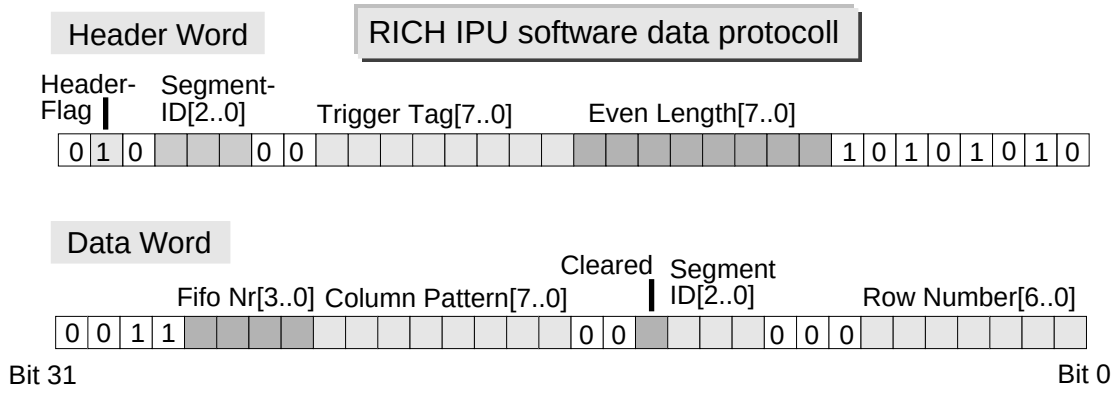

Fig. 4.16: *Structure of the Header and Data words sent from the RICH IPU to the MU. Hits are sent in patterns rather than separated to coordinates of hits.*

TOF IPU data

The TOF hit data is transferred via DMA to the MU. Therefore, the first 32-bit word is just the length of the following data block. Every TOF IPU sends the hit information of two sectors. The data structure is as shown in fig. 4.17.

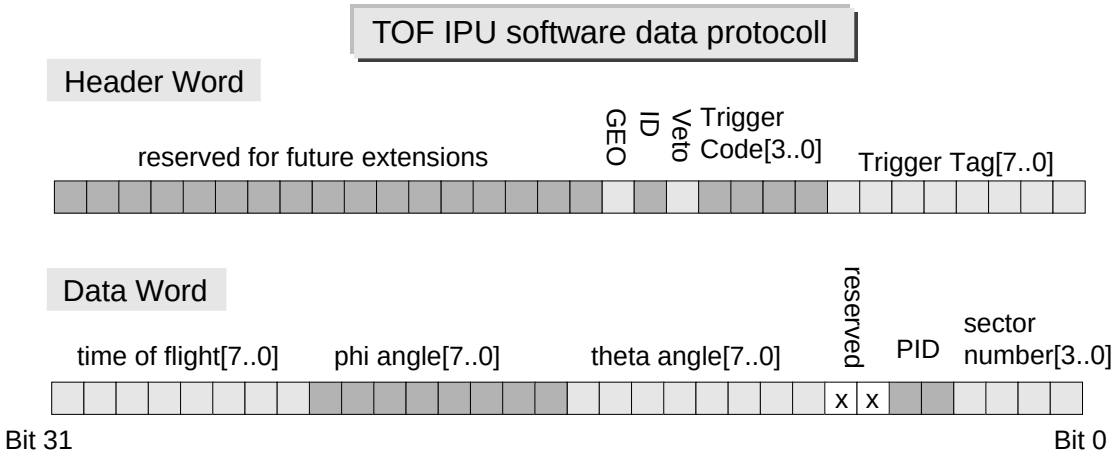

Fig. 4.17: *Structure of the data send from the TOF IPU to the MU.*

Here, the header word contains more information to allow a flexible trigger algorithm. The data words contain real θ and ϕ angles in a 8-bit resolution and information about the time of flight of the particle as well as its particle ID (if it is an electron or not).

Shower IPU data

The Shower data format is similar to the one for the RICH IPU, except that DMA is used for data transfer, due to the volume of data expected. Hence, the first 32-bit word

transferred is again the length of the following data. The format of header and data words is shown in fig. 4.18.

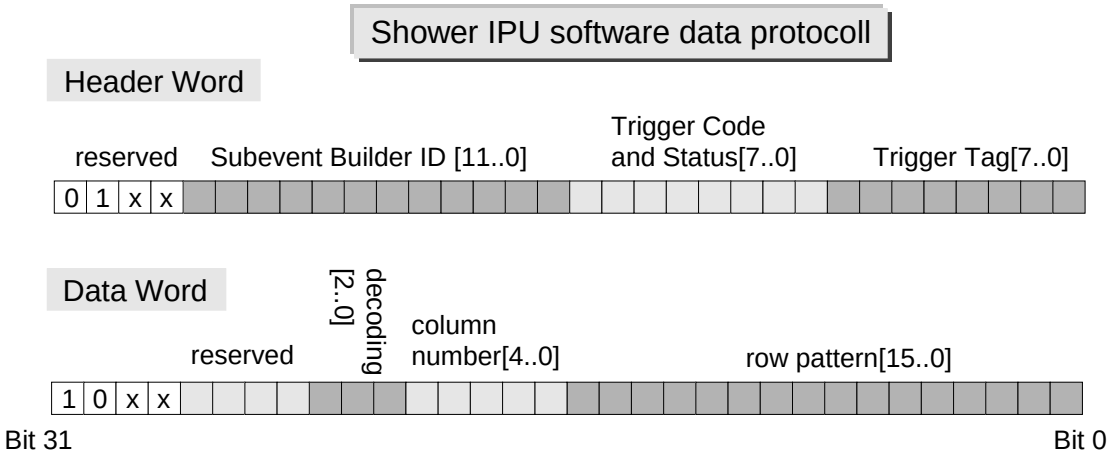

Fig. 4.18: *Structure of the data send from the Shower IPU to the MU. Data is sent as patterns rather than single hits.*

The data is sent as patterns rather than single hits. The reconstruction of single hits out of the patterns is done much more easily in a DSP than in a FPGA. The FPGA based IPUs process the data from the detector with a fixed timing, as the algorithm is always run for the whole pad plane, thus they have a fixed timing and can guarantee a processing time of less than 10 μs. The reconstruction time of hit patterns to single hits is undetermined (it depends on the coverage of the patterns). Thus, the reconstruction would have to run at a significantly higher clock speed.

The next difference is, that there are 12 IPUs (each sector is divided into upper and lower 15 rows and is then analyzed by 2 IPUs), which are identified by the Subevent-Builder-ID. With this number the MU can assign hits to a certain part of the detector.

Matching Unit SubEventData

As explained earlier the MU is just another readout controller from the data acquisition point of view. Therefore, the MU has to deliver data for every event which is conform to the HADES standard [Mue99].

After the standard header the MU sends all information it derived from the IPU hits. It puts the data of all the found leptons and dileptons in the event. This includes the θ and ϕ angles of the lepton when it traversed the RICH detector and its momentum (calculated by the deflection in the magnetic field). Furthermore, the dileptons with their opening angle and invariant mass are stored in the event data. This information is not only useful to speed up the offline analysis, it can also be used by the LVL3 trigger.

For test purposes, the MU can also embed many additional information, like the raw data sent from the IPUs to the MU. This helps to check offline the algorithm implemented in the MU. The details of this format also change (more frequently than for the IPUs) and are found also in [MUD01].

Additionally, counter information is stored (scalers), which allow online monitoring of event rate reduction and internal operation of the algorithm and are essential to determine the trigger efficiency.

4.3.2 The DSP Software

The DSP is programmed in C. Using C as the programming language has the great advantage, that it is easier to read, maintain and change code, as this language is a well known standard. The disadvantage with using C is the speed of execution of the code. As a DSP has very special features and possibilities (as described in chapter 4.2.3 “Digital Signal Processors” on page 67) a abstract language is not able to use these intensively. Therefore, for speed purposes it is recommended to program the DSPs in their special assembly language. But this has the big disadvantage, that every assembly language is different and anyone who has to change the code has first to learn the special language. Since for the prototype speed has never been the main focus, the language C has been chosen.

The program itself consists of several modules, which communicate with each other through the shared memory. The modules are the following ones:

Initialization

In this module all the internal registers are set to the appropriate values and the external devices are reset (for example the FIFOs which buffer the IPU data first). The various lookup tables are written with the help of control programs running on the local VME CPU. For each subdetector the first IPU is addressed and the DMA is set up. After this the MU falls into an idle mode. It works in an interrupt driven mode, so several tasks can be performed “at the same time”.

Interfaces

The different protocols on the various interfaces of the MU have to be implemented in software. The transfer of the LVL2 trigger decision is multiplexed and sent via the board controller CPLD to the CTU. The data sent to the data acquisition has to fulfill the HADES standard. The on board test display is programmed and routines are provided for online monitoring of the MU operation.

Event Building

This module is responsible for collecting the data from the various IPUs in the current configuration. The MU has to wait until the current data transfer of one IPU has finished, address the next in the row (which is also not fixed and can be configured by a table) and start a new DMA respectively single word transfer. This data collecting is concurrent for the three kinds of IPUs. After the last IPU has sent its data, the data is packed to an event.

Unpacking and Transformation of the IPU Data

This data is unpacked following the data format described above (chapter 4.3.1 on page 77). This also includes the transformation of hit patterns to single hits and the transformation of the x-y coordinates of the virtual pad planes to θ and ϕ coordinates.

Hit Matching

The single hits are then matched (rough tracking) according to the algorithm described in chapter 4.1 “The Algorithm” on page 59. This results into a table of possible leptons. For these leptons the momentum and their sign (electron or positron) is determined by their deflection in the magnetic field.

Dilepton Search

The found electrons and positrons are combined to form dileptons. For these an invariant mass is calculated. A window on the mass of these dileptons determines the final LVL2 trigger decision of the MU.

4.3.3 Control Software

For the proper operation of the Matching Unit various external programs have to be provided. Furthermore, the central position of the MU gives the opportunity for online monitoring of the operation of the LVL2 trigger system as well as the processing of the trigger algorithm within the MU. Therefore, programs on the local VME CPU have to access special monitoring registers on the MU and processes on the MU have to provide the required functionality. These programs are called *slow control programs* as they do not fulfill hard real time purposes, but are nevertheless essential for an operation of the whole system. Some of these features and programs are briefly introduced in the following:

Programming the DSPs

The DSPs have volatile memory and have to be programmed for every start of the system. The access to the DSPs is provided by a hardware host controller interface. The VME accesses on the MU board are arbitrated to the addressed DSP by the board controller CPLD, which also handles the handshake necessary to obtain the multiprocessor bus of the DSPs. The DSP program is then transferred by the control program running on the VME CPU to a special boot up register on the DSP and checked for integrity. Special care has to be taken to give the DSPs the opportunity to process their boot up program without further intervention from the slow control.

Loading the Tables and Trigger Registers

After the DSPs are running, they have to be provided with the required lookup tables. These are generated from tables which are output of simulations (xy to θ/ϕ mapping, $\theta/\Delta\theta/\phi$ to momentum mapping). The calibration with the actual magnetic field is applied and the floating point values are converted to fixed point values with the desired granularity. These numbers are then stored on the external memory of the board or in the internal memory of the DSPs.

Furthermore, many parameters controlling the operation of the MU and the applied trigger algorithm have to be transferred to the MU. With these parameters it is possible to control many aspects of the operation of the Matching Unit. In case of the data transport it is possible to run the experiment only with a subset of IPUs, in case a IPU goes out of operation or to remove a whole subdetector. The factor for *downscaled* events is configured, these are events, which are triggered positively in any

case, to assure to have not triggered (but marked) events in the analysis, to determine the efficiency the LVL2 is running with.
The trigger algorithm can be configured in various ways. It is possible to switch on or off all the steps explained in chapter 4.1 “The Algorithm” on page 59 and set thresholds for the each step. For example, one can demand just one found lepton candidate in the IPU data to trigger a positive decision.

Online Monitoring of the Internal Operation

Procedures have been employed to allow the online access to the Matching Unit via a VME CPU to monitor the current status of operation. This is done by directly accessing the memory in which the MU stores the current status in clear text. This gives the very important opportunity to immediately check the reasons for some error condition. In different levels all the steps the MU performs can be displayed and tracked of errors in the MU or the connected IPUs. Due to this very useful feature the MU has often been used to analyze problems on the IPUs occurred only in the common system at high rates.

Monitoring Tools for the Operator of the DAQ

The features and programs described above are intended just for the usage of an expert, who knows exactly how the MU operates.
Additionally, the MU provides some very useful information for the operator of the data acquisition. It is for example used to display the actual rates of LVL1 and LVL2 triggers during an experiment and even the momentarily rates during a spill structure of the accelerator. Problems with the accelerator as well as problems in the data acquisition system (which normally lead to “pumping” effects in the momentarily event rate) can instantly be seen in the event rate behavior, which are obscured by an average rate display.

Chapter 5

Results and Perspectives

The Matching Unit has been successfully used in the last year during several HADES commissioning beam times at GSI in Darmstadt.

The experiences and results of the last beam time (which was scheduled as a dedicated LVL2 test beam time) are summarized in this chapter. First the software necessary for analyzing the data is reviewed. The results of the performance of the hardware and the algorithms are shown. Then possible improvements to the Matching Unit are mentioned and the full performance Matching Unit (to be built) is described.

5.1 Analysis

To investigate the functionality of the HADES second level trigger system it is necessary to survey the data taken during beam times. This includes

a) to check the proper operation of the hardware,
b) to check the validity of the hardware algorithms and their functionality in hardware and
c) to optimize the parameters of the algorithms.

For example, lowering thresholds in the RICH IPU will increase the ring finding efficiency up to a certain limit (due to background), but at the same time the fake rate (i.e. falsely identified rings) will also increase. Tight θ and ϕ cuts used in the matching algorithm will reduce the event rate substantially, but also reduce the efficiency and will introduce momentum cuts. An optimum has to be found, without putting any physical bias on the trigger condition.

For this task the RICH IPU, TOF IPU, Shower IPU and the Matching Unit have to be simulated in software and the results of the offline analysis and hardware algorithms (performed in software as well as in the hardware IPUs) have to be compared.

5.1.1 LVL2 Trigger Efficiency

Definition:

For the further discussion it is necessary to define the LVL2 trigger efficiency:

The only meaningful definition for the efficiency can be a measure of the performance of the LVL2 trigger to find real electron/positron pairs which traversed the detector in a certain invariant mass window. Thus, the integral efficiency of an experiment is the number of identified electron/positron pairs (fakes not counted) divided by the number of real electron/positron pairs which actually were produced and traversed the detector. This is a very difficult quantity to measure, as one normally does not know exactly how many electron/positron pairs were produced.

A simulation of the detector is *not* sufficient for precision experiments, as it is not possible to simulate every aspect of the detector in detail. Thus, one has to use very well known processes to provide an external physical reference. This means, a known precision experiment has to be repeated with the HADES detector and the results compared to the already known results.

It is essential to point out the importance of this measurement. There is no other way to determine a reliable efficiency of the detector and the second level trigger system.

For example, one can use the η Dalitz decay to determine the HADES trigger efficiency. A possible experiment would be $pp \rightarrow pp\eta \rightarrow pp\gamma e^+e^-$.

The problem which arises when using this method is that the measured efficiencies are not directly transferable to for example heavy ion experiments, as the background is totally different.

A way to minimize this limitation is to use arbitrary real events taken during beam operation from a heavy ion experiment and artificially mix electron/positron signatures into the data. The result of the analysis of this data gives a good, but not exact, approximation of the efficiency of the detector and the trigger system.

RICH Efficiency, Fake Rate and Double Rings:

Important for the determination of the efficiency is the fact, that the RICH detector has the largest hadron suppression capability of all subdetectors. Therefore, it is important to optimize the operation of the RICH IPU.

To illustrate the difficulty involved in finding rings a real event with three rings found by the RICH IPU is shown in fig. 5.1.

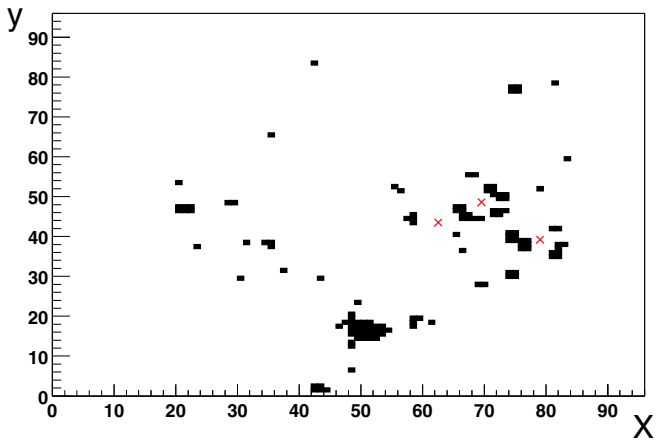

Fig. 5.1: *The 96x96 pad plane of the RICH IPU is displayed. The crosses mark ring centers the RICH IPU has found.*

This picture demonstrates that only a few pads provide a signal for a ring. There are several possible sources for such a ring, for example π^0 Dalitz decays ($\pi^0 \rightarrow \gamma e^+ e^-$), pair conversion of photons in the target or the radiator gas and decays of a vector mesons. The difference between these processes are, that only the decay of the vector mesons have a large opening angle of the electron/positron pair. The other processes can have opening angles that are so small that the centers of the Cherenkov rings are within the same pad in the RICH detector, and are denoted double rings.

Therefore, one has to optimize 3 parameters which depend on the threshold used for the ring finding algorithm used in the RICH IPU. For very low thresholds, the RICH IPU will find all rings and will therefore have an efficiency of 1. But on the other side it will also find many rings which are fakes, thus the event reduction factor of the LVL2 trigger will be low.

If one increases the thresholds to large values, the fake rate and the efficiency will drop. But additionally, the relative rate to trigger on double rings compared to single rings will increase, as the double rings produce more light and are more likely to be found by the RICH IPU.

Hence, high thresholds will bias the second level trigger on π^0 Dalitz decays and conversion pairs. The di-electrons from vector meson are suppressed.

This dependence is qualitatively shown in fig. 5.2.

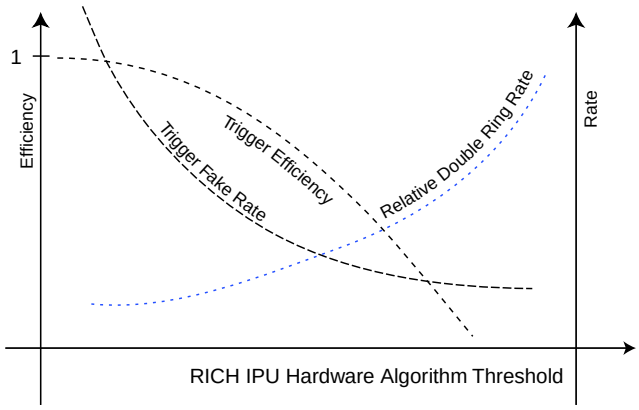

Fig. 5.2: *Qualitative plot illustrating the dependence of the efficiency, fake rate and fraction of double ring found by the algorithm on the thresholds set for the ring algorithm in the RICH IPU.*

This discussion demonstrates the importance to carefully select the thresholds for the ring finding algorithm in the RICH IPU, because they will influence the efficiency, fake rate and even can put a physical bias in the second level trigger.

Hardware Efficiencies:

Since we have not yet performed experiments such as measuring the η Dalitz decay, we can not quote an absolute trigger efficiency as defined above.

Nevertheless, we can make internal cross checks of the electrons and di-electrons found by the trigger hardware relative to the ones found by the offline analysis. The offline analysis offers a more sensitive method for lepton identification than is available online. The absolute efficiency for the offline analysis to find a lepton is defined as ε_{ana}.

In addition, the fraction of the leptons found by the offline analysis which also produces positive LVL2 triggers is defined as ε_{trig}. Thus the absolute trigger lepton finding efficiency is given by the product $\varepsilon_{ana} \times \varepsilon_{trig}$.

5.1.2 Analysis Software Framework

For the HADES analysis the *HYDRA* package has been written [Had01]. It is a C++ analysis package in the ROOT [Rot01] environment. ROOT is a C++ analysis environment, which provides all essential methods to store, retrieve and display data sets very efficiently.

HYDRA contains classes for the full event reconstruction and analysis.

The reconstruction is divided into several steps:

a) Reading event information from the data sets written by the data acquisition.
b) Retrieve all the parameters from a database describing the detector setup (position information, temperatures, calibration files) during the data taking.
c) Detecting particle hits in the subdetectors using pattern recognition techniques.
d) Reconstruct tracks
e) Fitting reconstructed tracks to obtain the momenta of the particles.
f) Correlate hits in the RICH with TOF and Shower.

The result of such a reconstruction and correlation can be lepton identification and hadron identification [San00b].

A Matching Unit and IPU analysis and simulation has been integrated into this HYDRA framework [Toi01]. The analysis includes the unpacking of the raw (binary) information stored in the data files, emulation of the IPUs and Matching Unit hardware algorithms in software and different comparisons to determine the efficiency ε_{trig} of the LVL2 trigger compared to the HYDRA analysis.

The comparison of software emulation and hardware algorithms is done in different stages (fig. 5.3):

a) The online pattern recognition of the IPUs is compared with an offline emulation of the IPUs: The IPU data can be accessed via the Matching Unit subevent and the IPU emulation is done with the raw event data from the detector readout (which is also the data source for the hardware IPUs).
b) The results of the matching algorithm is checked for consistency with an emulation of the Matching Unit using the hits found by the hardware IPUs.
c) The full LVL2 trigger is emulated using the raw detector data. The found leptons are compared with the leptons found by the offline Hydra analysis, which is taken as a reference. This results in a trigger efficiency for the LVL2 trigger, assuming that all IPUs worked as specified.
d) The Hydra analysis is compared with the results of the hardware LVL2 trigger. This gives the hardware LVL2 trigger efficiency, using the Hydra analysis as the reference.

The result of the efficiency determination is described in the following paragraph.

5.1.3 Second Level Trigger Algorithm Efficiency

Taking the data from the April 2001 beam time, the Hydra analysis was used to find all leptons in the data. Comparing this to the full LVL2 trigger emulation the following lepton finding efficiency ε_{trig} of the LVL2 trigger algorithm for a reduction factor of 16 was determined (fig. 5.4).

The data was taken for $^{12}C+^{12}C$ events at 1.5 AGeV.

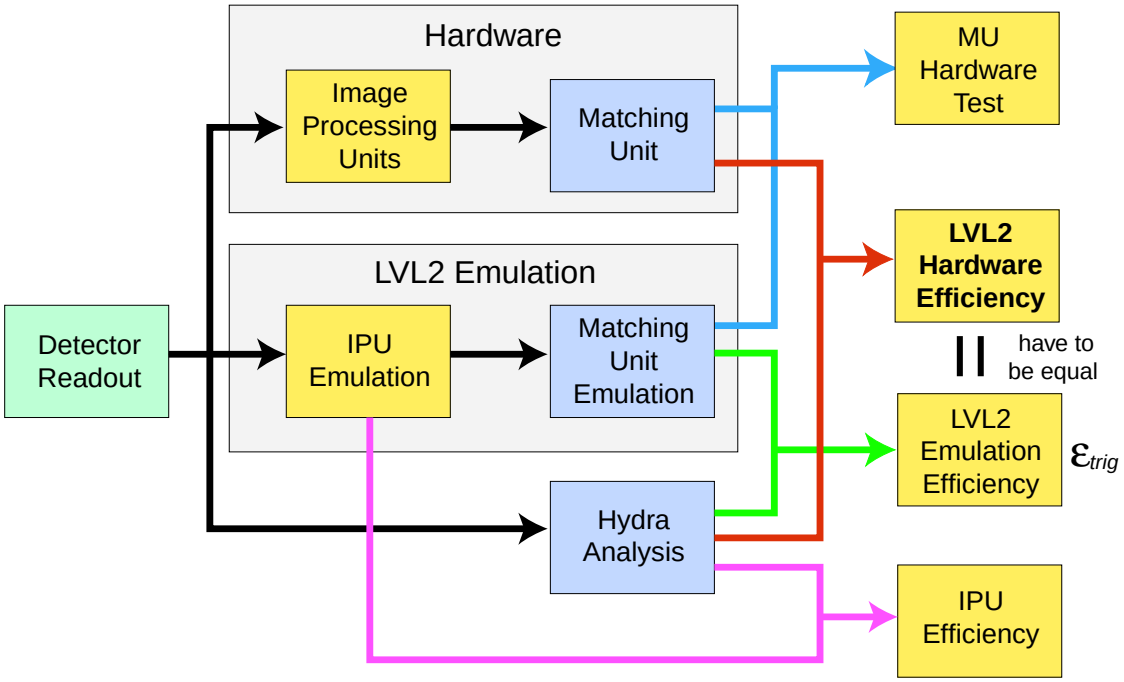

Fig. 5.3: *The data flow for the different consistency tests and determination of the LVL2 trigger efficiency compared to the offline analysis is shown. The results from the LVL2 trigger (stored in the Matching Unit subevent data) are compared with either the MU and IPU emulation or the results of the Hydra analysis as a reference. This is not the real di-electron trigger efficiency.*

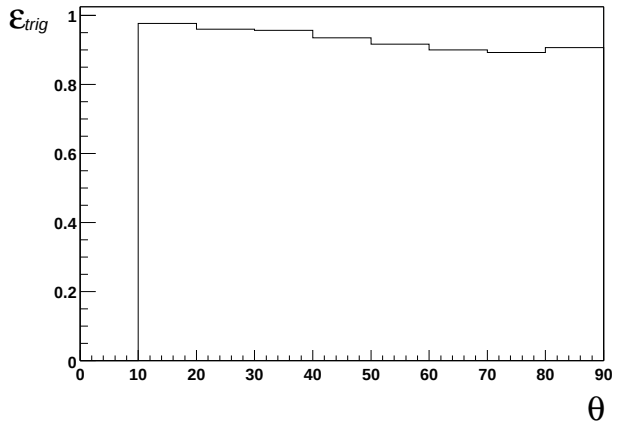

Fig. 5.4: *Trigger algorithm efficiency ε_{trig} versus polar angle θ for a reduction factor of 16. It is almost 1 for most of the leptons. The integrated efficiency amounts to about 93.7%. Below $\theta = 15°$ HADES has no acceptance.*

The Matching Unit trigger conditions were the requirement of one hit in RICH, at least one hit in TOF and Shower and a azimuthal ϕ window of $\pm 20°$. No polar θ cut was applied. For this calculation a run with 360000 events was used. The LVL2 trigger emulation reduced the number of events by a factor 16. There were 165 events dis-

carded by the emulation out of the 2648 events where at least 1 lepton was found by the Hydra analysis. This gives the mean efficiency

$$\varepsilon_{trig} = 1 - \frac{165}{2648} = 93.7\% . \quad (5.1)$$

The mean number of fakes per event is 0.24. This is larger than 1/16 because very often multiple fakes are found in a given event.

This comparison shows that the LVL2 trigger algorithms with the one lepton condition have a very high efficiency while reducing the number of events by only a factor of two.

Further analysis has to show an optimum for the thresholds of the LVL2 trigger algorithms and Matching Unit algorithm parameters and the achieved reduction rate. Tight conditions will increase the reduction rate but will at the same time decrease the efficiency and can put a bias on the trigger condition as discussed in chapter 5.1.1 on page 84.

5.2 Results from September 2001 Beam Time

In this section results of the IPUs and Matching Unit operation are presented. During the beam time in September 2001 ($^{12}C+^{12}C$ at 1 AGeV) the following setup concerning the LVL2 trigger was available:

a) 6 RICH IPUs (full setup, all six sectors operational)
b) 3 TOF IPUs (full setup, all TDCs were read out, but only ADCs for 1 sector)
c) Matching Unit with full implementation of the LVL2 trigger algorithm.

When positive triggers are given, the event rate is mainly limited by the readout of the subdetectors, which is currently at 2.5 kHz. The Matching Unit was tested with forced negative decisions which resulted in an event rate of about 25 kHz.

Therefore, during the beam time, the limited performance in event rate of the MU was not a limiting factor in data taking.

Before checking the operation of the MU, one first has to prove the operation of the connected IPUs. This is done by comparing the data delivered by the IPUs to the MU (stored in its subevent data) and the emulations with Hydra.

RICH IPUs:

The RICH IPU algorithm to find the centers of the Cherenkov rings is explained in chapter 3.2.1 “RICH IPU” on page 44. This algorithm is very different from the algorithm used in the Hydra analysis. Since the offline analysis has many more possibilities to optimize the ring finding, these offline rings are used as a reference. But nevertheless, one has to keep in mind, that also the offline analysis algorithm is based on thresholds which have to be optimized. Furthermore, there are principle limitations in increasing the ring finding efficiency, as the background in the RICH data will not allow a 100% identification of all rings, in software and hardware. Thus, only a known external physical reference can be used as reliable reference to measure real lepton recognition efficiencies (see chapter 5.1.1 on page 84).

The correlation of the ring centers found by the RICH IPUs to the centers found by the analysis is shown in fig. 5.5. The correlation shows a very good agreement of ring center coordinates found by the IPU and found by the offline ring finder.

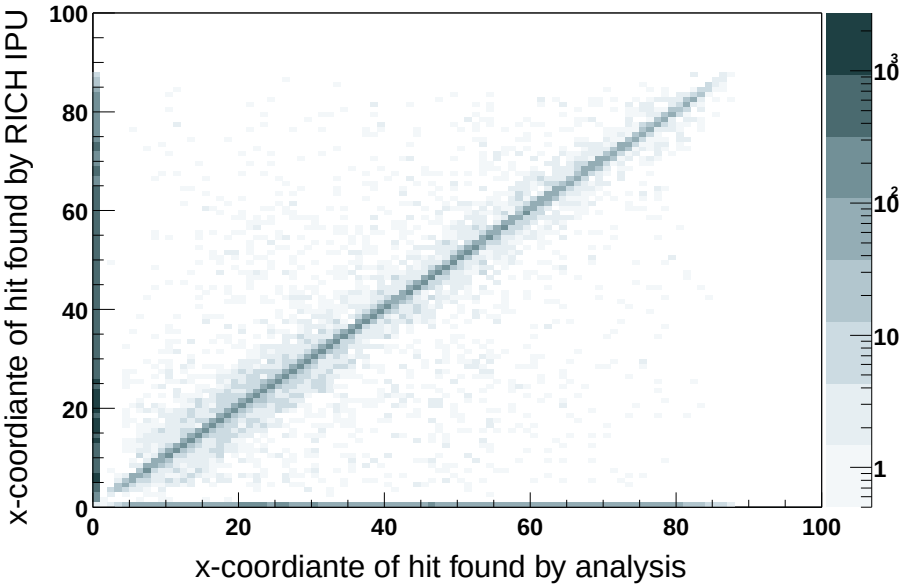

Fig. 5.5: *Correlation of ring center x-coordinates found by the offline analysis and the RICH IPU. The entries on the y-axis correspond to the fakes found by the IPU and not by the analysis. The entries on the x-axis show the events found by the offline analysis and not found by the IPU, so they reduce the efficiency of the RICH IPU.*

TOF IPU:

For the TOF IPU two correlations with the analysis can be done. One for the hit coordinates and one for the time of flight correlation. Since the algorithms are the same for the online and offline hit and time of flight determination, the correlations should be exact. They are shown in fig. 5.5 and fig. 5.7. Small variations are due to resolution differences in mapping the TOF hit angle, and because the TOF IPU uses integer values whereas the analysis is using floating point calculations.

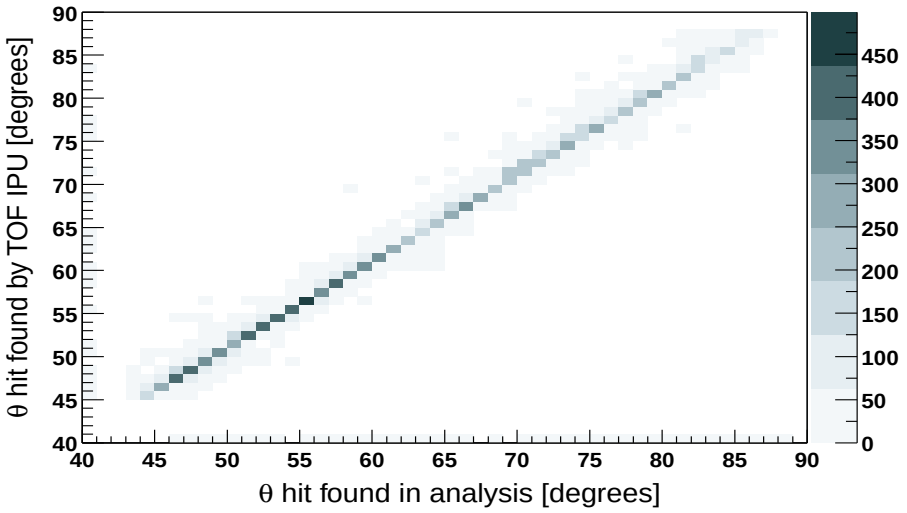

Fig. 5.6: *Correlation of the θ angle of hits in the TOF found by the TOF IPU and the offline analysis.*

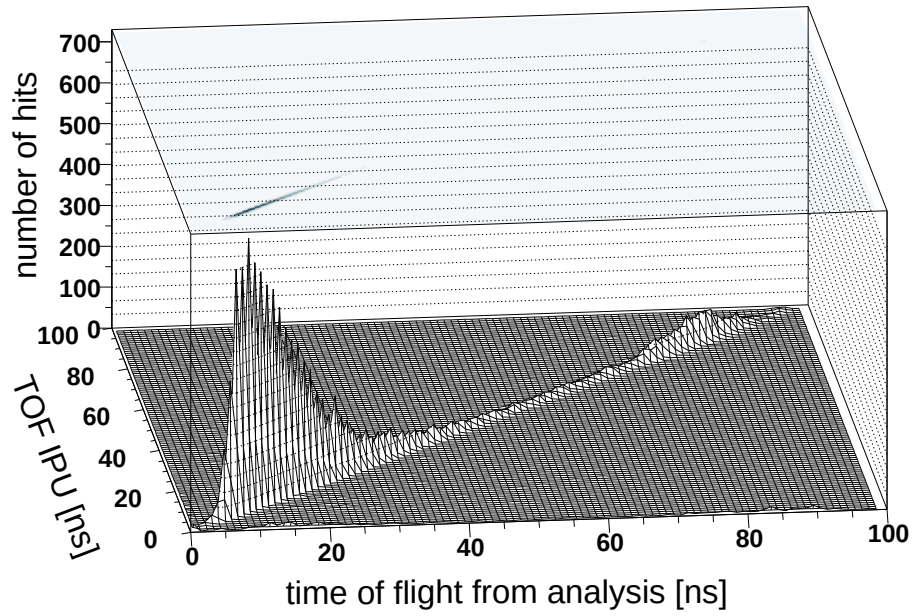

Fig. 5.7: *Correlation of the time of flight calculated by the TOF IPU and the offline analysis.*

5.2.1 Experiments with the Matching Unit Using Beam

The Matching Unit with the full trigger algorithm implemented was used during the september and November 2001 beam time. The reaction used was $^{12}C+^{12}C$ at 1.5 AGeV and 2.0 AGeV. Extensive tests have been performed to test the functionality and accuracy of the algorithm. The information the Matching Unit delivers for each event is the following:

a) Number of hits found in the IPU data for RICH, TOF and Shower IPU.
b) Sector hit pattern for each IPU (information in which sector there were hits found).
c) Number of leptons found.
d) A list of all leptons with their corresponding RICH-TOF or RICH-Shower pairs and the momentum of the lepton.
e) Number of dileptons found.
f) A list of all dileptons found with their opening angle and invariant mass and the identifiers of the corresponding leptons.

With this information all steps of the MU can be tested and possible errors in the implementation of the algorithms can be found.

To demonstrate the functionality of the MU one has to compare the results from the MU with the emulation of it. Therefore, the effect of the Matching Unit emulation on the raw events is shown and compared with the output of the hardware MU.

In fig. 5.8 the differences in ϕ (azimuthal) angles of the hits found by the RICH IPU to the hits found by the TOF IPU are plotted versus their differences in θ (polar). In this plot all matched RICH hits with TOF hits (which belong to the same sector) of all 80000 hits are displayed, no emulation and no trigger algorithm in the data taking was used.

The reason for the asymmetry in $\Delta\theta$ of approx. 40° is due to the geometry of the RICH and TOF detectors. The RICH detector covers the θ angles from approx. 15° to 85°, whereas the TOF detector only covers 45° to 85°. This results in a $\Delta\theta$ range from -70° to +40° which also is seen in the plot. Due to the reduced ring recognition efficiency at the edges of the RICH detector the full range for $\Delta\phi$ angles is not covered.

The Matching Unit with the following trigger conditions was used:

a) exactly one hit found in the RICH IPU
b) at least one corresponding hit found in the TOF IPU
c) a $\Delta\phi$ window of $\pm 15°$

Hits which fulfill these requirements are called lepton candidates in the following.

The positively triggered data from the hardware Matching Unit is displayed in fig. 5.9. Here, 5885 leptons were found. This very conservative trigger condition results in a trigger rate reduction by a factor of 80000/5885 = 13.6. The main reduction originates from the ring finding in the RICH IPU. There were 71627 events with no hit found in the RICH IPU. The remaining 8373 hits were then matched by the MU with the hits found by the TOF IPU, which then discarded 2488 events and 5885 lepton candidates remain.

The results of the emulation and the hardware MU are the same, no discrepancies are found. This comparison includes the search for leptons found by the emulation and not found by the hardware MU and vice versa.

This analysis proves the functionality of the Matching Unit in beam conditions. The hardware works correctly and reliably. The basic algorithm is performing as expected. A detailed analysis of the matching algorithm is in progress, to check the more complex

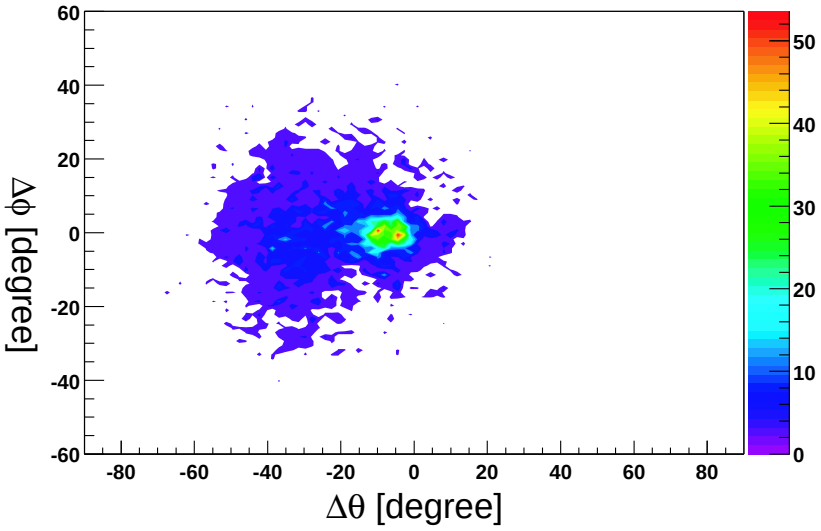

Fig. 5.8: Δθ *versus* Δϕ *for the RICH and TOF IPU. No trigger condition was applied. From the total of 80000 events only the events are shown, where at least one hit in the RICH and one hit in the TOF in the same sector were found.*

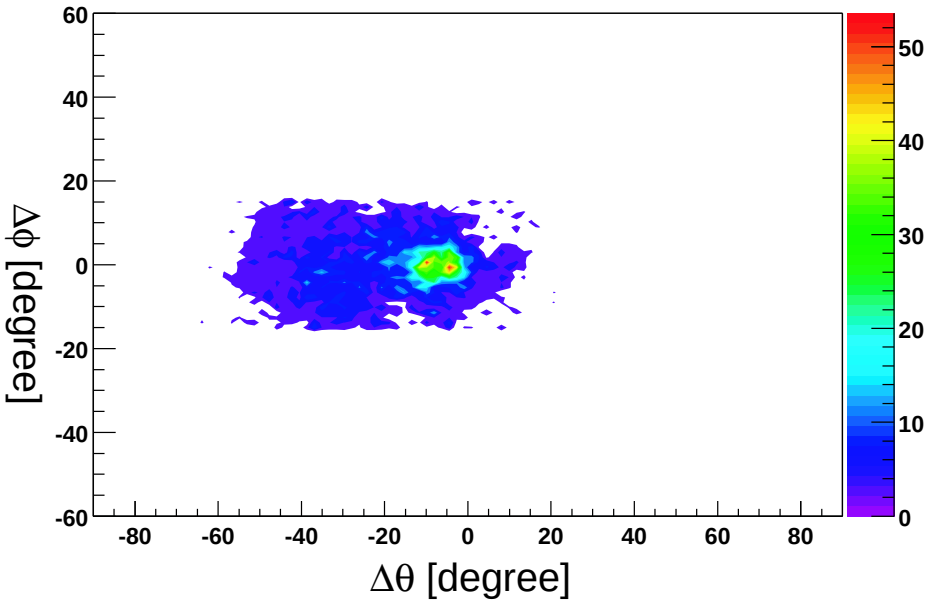

Fig. 5.9: Δθ *versus* Δϕ *for the RICH and TOF IPU. The hardware Matching Unit was used, with the condition: 1 hit in the RICH, at least 1 hit in the TOF and a* ϕ *window of 15°. 5885 found leptons are displayed. The cut in the* ϕ *angle can be easily recognized in the plot, no entries for* Δϕ *larger than 15° can be found.*

dilepton invariant mass determination. This is done in a step by step process, as one also needs large statistics to test the Matching Unit for problems which can occur very rarely.

In the following possible improvements to the MU are discussed and a concept of the next version of the MU hardware is introduced.

5.3 Outlook

The experiences with the Matching Unit allowed the functionality of the hardware concept as explained in chapter 4.2 on page 64 and the correctness of the matching algorithm to be demonstrated.

The differential interfaces to the IPUs have proven to be fast, reliable and not prone to transfer errors due to noise. The connection to the CTU worked without problems. Also the concept of the parallel execution of programs in independent DSPs proved to be adequate for the task the MU is designed for.

5.3.1 Possible Improvements

The MU uses a *scheduling* DSP for receiving the data from the three IPUs and building subevents before sending this data to one of the other DSPs for performing the matching algorithm. This concept turned out to be not ideal for the HADES LVL2 trigger. The work done by this scheduling DSP was underestimated, as the real world overhead has not been taken into account, namely the check of data consistency and the size of the IPU data is larger for test purposes. Therefore, the data transport alone can exceed 10 µs on average in certain configurations (more than 6 IPUs used by future extensions to the LVL2 trigger). Additionally, the software development and maintenance demands the lowest complexity as possible (using KISS, **k**eep **i**t **s**mall and **s**imple, as a guideline). For these reasons, the architecture should be changed in a way, that from the IPUs to the data processing DSP no additional pipelined step is introduced. This means, that the data from the three IPUs is transferred directly to each DSP, without the scheduling DSP used in the prototype MU.

Additionally, there are plans for the extension of the HADES detector with additional subdetectors which also should be included into the LVL2 trigger. Therefore, an additional IPU input has to be foreseen.

Moreover, it would be useful to connect the Matching Unit also to the LVL1 and LVL2 trigger bus, to monitor the LVL1 triggers and to have the possibility to issue a busy condition.

The next Matching Unit will incorporate the improvements explained in the last section. The concept is shown in the block diagram in fig. 5.10.

The new features include:

a) the connection of up to 4 IPUs
b) a crossbar switch redirects the data streams directly to a certain DSP, without going through a scheduling DSP
c) an interface to the HADES trigger bus allows the monitoring of the LVL1 triggers by the CTU and comparing them with the data from the IPUs and the possibility to signal a busy condition on the MU

The main advantage is the missing scheduler, which removes the pipelined step of data receiving and event packing. This increases speed and reduces the complexity of the code necessary for operation of the MU. Using this approach, essentially the same code can run in all DSPs. The DSPs used on the new version of the MU are the next generation of the SHARC DSPs. Their execution time is 3-4 times as fast as the old DSPs which will give the possibility for new and more complex trigger algorithms.

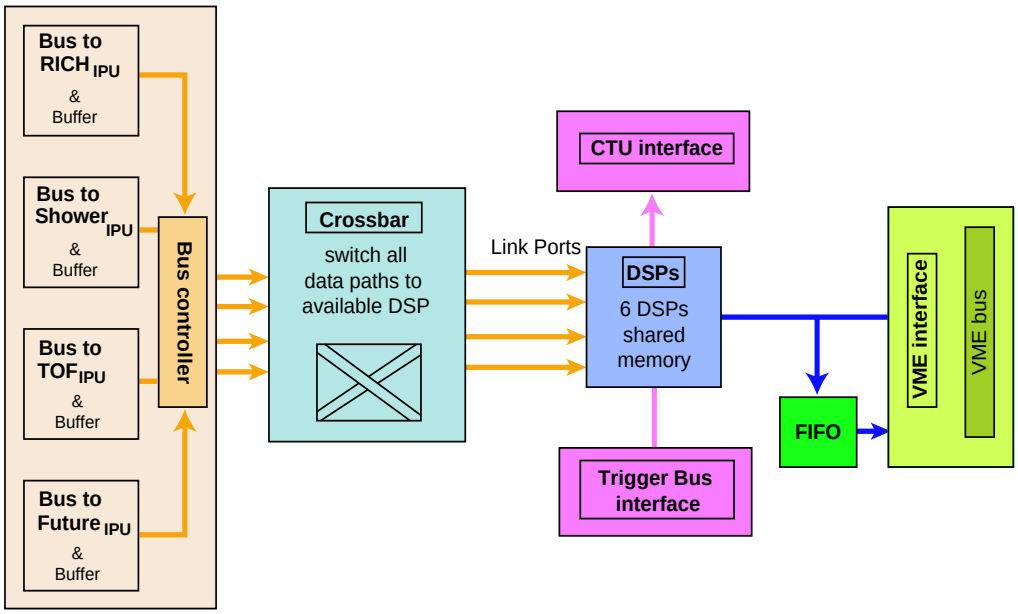

Fig. 5.10: *Block diagram of the next Matching Unit. Important changes: Crossbar switched data streams to DSPs, connection of up to 4 IPUs, interface to the HADES trigger bus.*

Additionally, a concentrator board is planed to be built, which simultaneously addresses the different IPUs of a given type, collects the data and sends the data in one packet the MU. This will reduce the latency introduced by subsequent addressing of the IPUs on the long cables where the signals have a transit time of about 400 ns.

References

[Abr96]: Abreu, M.C. et al., (NA38 collaboration), Phys. Lett. B 368, 230 (1996); Abreu, M.C. et al., (NA50 collaboration), Nucl.Phys. A610, 331 (1996).

[Amb99]: Ambrogiani, M. et. al., Phys. Rev. D60 (1999).

[Ana00]: Analog Devices, *ADSP-2106x SHARC, DSP Microcomputer Family Rev. D,* Analog Devices, 2000

[Ant98]: Antonelli, A. et al., Nucl.Phys. B517 (1998) 3.

[Ale80]: Alekseev, G.D., et al.: *Investigation of Self-Quenching Streamer Discharge in a Wire Chamber,* Nucl. Inst. Meth. 177 (1980) 385

[Ata82]: Atac, M., Tollestrup, A.V.: *Self-Quenching Streamers,* Nucl. Inst. Meth. 200 (1982) 345

[Bal98]: Balanda, A., et al.: *Development of a fast pad readout system for the HADES shower detector.* Nuclear Instruments and Methods in Physics Research A417 (1998) 360

[Bar85]: Barkov, L.M., et al., Nucl. Phys. B 256 (1985) 365.

[Bas98]: Bassini, R.: *A 32 Channel TDC (ADC) on VME Board*. Istituto Nazionale di Fisca Nucleare - Sezione di Milano, 1998

[Bat70]: Bathow, G., et al., Nucl. Phys. B20, 592 (1970)

[Bet30]: Bethe, H.A.: Ann. d. Phys. 5, (1930)

[Bir64]: Birks, J.B.: *The Theory and Practice of Scintillation Counting* (Pergamon, London, 1964).

[BMu98]: Braun-Munzinger, P., Stachel, J., Nucl. Phys. A638 (1998) 3c

[Böh99]: Böhmer, M.: *Das Auslesesystem für den Ringabbildenden Cherenkovdetektor im HADES Spektrometer.* Diplomarbeit, Physik-Department der Technischen Universität München, Institut E12, 1999

[Bra98]: Bratkovskaya, E.L., Cassing, W., Rapp, R., Wambach, J.: *Dilepton production and mT-scaling at BEVALAC/SIS energies.* Nucl. Phys. A 634 (1998) 168.

[Bro91]: Brown, G.E., Roh, M.: Phys. Rev. Lett. 66 (1991) 2720

[Cal01]: Calabrese, R., *Experimental Status Report on Time-Like Baryon Form Factors*, Proceedings of the 2001 e+e- Physics at Intermediate Energies Workshop, http://www.slac.stanford.edu/econf/C010430/W07.html, (2001)

[Cer37]: Cherenkov, P.A.: *The visible glow of pure liquids under the action of gamma-rays*. Dokl. Akad. Nauk. SSSR [Sov. Phys. Dokl.] 2:451 (1934)

[DLS95]: DLS Collaboration, Dilepton Production from p-p to Ca-Ca at the BEVALAC, Nuclear Physics A583 (1995) 617c-622c

[Dov71]: Dover, C.D., Hüfner, J., Lemmer, R.H.: Ann. Phys. 66 (1971) 248

[Dre97]: Drees, A. et al: *Open charm contribution to dilepton spectra produced in nuclear collisions at SPS energies*, Z. Phys. C. (1997)

[Dru93]: Druzhinin, V.P. et al., Preprint, INP84-93 Novosibirsk

[Dzh83]: Dzhelyadin, R.I. et al., Phys. Lett. B102, 296 (1981)

[Fey72]: Feynman, R.P.: *Photon Hadron Interactions*, Benjamin, Reading (1972).

[Fri98]: Friedman, E. and Gal, A.: *On the determination of the pion effective mass in nuclei from pionic atoms*, nucl-th/9805004

[Gar93]: Garrow, K.: *HADES Simulation of TOF and SHOWER*, (1993)

[Gar98A]: Garabatos, C. et al.: *The HADES dilepton spectrometer.* Nuclear Physics B 61B (1998) 607

[Gar98]: Garabatos, C. et al.: *Optimisation of low-mass drift chambers for HADES*. Nuclear Instruments and Methods in Physics Research A412 (1998) 38

[Gil97]: Gilg, H. et al, *Effective pion mass in the nuclear medium deduced from deeply bound pionic states in* ^{207}Pb, Phys. Lett. B 418 (1998) 246-251

[HaC01]: The HADES Collaboration: *Dilepton Production in CC and* $\pi^{\pm}$ *p Reactions*, http://www-hades.gsi.de, May 2001

[Had01]: Hades Analysis Group: *The Hydra Analysis Package*. http://www-hades.gsi.de/computing (2001)

[Had94]: HADES-Kollaboration: *HADES: A proposal for a high acceptance di-electron spectrometer.* GSI Darmstadt, 1994

[Hel95]: Masera, M. for the HELIOS-3 Collaboration, Nucl. Phys. A590, 93c (1995); A.L.S. Angelis, et al. (HELIOS-3 Collaboration), Eur. Phys. J. C.

[Hol97]: Holzmann,R. et al., Phys. Rev. C 56, R2920 (1997)

[Hye93]: Hyer, T., Phys.Rev. D47 (1993) 3875.

[ICR84]: *Stopping Powers of Electrons and Positrons*, ICRU Report No. 37 (1984)

[Kli90]: Klimt, S. et al.: *Chiral phase transition in the SU(3) Nambu and Jona-Lasinio model.* Phys. Lett. B 249 (1990) 386

[Kli96]: Klingl, F., Kaiser, N., Weise, W.: *Effective Lagrangian approach to vector mesons, their structure and decays*. Z. Phys. A 356, 193-206 (1996)

[Kli97]: Klingl, F., Kaiser, N., Weise, W.: Nucl. Phys. A 624 (1997) 527

[Koc95]: Koch, V.: *Introduction to Chiral Symmetry.* LBNL-Report 38000, 1995

[Lan85]: Landsberg, L.G.: Phys. Rep. 128(1985) 301

[Leh97]: Lehnert, J. et al: *The trigger system for the HADES detector.* Proceedings of the Xth IEEE Real Time Conference, Beaune 1997, p. 51

[Leh00]: Lehnert, J.: *Echtzeit-Mustererkennung zum Elektronennachweis mit einem RICH-Detektor in relativistischen Schwerionenkollisionen*, PhD. thesis, Universität Gießen, 2000

[Lep79]: Lepage, G., Brodsky, S., Phys. Rev. Lett. 43 (1979) 545; Phys. Rev D22 (1980) 2157.

[Lic99]: Lichtblau, C.: *Entwicklung schneller Elektronik für das HADES-Flugzeitsystem.* Diplomarbeit, 2. Physikalisches Institut, 1999

[Lin01]: Lins, E.: *Entwicklung eines Auslese- und Triggersystems zur Leptonenidentifizierung mit dem HADES-Flugzeitdetektor*, PhD. thesis, Universität Gießen, 2001

[Mue99]: Münch, M.: *A new ATM-based Data Acquisition System for the HADES Spectrometer*, Proceedings of the 37. International Winter Meeting on Nuclear Physics, Bormio (1999)

[MUD01]: *Matching Unit SubEvent data format*, committed to the HADES CVS repository, "/u/hades/CVS/debug/mu/MU_subevent_dataformat.txt"

[Nel66]: Nelson, W.R., Jenkins, T.M., McCall, R.C., and Cobb, J.K. Phys. Rev. 149, 201(1966)

[Oza01]: Ozawa, K. et al.: *Observation of ρ/ω Meson Modification in Nuclear Matter*, Phys. Rev. Letters. 86, 22 (2001)

[PDG00]: Particle Data Group, *Review of Particle Physics*, The European Physical Journal C15 (2000) 1

[Pet00]: Petri, M.: *Entwicklung eines kombinierten Auslese- und Triggersystems zum Nachweis von Elektron/Positronen-Signaturen in einem elektromagnetischen Schauerdetektor*, PhD. thesis, Universität Gießen, 2001

[Phi98]: Philips Semiconductor, *960 macrocell SRAM CPLD, Datasheet.* Philips, 1998

[Pos00]: Post, M., Leupold, S., Mosel, U.: *The spectral function in a relativistic resonance model*, Nucl. Phys. A 689 (2001) 753-783

[Rap98]: Rapp, R., Urban, M., Buballa, M., Wambach, J.: Phys. Lett B 417 (1998) 1

[Rap99]: Rapp, R., Wambach, J.: *Chiral Symmetry Restoration and Dileptons in Relativistic Heavy-Ion Collisions*, hep-ph/9909229

[Ros50]: Rosenbluth, M.N.: Phys. Rev. 79 (1950) 615

[Rot01]: ROOT: *ROOT, an Object-Oriented Data Analysis Framework*. http://root.cern.ch (2001)

[Sal95]: Salabura, P. et al.: *HADES - a high acceptance di-electron spectrometer.* Nuclear Physics B44 (1995) 701

[Sak69]: Sakurai, J. J., *Currents and Mesons*, The University of Chicago Press (1969)

[San00]: Sánchez, M.: *Kick Plane (Beamtime Edition)*, Internal Paper, GSI, 22.12.2000

[San00b]: Sánchez, M.: *The Hydra Analysis Package*, Internal Paper, GSI (2000)

[Sch95]: Schön, H.: *HADES - Ein Dileptonenspektrometer hoher Akzeptanz für relativistische Schwerionenkollisionen*, Doktorarbeit, Institut für Kernphysik, Johann-Wolfgang-Goethe-Universität Frankfurt am Main, 1995

[Seg94]: Seguinot, J. et al.: *A historical survey of ring imaging Cherenkov counters.* Nuclear Instruments and Methods in Physics Research A343 (1994) 1

[Tho01]: Thomas, A.W., Weise, W.: *The Structure of the Nucleon*. WILEY-VCH (2001)

[Toi01]: Toia, A.: *Analysis and Simulation of the HADES LVL2 Trigger.* Internal report, University of Gießen (2001)

[Tra99]: Traxler, M. et al.: *The HADES second level trigger system.* IEEE Transactions on Nuclear Science 47 (2000) 376

[Yps94]: Ypsilantis, T. et al.: *Theory of ring imaging Cherenkov counters*. Nuclear Instruments and Methods in Physics Research A343 (1994) 30

[Zei99]: Zeitelhack, K. et al.: *The HADES RICH Detector.* Nuclear Instruments and Methods in Physics Research A433 (1999) 201

HADES Collaboration

Czech Academy of Sciences , Rez, Czech Republic
Nuclear Physics Institute
A. Kugler , R. Pleskac , A. Taranenko , P. Tlusty , V. Wagner

Forschungszentrum Rossendorf , Dresden, Germany
Institut für Kern- und Hadronenphysik
R. Dressler , W. Enghardt , E. Grosse , R. Kotte , L. Naumann , J. Seibert

Gesellschaft für Schwerionenforschung , Darmstadt, Germany
Kernphysik I (Nuclear Reactions)
H. Agakichiev , D. Bertini , J. Bielcik , H. Bokemeyer , P. Braun-Munzinger , O. Goepfert , R. Holzmann , I. Koenig , W. Koenig , B. Kolb , D. Magestro , W. Niebur , C. Schroeder , P. Senger , R. Simon , P. Zumbruch
Detector Laboratory
H. Daues , J. Hehner , H. Stelzer
Datenverarbeitung und Elektronik Experimente
E. Badura , M. Dahlinger , H. Göringer , J. Hoffmann , W. Ott
Zentrale Technik
U. Kopf

Institut de Physique Nucleaire Orsay , Orsay, France
Division de Recherche
J. Boyard , T. Hennino , J. Jourdain , J. Pouthas , B. Ramstein , M. Roy-Stephan

Institute for Nuclear Research , Moscow, Russia
Experimental Physics
M. Golubeva , F. Guber , T. Karavicheva , A. Kurepin , A. Reshetin , K. Shileev , V. Tiflov

Institute of Theorectical and Experimental Physics , Moscow, Russia
A. Nekhaev , N. Rabin , V. Smolyankin

Istituto Nazionale di Fisica Nucleare Laboratorio Nazionale del Sud , Catania, Italy
C. Agodi , G. Bellia , R. Coniglione , P. Finocchiaro , C. Maiolino , P. Piattelli , P. Sapienza

Jagiellonian University , Cracow, Poland
Smoluchowski Institute of Physics
A. Balanda , M. Jaskula , M. Kajetanowicz , R. Kulessa , J. Otwinowski , M. Ploskon, W. Prokopowicz , W. Przygoda , P. Salabura , J. Sowa , E. Wajda , W. Walus , T. Wojcik

Johann Wolfgang Goethe-Universität Frankfurt , Frankfurt, Germany
Institut für Kernphysik
J. Markert , C. Müntz , Y. Pachmayer , K. Rosenkranz , H. Stroebele , J. Stroth , Y. Wang , J. Wüstenfeld

Joint Institute of Nuclear Research , Dubna, Russia
Lab. of High Energy Physics
S. Chernenko , O. Fateev , L. Glonti , Y. Panebratsev , V. Pechenov , L. Smykov , A. Titov , Y. Zanevsky

Justus Liebig Universität Giessen , Giessen, Germany
II. Physikalisches Institut
I. Froehlich , W. Kühn , J. Lehnert , E. Lins , V. Metag , M. Petri , J. Ritman, A. Toia, M. Traxler

Moscow Engineering Physics Institute , Moscow, Russia
E. Atkin , Y. Mishin , Y. Volkov

Slovak Academy of Sciences , Bratislava, Slovakia
S. Hlavac , I. Turzo

Technische Universität München , München (Garching), Germany
Department E12
M. Boehmer , T. Eberl , L. Fabbietti , J. Friese , R. Gernhäuser , J. Homolka , A. Kastenmüller, P. Kienle , H. Koerner , P. Maier-Komor , M. Münch , B. Sailer , S. Schroeder , W. Schön , A. Ulrich , S. Winkler

Universidade de Santiago de Compostela , Santiago de Compostela, Spain
Departamento de Fisica de Particulas
H. Alvarez-Pol , I. Duran , B. Fuentes , J. Garzon , R. Lorenzo , M. Sanchez , A. Vazquez

Universita degli Studi di Milano , Milano, Italy
R. Bassini , C. Boiano , S. Brambilla , I. Iori

Universite Blaise Pascal/Clermont II , Clermont (Aubiere Cedex), France
Lab. de Physique Corpusculaire
H. Meunier , G. Roche

University of Cyprus , Nicosia, Cyprus
R. Ispiryan , H. Tsertos

University of Valencia , Valencia (Burjasot), Spain
Instituto de Fisica Corpuscular
F. Ballester , J. Diaz , M. Pardo , N. Yahlali

Appendix A

Trigger Codes

In this appendix the LVL1 trigger codes with their corresponding LVL2 codes are listed.

Each legal code on LVL1 and LVL2 has a defined consequence for the readout. The second level trigger decisions are divided into positive and negative decisions, which the Matching Unit has to determine. Due to the usage of special trigger codes for the calibration events, the subdetectors have the opportunity to react differently to such events. Therefore, it is possible, that during MDC calibration events (ca. 10 Hz) the other detectors do not generate data, even if the Matching Unit triggers this event positively.

The table with all possible 16 trigger codes is listed below.

LVL1			LVL2			
Code	**Name**	**Usage/Reaction of Readout**	**pos.**	**neg.**	**Name**	**Reaction of Readout**
0x0	Illegal	error	NA	NA	Illegal	NA
0x1	Norm1	generate data	0x1	0x9	Norm	MU decision
0x2	Norm2	generate data	0x1	0x9	Norm	MU decision
0x3	Norm3	generate data	0x1	0x9	Norm	MU decision
0x4	Norm4	generate data	0x1	0x9	Norm	MU decision
0x5	Norm5	generate data	0x1	0x9	Norm	MU decision
0x6	Spec1	calibration event	0x2	0xa	Spec1	own decision
0x7	Spec2	calibration event	0x3	0xb	Spec2	own decision
0x8	Spec3	calibration event	0x4	0xc	Spec3	own decision
0x9	Spec4	calibration event	0x5	0xd	Spec4	own decision
0xa	Spec5	calibration event	0x6	0xe	Spec5	own decision

Table A.1: Overview of the trigger codes in LVL1, their name and usage. Corresponding positive and negative LVL2 trigger codes sent by Matching Unit/CTU are shown.

LVL1			LVL2			
Code	**Name**	**Usage/Reaction of Readout**	**pos.**	**neg.**	**Name**	**Reaction of Readout**
0xb	Illegal	NA	NA	NA	Illegal	NA
0xc	Illegal	NA	NA	NA	Illegal	NA
0xd	BeginRun	send first trigger tag	NA	NA	NA	NA
0xe	EndRun	empty pipes	NA	NA	NA	NA
0xf	Illegal	NA	NA	NA	Illegal	NA

Table A.1: Overview of the trigger codes in LVL1, their name and usage. Corresponding positive and negative LVL2 trigger codes sent by Matching Unit/CTU are shown.

Appendix B

Matching Unit Registers

In this appendix the basic usage and the registers of the Matching Unit are documented. The MU is a VME module and the configuration and all settings are done by accesses from the local VME CPU.
The MU basis address can be configured via a hex-switch on the PCB. The upper 5 bits of the VME address space are selectable. The standard basis address used at GSI is `0xd0000000`.
The offsets for the different components on the board are listed in table B.1.

Component	Offset	Description
Lattice control register	`0x07000000`	This chip provides a basic VME interface and is automatically usable directly after power up. It is used to program the board controller.
Philips control register (board controller CPLD)	`0x06000000`	The board controller CPLD is responsible for the coordination of all data transfers happening on the MU. It has to be programed after power up. Important register are shown in table B.3.

Table B.1: Offsets to the basis address of the MU to access components on the board.

Component	Offset	Description
FIFO	0x04000000	The MU event FIFO. It is used to store all data from the MU and is read out by the local VME CPU and its data is sent to the Event Builder. It has a depth of 64k words and a width of 16-bit. It is directly accessible by VME without interrupting the operation of the DSPs.
External Memory	0x02000000	Static RAM on the MU. It is used to store large tables. It has 512 kBytes of memory.
DSPs	0x00000000	The basis address for the host bus access to the DSPs. A second offset is needed to determine the number of DSP accessed (table B.2).

Table B.1: Offsets to the basis address of the MU to access components on the board.

The offsets for the 3 DSPs on the MU are shown in table B.2.

DSP Nr.	Offset
1	0x00000000
2	0x02000000
3	0x04000000

Table B.2: DSP offsets.

Important registers in the board controller CPLD (table B.3).

Register Offset	Name
0x0	MU setup register (table B.4)
0x4	MU board status register (table B.5)
0x8	IPU addressing register (table B.6)

Table B.3: Register names in the board controller CPLD.

MU setup register:

Bit Number	Name and Function
0	$\overline{\text{SBTS}}$: Sets the SHARC multiprocessor bus into a tri-state condition.
1	$\overline{\text{SH\_RESET}}$: Resets all SHARC DPSs on board.
2	$\overline{\text{IPU\_FIFO\_RESET}}$: Resets all IPU FIFOs.
3	$\overline{\text{FIFO\_RESET}}$: Resets the Event FIFO of the MU.
4	$\overline{\text{SELF\_DATA}}$: The board controller will produce fake IPU data, for testing purposes only.
5	EN_FIFO_CLOCK: Enables the clock line on the IPU FIFOs.

Table B.4: MU setup register

MU board status register:

Bit Number	Name and Function
0	CTU_BUSY: Signals a BUSY condition from the CTU, no further LVL2 trigger decisions can be sent to the CTU.
1	$\overline{\text{FIFO\_FF}}$: Full flag of the event FIFO, no further event data can be written to the event FIFO.
2	$\overline{\text{FIFO\_AF}}$: Event FIFO is almost full (127 words).
3	$\overline{\text{FIFO\_EF}}$: Empty flag of the event FIFO.
4	$\overline{\text{FIFO\_A}}$: Event FIFO is almost empty (127 words).

Table B.5: MU board status register

IPU addressing register:

Bit Number	Name and Function
2-0	IPU_ADDRESS: Number of IPU to be addressed.
3	LINK_SPEED: 1 for 10 MHz, 0 for 20 MHz frequency of the serial protocol to address the IPUs.

Table B.6: IPU addressing register

DSP registers:

In table B.7 the most important registers of the DSPs, their offset to the DSP Nr. and the description of their function are listed.

Register Name	Offset	Function
RICH IPU addressing	0xE800	Writing a number to this register will address the corresponding the RICH IPU.
SHOWER IPU addressing	0xE804	Writing a number to this register will address the corresponding the SHOWER IPU.
TOF IPU addressing	0xE808	Writing a number to this register will address the corresponding the TOF IPU.
LVL2 Triggers	0xE80C	Number of LVL2 triggers given by the MU, read only.
MU_STATUS_REG	0xE8010	Status register of the MU operation. The bits are explained in table B.8. (read only)
Pos_LVL2_Triggers	0xE8014	Number of positive LVL2 trigger decisions. (read only)
Debug_Level	0xE801C	If set to 0, only error messages are written to the debug memory. Bits 3-0 set the debug level for data transport, bits 7-4 set the debug level for the matching algorithm.
Not_connected_IPU	0xE8020	Register to mask out IPUs which do not send data to the MU. bit 0: RICH IPU bit 1: SHOWER IPU bit 2: TOF IPU
Trigger_condition_mask	0xE8024	Register to mask out IPUs which should not be used for a trigger decision. bit 0: allow positive triggers at all (default: 1) bit 1: RICH IPU bit 2: SHOWER IPU bit 3: TOF IPU
Number of IPUs: RICH	0xE8048	Number of RICH IPUs connected to the MU.
Number of IPUs: Shower	0xE804C	Number of Shower IPUs connected to the MU.

Table B.7: Matching Unit DSP registers with offset and description.

Register Name	Offset	Function
Number of IPUs: TOF	0xE8050	Number of TOF IPUs connected to the MU.
Current_IPU_address: RICH	0xE8058	This register contains the RICH IPU which has been addressed most recently.
Current_IPU_address: Shower	0xE805C	This register contains the Shower IPU which has been addressed most recently.
Current_IPU_address: TOF	0xE8060	This register contains the TOF IPU which has been addressed most recently.
Disable_MU_Algorithm	0xE80A0	Enables (0) or disables (1) the processing of the MU trigger algorithm. Downscaling still works.
Downscaling_value	0xE8028	Downscaling value can be read and set. Downscaling is defined as: (1/value) is the fraction of forced positive triggers.
Error_message_print	0xE8040	Enables (1: default) or disables (0) error messages to be print to the debug memory.
LVL2_to_CTU	0xE8064	Enables (1: default) or disables (0) sending of the LVL2 decision to the CTU.
Trigger_Condition1: RICH	0xE80B0	Minimal number of hits which have to be found in the RICH IPU to give a positive LVL2 trigger decision. All conditions from 1 to 4 must be met.
Trigger_Condition 2: TOF and SHOWER	0xE80B4	Minimal number of hits which have to be found in the TOF IPU and SHOWER IPU.
Trigger_Condition 3: Leptons	0xE80B8	Minimal number of leptons which have to be found.
Trigger_Condition 4: DiLeptons	0xE80BC	Minimal number of dileptons which have to be found.
Trigger_Cond_met1-5	0xE808C-0xE809C	MU scalers. They show the number of events, which met each of the trigger conditions described above.

Table B.7: Matching Unit DSP registers with offset and description.

Register Name	Offset	Function
Delta_Phi_Cut	0xE807C	Delta phi (the size of the hit matching window): 0=0°, 255 = 60°.
Delta_Theta_Cut	0xE8084	Delta theta cut: 0=0°, 255 = 90°.
Invariant_Mass_Cut	0xE8080	Invariant mass squared cut. IEEE 32-bit floating point number.

Table B.7: Matching Unit DSP registers with offset and description.

MU_STATUS_REGISTER (read only):

Bit Number	Name and Function
0 and 1	If one of these bits is set, the event FIFO on the MU is full and the MU can not send the data to the DAQ. As long as the readout does not continue, the MU will not address the IPUs.
2	This bit signals that the MU stopped accepting new data, since the CTU is BUSY and can not accept more LVL2 trigger decision.
3	Fatal Error: Too many data words have been sent by a IPU. MU stopped.
4	Global_Stop: Set to one, if the global stop bit is set.

Table B.8: MU_STATUS_REGISTER

Slow Control Software: (at GSI)

The status of the Matching Unit can be displayed with the command:
`printf_daemon 0xd2004000.`
The LVL2 and positive LVL2 rate can be displayed with the command:
mu_fastrate d00E800C d00E8014
Registers can be read by:
`rw r <address>`
Writing to registers:
`rw w <address> <value>` , where value is hexadecimal.

Normal operation is done with the `muctrl` program. The configuration and all necessary parameters for the operation (trigger condition) are read from the file:
`trigconc.tcl`
The registers of the MU described above, are defined and set in this file.

Index

Danksagung

An erster Stelle möchte ich Prof. Dr. Wolfgang Kühn danken, der mir die Mitarbeit an diesem sehr interessanten internationalen Projekt ermöglichte und sein Team aus Gießen immer wieder mit vollem Einsatz unterstützt und unsere Interessen vor der Kollaboration verteidigt.

Ich danke auch Jim Ritman, der immer kompetent und wohlwollend jede Frage zum tieferen Sinn und Unsinn des Quark-Gluon-Plasmas und anderer Physik beantwortet, auch wenn ich zum Dritten mal nachfragen muß.

Danke an das Gießener HADES-Team Erik, Jörg, Ingo, Markus und Alberica für die (fast durchgehend) überaus gelungene Teamarbeit. Gemeinsam sind wir stark....

Weiterhin möchte ich Erik und Jörg für das freundschaftliche Verhältnis danken!

Danke auch an all die Ehemaligen, die noch vor nicht allzu langer Zeit das Institut bereichert haben:
Hans: sein hallendes Lachen über den Flur fehlt einfach.
Carsten: mein Freund, der unsere “Klassenfahrten” immer sehr lustig machte.
Rene: der fluchtartig das Land verließ, um in Australien sein Glück zu suchen. Übrigens, deine Sandalen stehen immer noch hier rum... :-)
und so weiter und so fort....

Natürlich danke ich auch allen “festen” Mitarbeitern im Institut, ohne die hier alles drunter und drüber laufen würde.

Bei meinen Eltern möchte ich mich dafür bedanken, daß sie mich während der ganzen Studienzeit (nicht nur finanziell!) unterstützt haben.

Und natürlich vielen Dank an mein Schatz Tanja, sie gibt der ganzen Sache den Glanz! Außerdem wäre ich ohne sie während des Schreibens der Arbeit verhungert.